nagra.

Technical Report 14-12

Montmorillonite stability under near-field conditions

July 2014

O.X. Leupin (ed.), M. Birgersson,
O. Karnland, P. Korkeakoski,
P. Sellin, U. Mäder, P. Wersin

National Cooperative
for the Disposal of
Radioactive Waste

Hardstrasse 73
CH-5430 Wettingen
Switzerland
Tel. +41 56 437 11 11

www.nagra.ch

nagra.

Technical Report 14-12

Montmorillonite stability under near-field conditions

July 2014

O.X. Leupin (ed.) [1], M. Birgersson [2], O. Karnland [2], P. Korkeakoski [3], P. Sellin [4], U. Mäder [5], P. Wersin [5]

[1] Nagra, [2] Clay Technology AB, [3] Posiva, [4] SKB, [5] University of Berne

National Cooperative for the Disposal of Radioactive Waste

Hardstrasse 73
CH-5430 Wettingen
Switzerland
Tel. +41 56 437 11 11

www.nagra.ch

This report was prepared on behalf of Nagra. The viewpoints presented and conclusions reached are those of the author(s) and do not necessarily represent those of Nagra.

ISSN 1015-2636

Abstract

Clay-based engineered barriers comprising bentonite and bentonite/sand mixtures are the favoured option in geological repositories for high-level waste due to their inherently low hydraulic conductivity at full saturation. This ensures that diffusion of solutes such as radionuclides will be the dominating mechanism for transport through the engineered barriers. Another advantageous property of bentonite is the development of swelling pressure in contact with water under the constant volume conditions of repository excavations, ensuring the closure of unintentional gaps or openings. The predictability of the long-term behaviour of bentonite (up to a million years) is thus key to the safety analysis.

The thermal pulse from the radioactive decay of the radionuclides in the high-level waste and spent fuel will lead to temperatures significantly higher than in the undisturbed host rock for hundreds of years, which may influence the thermodynamic stability and kinetics of alteration reactions of montmorillonite, the smectite that is the main constituent of the bentonite. The aim of this report is to review the present understanding of potential alteration of bentonite by focusing on experimental and modeling results under the thermal conditions of a repository.

Many studies show that the transformation of smectite-to-illite is induced by increasing temperature and potassium activity. The conversion process is complex and still not completely understood. Nonetheless, it displays very slow kinetics over a wide range of environmental conditions for the temperatures of interest.

The various models for illitisation of smectites suggest negligible transformation in a repository due to the relatively short period of elevated temperatures and slow mass transport. However, because of uncertainties and a number of conservatisms in the application of such models, the results of such calculations should be considered as bounding and indicative and not as quantitative predictions.

In addition to the review of published studies, three sets of experiments were performed to study potential changes to the safety-relevant properties of bentonite during the high temperature period of a repository and the results may be summarized as follows:

- Smectite-to-illite hydrothermal experiments with MX-80 bentonite at 270 °C and variable potassium activity conditions did not evidence any illitisation in reacted samples for either raw bentonite or Na-exchanged bentonite reacted in "granite-type" solution regardless of the presence of added K-feldspar or the more abundant accessory mineral content in the raw bentonite.
- Experiments on thermal stability of montmorillonite at 90 – 150 °C showed that montmorillonite dissolved and released silica, which resulted in a layer charge increase located in the tetrahedral sheets. The montmorillonite was consequently altered in the direction towards beidellite – a swelling smectite mineral.
- Experiments on the effect of steam on the swelling capacity of bentonite showed that water vapor at temperatures up to 200 °C and water unsaturated conditions do not cause a significant reduction of the water uptake capacity of montmorillonite.

Based on the review and additional studies performed, it can be concluded that the swelling pressure and the hydraulic conductivity, which are important safety function indicators for clay barriers, are not expected to be significantly affected by the thermal transient that will occur in the discussed repositories.

Zusammenfassung

Technische Barrieren aus Ton, die Bentonit- oder Sand-Bentonit-Mischungen enthalten, werden im geologischen Tiefenlager für hochaktive Abfälle aufgrund der inhärent tiefen hydraulischen Leitfähigkeit bei Vollsättigung bevorzugt. Diese gewährleisten, dass die Diffusion der prioritäre Transportmechanismus von gelösten Stoffen, wie etwa Radionuklide, innerhalb der technischen Barrieren ist. Ein weiterer Vorteil von Bentonit ist dessen Quellfähigkeit, die bewirkt, dass der Bentonit bei konstantem Volumen und in Kontakt mit Wasser einen Quelldruck entwickelt, der dazu führt, dass unerwünschte Ausbrüche und Risse in den Lagertunneln geschlossen werden. Die Prognostizierbarkeit des Verhaltens von Bentonit ist daher für die Langzeit-Sicherheitsanalyse (bis zu einer Million Jahre) eines geologischen Tiefenlagers von zentraler Bedeutung.

Die Zerfallswärme des hochaktiven verglasten Abfalls und der abgebrannten Brennelemente wird in direkter Umgebung zu einer Temperatur führen, die während hunderten von Jahren signifikant höher als diejenige im ungestörten Opalinuston sein wird und damit die thermodynamische Stabilität und Umwandlungskinetik vom Smektitmineral Montmorillonit, dem Hauptmineral von Bentonit, beeinflussen könnte. Das Ziel dieses Berichts ist es, das heutige Verständnis von potenziellen Änderungen des Bentonits aufgrund von Experimenten und Modellierungen unter thermischen Bedingungen, die relevant für ein Tiefenlager sind, zu beurteilen.

Viele Studien zeigen, dass die Umwandlung von Smektit zu Illit durch steigende Temperaturen und Kaliumaktivität bewirkt wird. Der Umwandlungsprozess ist komplex und noch nicht vollständig verstanden. Nichtdestotrotz zeichnet ihn im Bereich der Temperaturen von Interesse und für ein breites Spektrum von Umgebungsbedingungen eine langsame Kinetik aus.

Aufgrund der relativ kurzen Dauer erhöhter Temperaturen und des langsamen diffusiven Stofftransports deuten die verschiedenen Modelle für die Illitisierung von Smektit auf eine vernachlässigbare Umwandlung hin. Wegen einer Anzahl von Ungewissheiten und konservativen Annahmen in der Anwendung solcher Modelle sind deren Resultate in erster Linie als abdeckend und indikativ und nicht als quantitative Vorhersagen zu betrachten.

Um potenzielle Änderung von sicherheitsrelevanten Eigenschaften von Bentonit während der Dauer erhöhter Temperaturen in einem geologischen Tiefenlager zu untersuchen, wurden zusätzlich zur Durchsicht von publizierten Studien drei Typen von Experimenten durchgeführt, deren Resultate wie folgt zusammengefasst werden können:

- Hydrothermal-Experimente zur Smektit-zu-Illit-Umwandlung mit MX-80 Bentonit bei 270 °C und variabler Kaliumaktivität liessen keine Illitisierung nachweisen, weder im unbehandelten noch im mit Natrium ausgetauschten Bentonit, welcher mit "granitischem" Porenwasser reagierte, unabhängig davon, ob Kalifeldspat dazugegeben wurde oder in der Gegenwart eines erhöhten Sekundärmineralgehalts im ursprünglichen Bentonit.
- Experimente zur thermischen Stabilität von Montmorillonit bei 90 – 150 °C zeigen auf, dass Montmorillonit sich auflöst und Silikat freisetzt, was in einer Zunahme der Schichtladung in den Tetraederschicht führt. Montmorillonit wurde folglich in Richtung auf Beidellit umgewandelt – ein quellfähiges Smektitmineral.
- Experimente zum Einfluss von Wasserdampf auf die Quellfähigkeit von Montmorillonit zeigen auf, dass bis zu Temperaturen von 200 °C und unter Wasser-ungesättigten Bedingungen keine signifikante Reduktion der Quellfähigkeit von Montmorillonit auftritt.

Aufgrund der durchgeführten Versuche und der Durchsicht von publizierten Studien kann der Schluss gezogen werden, dass weder der Quelldruck noch die hydraulische Leitfähigkeit, welche wichtige Indikatoren für die Sicherheitsfunktionen der tonhaltigen Barriere sind, durch die thermisch transiente Phase in den besprochenen geologischen Tiefenlagern signifikant beeinflusst werden.

Résumé

Pour les dépôts géologiques destinés aux déchets de haute activité, on prévoit des barrières ouvragées composées de matériaux argileux – bentonite ou mélanges de bentonite et de sable –, du fait de leur faible conductivité hydraulique à saturation. Cette propriété fait que le transport de solutés, tels que les radionucléides, au travers des barrières ouvragées s'effectuera en priorité par diffusion. La bentonite a également pour avantage de gonfler lorsqu'elle entre en contact avec de l'eau. Du fait que les volumes des cavernes de stockage sont constants, on estime que la bentonite parviendra donc à combler les vides éventuels qui pourraient subsister. La possibilité de prévoir le comportement à long terme (jusqu'à un million d'années) de la bentonite est par conséquent un élément-clé des analyses de sûreté.

La chaleur émanant des déchets de haute activité et des éléments combustibles usés pendant la phase de décroissance radioactive entrainera des températures nettement plus élevées que celles qui règnent dans une roche non perturbée, et ceci sur plusieurs centaines d'années. Ces conditions pourraient avoir un impact sur la stabilité thermodynamique et la cinétique de l'altération de la montmorillonite (la smectite qui est le principal composant de la bentonite). L'objectif du présent rapport est de résumer les connaissances actuelles sur les mécanismes d'altération potentiels de la bentonite, en mettant l'accent sur les résultats issus d'expérimentations et de modélisations reproduisant les conditions thermiques d'un dépôt en profondeur.

De nombreuses études montrent qu'une augmentation de la température et l'activité du potassium peuvent induire la transformation de smectite en illite. Complexe, cette transition n'est pas encore bien comprise. On sait toutefois que la cinétique est très lente pour une vaste palette de conditions environnementales aux températures considérées.

Les différents modèles relatifs au processus d'illitisation des smectites suggèrent que la transformation s'opérant dans un dépôt géologique est négligeable du fait de la période relativement courte pendant laquelle règnent des températures élevées, mais aussi de la lenteur du transport diffusif de masse. Cependant, étant donné les incertitudes qui accompagnent l'application de tels modèles et le fait que les calculs reposent en partie sur des hypothèses pessimistes, les résultats obtenus doivent plutôt être considérés à titre indicatif, comme reflétant des conditions limites, et non pas comme des prédictions quantitatives.

En plus de l'analyse des études existantes, trois séries d'expériences ont été mises en œuvre pour étudier les transformations potentielles de la bentonite pendant la période de hautes températures, plus spécifiquement les altérations qui pourraient affecter négativement les propriétés de la bentonite qui sont pertinentes pour la sûreté du dépôt. Les résultats peuvent être résumés comme suit:

- Les expériences hydrothermiques «transformation smectite – illite» effectuées avec de la bentonite MX-80 à 270 °C, avec une activité du potassium variable, n'a produit aucun indice d'illitisation dans les échantillons testés, ni pour la bentonite brute, ni pour la bentonite ayant subi un échange d'ions de sodium dans une solution de « type granit ». Les résultats ont été les mêmes, indépendamment de la présence, dans la bentonite brute, de feldspath potassique ajouté ou d'une teneur plus élevée en minéraux accessoires.
- Les expériences portant sur la stabilité de la montmorillonite à des températures de 90 à 150 °C ont conduit à une dissolution accompagnée d'un dégagement de silice, entrainant une augmentation de charge dans les couches tétraédriques. En conséquence, la transformation de la montmorillonite est allée en direction de la beidellite.

- Les expériences menées sur les effets de la vapeur sur la capacité de gonflement de la bentonite ont révélé que la vapeur d'eau à des températures allant jusqu'à 200 °C et dans des conditions non saturées n'entrainait pas de réduction significative de la capacité d'absorption d'eau de la montmorillonite.

Sur la base des analyses et des études complémentaires effectuées, il est permis de conclure que la pression de gonflement et la conductivité hydraulique, qui sont des indicateurs importants pour la sûreté des barrières ouvragées composées de matériaux argileux, ne seront pas affectées de manière significative par l'augmentation temporaire de la température qui surviendra dans les dépôts géologiques.

Table of Contents

Abstract I

Zusammenfassung III

Résumé V

Table of Contents VII

List of Tables IX

List of Figures X

1 Introduction 1
1.1 Desired properties of bentonite – safety functions 2
1.1.1 Specific Nagra required properties – safety functions 2
1.1.2 Specific SKB and Posiva required properties – safety functions 6
1.2 SF/HLW repository expected evolution and repository conditions in Opalinus Clay 8
1.3 SF/HLW repository reference evolution and repository conditions in crystalline rock 14

2 Smectite stability at increased temperatures – insights from literature 29
2.1 Formation conditions of smectite 29
2.2 Modes of smectite alteration 34
2.2.1 Transformation to illite 34
2.2.2 Transformation to beidellite and saponite 34
2.2.3 Transformation to chlorite 35
2.2.4 Effects of high pH 36
2.2.5 Effects of unsaturated conditions 36
2.2.6 Effects of cementation 37
2.2.7 Hoffmann-Klemen effect 37
2.2.8 Possible reduction of structural Fe^{3+} 37
2.2.9 Summary considerations 38
2.3 Illitisation 38
2.3.1 Introduction 38
2.3.2 Process description 39
2.3.3 Influence of temperature 40
2.3.4 Influence of potassium 41
2.3.5 Influence of pressure 42
2.3.6 Influence of smectite mineralogy 42
2.3.7 Influence of cations in the interlayer and in solution 42
2.3.8 Influence of water activity and transport 43
2.3.9 Compilation of activation energies 43
2.4 Implications for the bentonite buffer 46

2.4.1 Summary considerations based on literature data ... 46
2.4.2 Transport limitation ... 47

3 Smectite-to-illite conversion: hydrothermal experiments with MX-80 bentonite at 270 °C and variable potassium activity conditions ... 49
3.1 Objectives and design of experiments ... 49
3.2 Materials and methods ... 50
3.2.1 Overview of the experimental procedures ... 50
3.2.2 Equipment ... 51
3.2.3 Methods ... 51
3.2.4 Mixed-layer clay quantification by computed XRD patterns ... 55
3.3 Results ... 59
3.3.1 XRD peak distance quantification of homo-ionised samples ... 59
3.3.2 Illite content of thermally reacted samples ... 62
3.4 Summary and conclusions ... 63

4 Experiments on thermal stability of montmorillonite at 90 – 150 °C ... 65
4.1 Introduction ... 65
4.1.1 General experimental principles ... 65
4.2 Test material ... 66
4.2.1 Equipment and test method in the 90 °C test series ... 66
4.2.2 Equipment and test method in the 150 °C test series ... 68
4.3 Analyses ... 69
4.3.1 Water content and density ... 69
4.3.2 Water analyses ... 69
4.3.3 Cation exchange capacity ... 69
4.3.4 Exchangeable cations ... 70
4.3.5 SEM/EDX element analyses of the solids ... 70
4.4 Results and discussion ... 71
4.4.1 90 °C test series ... 71
4.4.2 150 °C test series ... 76
4.5 Conclusions ... 81

5 Effect of steam on the swelling capacity of bentonite ... 83
5.1 Introduction ... 83
5.2 Test materials ... 83
5.3 Equipment and test technique ... 84
5.4 Results and discussion ... 85
5.5 Conclusions ... 90

6 Summary and conclusions ... 91

Acknowledgements ... 93

7 References ... 95

List of Tables

Tab. 1-1: Compilation of attributes for the buffer material around the canister for the different repository design and concepts. 4

Tab. 1-2: "Initial state" Opalinus Clay pore water chemistry..... 12

Tab. 1-3: Bentonite pore water (adapted from Bradbury et al. 2014) composition for 36 % bulk porosity obtained with the novel approach ("New model"). 13

Tab. 1-4: Process table for the buffer describing how buffer processes are handled in different time frames and for the special case of an earthquake for the SR-Site. 15

Tab. 2-1: Selected data of smectite-to-illite reaction experiments. 44

Tab. 2-2: Activation energies applied in modelling studies to simulate illitisation. 45

Tab. 3-1: Recipe for the synthetic "granite" pore water. 52

Tab. 3-2: List of experiments, charges and conditions, all at 270 °C..... 54

Tab. 3-3: Reference table for quantifying illite content in glycolated illite/smectite. 57

Tab. 3-4: Peak distances between 001/002 and 002/003 peaks in °Δ2Θ..... 59

Tab. 3-5: Percentage of illite in reacted samples (270 °C) and starting materials. 62

Tab. 4-1: Results from test series MmS-A concerning water content (w), saturated density (ρ_m), pore ratio e, porosity (n), dry density (ρ_d), initial swelling pressure ($P_{s,\,ini}$) and final swelling pressure($P_{s,\,fin}$). 71

Tab. 4-2: Silica dissolution rates evaluated for all sampled solutions..... 73

Tab. 4-3: Total amount of released silica into the external water solutions according to ICP/AES analyses. 73

Tab. 4-4: Structural formula based on SEM/EDX element analyses of all samples in the 90 °C test series. 75

Tab. 4-5: Total mass of ions in the solutions. 76

Tab. 4-6: Sum of exchanged cation equivalents from all test solutions. 77

Tab. 4-7: Measured magnesium mass, and total magnesium equivalents per mass, in relevant test solutions. 77

Tab. 4-8: Total release of Si (and as SiO_2) from all samples according to the ICP/AES water analyses. 78

Tab. 4-9: Silicon release rates (mole Si/g clay/s) for each exchange period of the water solutions. 78

Tab. 4-10: Measured CEC after heating tests, but before the K/Na exchange procedure. 79

Tab. 4-11: Measured CEC after heating tests, and after exchange to K- and subsequent exchange to Na-state. MmS-BR represents reference material. 80

Tab. 4-12: Structural formula based on SEM/EDX element analyses of all samples in the 150 °C test series. 80

Tab. 5-1: Layout and major results from all steam tests. 86

List of Figures

Fig. 1-1: Nagra disposal concept for SF and HLW: (a) repository layout and detail of EBS; (b) longitudinal section of emplacement tunnel showing liner and hydraulic seal. 9

Fig. 1-2: Rock wall temperature (1), temperature drop across bentonite (2), maximum bentonite temperature (3) located at the top of the canister in dry deposition holes (left) and at canister mid-height in wet deposition holes (right). 20

Fig. 1-3: Distribution of buffer peak temperature in two different rock domains in the Forsmark site (rock domains RFM029 above and RFM045 below), with and without correction for spatial variability. 21

Fig. 1-4: Sketch of a vertical cross section of the near-field of a KBS-3 repository showing the thermo-hydraulic and transport processes that are believed to occur during the saturation period of the bentonite buffer (after Sena et al. 2010). 24

Fig. 1-5: Calculated evolution of the amount of anhydrite in the MX-80 bentonite buffer as a function of buffer saturation time (Sena et al. 2010). 25

Fig. 1-6: Calculated evolution of the amount of SiO_2 in the modelled domain of MX-80 bentonite, for a saturation time of the bentonite of 10 years (Sena et al. 2010). 26

Fig. 2-1: Mineral assemblages as function of temperature in intermediate to alkaline types of hydrothermally altered rocks (from Inoue 1995). 29

Fig. 2-2: Ideal end members in the pyrophyllite – mica series with potassium as charge compensating cation, and approximate compositional ranges for illite and smectite. 30

Fig. 2-3: Activity ratio diagram in the Si-Al-K-O-H_2O system at 25 °C (from Aagard & Helgeson 1983). 31

Fig. 2-4: Sketch of illitisation with a dissolution/precipitation model (from Ahn & Peacor 1986). 35

Fig. 2-5: Illitisation rates sketched for sedimentary basins with a low geothermal gradient (left) and a high gradient (right) (from Meunier & Velde 2004) (see text). 40

Fig. 2-6: Illitisation degree (shown as % loss smectite) in three different experimental studies at 250 °C (left) and illitisation rate (% illite per day) as function of K content (% K_2O) for the same three studies (right, from Meunier & Velde 2004). 41

Fig. 2-7: The extent of transformation of the bentonite buffer in a KBS-3 deposition hole after 100'000 years of interaction with the ground water as modelled in (Birgersson *in prep.*). 48

Fig. 3-1: Details of titanium autoclaves (left), mounting arrangement of autoclaves in the oven (middle), and oven with external motor drive for the rotation system (right). 51

Fig. 3-2: XRD pattern of an illite and smectite clay mixture computed with NEWMOD (Reynolds & Reynolds 1995). 56

Fig. 3-3: Calibration curve for illite content in I/S using computed XRD patterns and data from Tab. 3-3. 58

Fig. 3-4: XRD patterns of oriented clay samples. 61

Fig. 4-1: Principle drawing of the test setup for the 90 °C test series (top) and a photo of the 6 test cells placed in the laboratory oven (bottom). 67

Fig. 4-2: Test equipment for the 150 °C series. 68

Fig. 4-3: Swelling pressure evolution during water saturation and initial heating phases. 71

Fig. 4-4: Concentration in external solutions (left) and released silica mass (right) versus time in the six tests. 72

Fig. 4-5: Ion distribution in the reference material and in the test samples after the heating phase. 74

Fig. 4-6: First set of CEC results from reference and test samples in the 90 °C-series after the heating phase but before ion exchange to K^+- and subsequently Na^+-form. 74

Fig. 4-7: Second set of CEC results from reference and test samples in the 90 °C-series after the heating phase after ion exchange to K^+- and subsequently Na^+-form. 75

Fig. 4-8: Measured CEC after heating tests, and after exchange to K- and subsequent exchange to Na-state. 79

Fig. 5-1: Test equipment showing the pressure controlling device and the various parts used for steam exposure of the clay. 85

Fig. 5-2: Clay/water volumes for five materials in Series MmS-1000. 87

Fig. 5-3: Illustration of the clay/water volume after active dispersion and settlement for five materials in Series MmS-1000. 88

Fig. 5-4: Left photo: reference (left) and steam (150 °C) exposed (right) montmorillonites from Series MmS-800, right photo: reference (left) and steam (200 °C) exposed (right) materials from the Series MmS-700. 88

Fig. 5-5: "Swelling capacity" of different materials according to the publication by Couture (1985). 89

1 Introduction

Bentonite and bentonite/sand mixtures are the favoured option for clay-based engineered barriers for nuclear waste repositories due to their inherently low hydraulic conductivity at full saturation. This ensures that diffusion of solutes such as radionuclides will be the dominating mechanism for transport through the engineered barriers. Another advantageous property of smectite-rich bentonite is the build-up of swelling pressure in contact with water, ensuring the closure of unintentional gaps or openings, thus providing self-sealing capacity. The predictability of the long-term behaviour of bentonite (up to a million years) is thus important for the safety analysis.

The long time frame requires an in-depth understanding of possible alteration processes affecting the bentonite:

- Initially when the repository is being resaturated, strong hydraulic gradients will prevail and this may cause – in a fractured host rock – mechanical erosion of the bentonite. Here, ion exchange composition may be very important since the contact zone between the groundwater and the bentonite is small and erosion properties of Ca- and Na-bentonite are very different.
- The steep thermal gradient during the early repository evolution when the near-field is still being resaturated may induce internal mass redistribution (i.e. dissolution and re-precipitation of accessory minerals) in the bentonite resulting in some cementation of the bentonite matrix. In the long run, if elevated temperature persists, the smectite component in the bentonite may also undergo some mineralogical changes.
- It is expected that bentonite will interact with tunnel supporting structures as well as with the groundwater. Chemical interactions with the metal disposal canisters and cement-based tunnel reinforcements may also occur. The concentrations of cations in the local groundwater will determine the final composition of the exchanger in the bentonite. An intruding groundwater with a very low concentration of ions may also affect the mechanical stability of the bentonite.

All these alteration and transformation processes are safety-relevant as they may affect the hydro-mechanical and chemical properties of the bentonite. Therefore it is crucial to have an in-depth understanding of expected processes in order to be able to quantify the extent of the alteration in a long-term perspective and to finally assess the alteration in the perspective of the safety analysis.

The aim of this report is to review today's understanding of potential alteration of bentonite by focusing on experimental and modelling results under thermal conditions as might be found in a repository. To complement the findings in the literature review of published studies, three sets of experiments were performed to study potential changes to the safety-relevant properties of bentonite during the high temperature period of a repository. Even though the thermal pulse from the decay heat from the high level waste (HLW) and spent fuel (SF) will last only for up to a few hundred years for temperatures significantly higher than the undisturbed host rock temperature at repository level (depending on the thermal load, the repository design, host rock and resaturation etc.) it is nevertheless expected to have the biggest impact on the stability of the bentonite by influencing thermodynamic stability or accelerating reactions.

1.1 Desired properties of bentonite – safety functions

Overall required properties

The overall safety functions of a nuclear waste repository are confinement and attenuation. Confinement is defined as the complete isolation of the waste, while retardation slows down any releases in the case of a failed confinement.

The overall criterion for evaluating repository safety is the risk criterion issued by national regulators which is usually expressed as a maximum dose, or risk, to a representative individual in the group in the biosphere exposed to the greatest risk.

To evaluate the dose or risk from a repository a detailed and quantitative understanding of all processes that affect the repository together with the associated uncertainties is needed. Dose and risk are therefore not very practical entities to use for the study of individual repository components. To resolve this, the concept of "safety functions" has been introduced. A safety function is a description of how an individual barrier contributes to the confinement and retardation of radionuclides. Safety functions can be defined based on the understanding of the properties of the components and the long-term evolution of the system.

To safely contain the waste and to be compliant with the overriding safety principles the key requirements for a buffer material in the case of high level nuclear waste disposal independently of the host rock are: (1) a low hydraulic permeability/conductivity; (2) a self-sealing ability; and (3) durability of properties in the very long-term.

1.1.1 Specific Nagra required properties – safety functions

The required properties for bentonite buffer specific to the Nagra context (*cf.* Tab. 1-1) have been defined and described in more details in Leupin & Johnson (2014).

The attenuation of radionuclide release from the repository system is strongly dominated by sorption and diffusive transport in the clay-rich rock, which is much thicker than the bentonite engineered barrier. As a result, in a scenario in which diffusion dominates transport in the host rock, bentonite makes a limited contribution to retarding radionuclide transport, but nonetheless provides redundancy and a suitable chemical (low microbial activity) and hydromechanical (isotropic loads on the canister) environment.

Bentonite plays a particularly important role in alternative scenarios or assessment cases. These assessment cases are based on what-if cases that investigate the robustness of the disposal system (Nagra 2002), such as i) unintentional borehole intrusion of the near-field and ii) occurrence of hydraulically transmissive discontinuities intersecting the emplacement tunnels. Both cases incorporate the assumption that the emplacement tunnels, including the bentonite, have low hydraulic conductivity. This attribute contributes to ensuring low dose consequences. As a result, the most important requirement in relation to long-term safety assessment is to maintain overall low hydraulic conductivity in the waste emplacement tunnels. This requires also that all voids are filled by swelling clay, i.e. some swelling pressure must be provided by the bentonite.

In order to achieve the two safety functions (i.e. low hydraulic permeability and self-sealing ability), safety-relevant attributes are defined. The safety-relevant attributes of the buffer include those that contribute to the safety functions of other barriers or those that directly involve the safety functions of the buffer itself.

Low hydraulic conductivity

This requirement supports the buffer safety function "attenuate releases". The hydraulic parameters of the saturated buffer should prevent advective flow through the buffer and therefore result in an effective transport barrier. Possible cracks in the buffer should close due to self-sealing.

Chemical retention of radionuclides

This requirement supports the buffer safety function "attenuate releases" by retarding transport of radionuclides from the buffer.

Sufficient density

This requirement supports the buffer safety function "attenuate releases" by ensuring that the density of the buffer will be high enough that the resulting microporous structure provides an effective barrier for colloid transport.

Sufficient swelling pressure

This requirement supports the rock safety function "attenuate releases". Emplacement tunnels in the Opalinus Clay may be supported with rock bolts and liner. In either case the lifetime of the support is designed to provide stable conditions during construction and operation (up to several years). After waste and buffer emplacement there may be interactions of the support system with other system components (host rock, buffer, canister, waste form). These interactions should not be detrimental to the safety of the system. The support will eventually fail due to corrosion and deformation and allow additional time-dependent deformations of the near-field host rock and compaction of the buffer. The maximum convergence induced compaction of the buffer, which is controlled by the stress field and the mechanical properties of host rock and swelling pressure of the buffer material, should be limited to avoid significant extension of the excavated damage zone (EDZ) of the host rock. Limited convergence will also enhance the self-sealing capacity of Opalinus Clay in the EDZ. The consequences of such an extension may include significant increases in permeability of the EDZ that are difficult to evaluate quantitatively. In addition, a too high swelling pressure could also initiate fracturing of the rock. Furthermore, an adequate swelling pressure will prevent canister sinking. The canister should be placed in a way that its distance to the tunnel wall is constant and so that it is encased by a thick layer of buffer material to avoid hydraulic short-cuts to the EDZ of the tunnels. Having sufficient swelling pressure also supports the buffer safety function "protect the canister" (Leupin & Johnson 2014). The rheology of the buffer material (viscous material behaviour) should keep deviant stresses and stress inhomogeneity as low as possible to protect the canisters (e.g. avoid point loading of canister). Potential larger deformations of the host rock resulting from tectonic events (e.g. earthquakes) should be attenuated.

Sufficient gas transport capacity

This requirement supports the buffer safety function "attenuate releases". The buffer should transport corrosion gases without significant reduction of its function as a hydraulic barrier.

Tab. 1-1: Compilation of attributes for the buffer material around the canister for the different repository design and concepts.

Safety-relevant attributes	**Favours/contributes to ...**	**Preferred values for Nagra**	**Favours/contributes to ...**	**Preferred values for SKB**	**Preferred values for Posiva**
Low hydraulic conductivity	Attenuation safety function of buffer, by ensuring diffusive transport	$K < 10^{-11}$ m s^{-1} for buffer around canister	Limit advective transport	$< 10^{-12}$ m s^{-1}	$10^{-11} – 10^{-12}$ m s^{-1}
Chemical retention of radionuclides	Attenuation safety function of buffer, by retarding transportfrom the buffer	No quantitative criterion [1], strong sorption is favoured	-	No requirement	No requirement
Sufficient density	Attenuation safety function of buffer, by preventing colloid transport	$\rho_s > 1.650$ Mg m^{-3} [2]	Attenuation safety function Damp shear movement	$\rho_d > 1'000$ kg m^3	2'050 kg m^{-3} (for a saturated buffer)
Sufficient swelling pressure (P_s)	Attenuation safety function of rock, by providing mechanical stabilisation of rooms, and hence avoiding significant extension of EDZ	0.2 MPa $< P_s <$ minimum principal stress	Attenuation safety function of rock, by providing mechanical stabilisation of rooms	1 MPa $\leq P_s \leq$ 15 MPa	5 MPa $\leq P_s \leq$ 15 MPa
Mechanical support	Safety function of canister, by ensuring it is surrounded by a protective layer of buffer (stress buffering)	Buffer must be sufficiently viscous to avoid canister sinking [1]	Safety function to prevent canister sinking by a protective layer of buffer (stress buffering)	$P_s > 0.1$ MPa	$P_s > 0.1$ MPa
Sufficient gas transport capacity	Attenuation safety function of buffer, by ensuring gas can migrate without compromising hydraulic barrier	No quantitative criterion [1], less than the minimum principal stress	-	"Sufficient"	-
Minimise microbial corrosion	Safety function of canister, by ensuring conditions favorable to slow corrosion	No quantitative criterion but higher densities are prefered to limit microbial activity [1]	Safety function of canister, by ensuring conditions favorable to slow corrosion	No quantitative criterion at this stage, but higher densities are prefered to limit microbial activity	No quantitative criterion but higher densities are prefered to limit microbial activity [1]

Tab. 1-1: (continued)

Safety-relevant attributes	Favours/contributes to ...	Preferred values for Nagra	Favours/contributes to ...	Preferred values for SKB	Preferred values for Posiva
Resistance to mineral transformation	Longevity of other safety-relevant attributes of buffer	No quantitative criterion [1]	Longevity of other safety-relevant attributes of buffer	T max ≤ 100 °C	Non quantitative criterion but limit pyrit content of the bentonite
Mechanical support	Safety function of canister, by providing stress buffering	Not a required property	No quantitative requirement for stress buffering. Canister must be designed to handle variations in swelling pressure	-	-
Suitable heat conduction (T_c)	Safety function of canister, by ensuring favorable maximum temperature conditions	$0.4 < T_c < 2$ W m^{-1} K^{-1} (for a specific thermal heat load of 1'500 W)	Safety function of canister, by ensuring favorable maximum temperature conditions	T max ≤ 100 °C	T max ≤ 100 °C
	Safety functions of buffer and rock, by ensuring favorable maximum temperature conditions	$0.4 < T_c < 2$ W m^{-1} K^{-1} (for a specific thermal heat load of 1'500 W)	Safety functions of buffer and rock, by ensuring favorable maximum temperature conditions	T max ≤ 100 °C	T max ≤ 100 °C

[1] Where no quantitative criterion is indicated, the impacts on safety of the process must nonetheless be evaluated.

[2] ρ_s values are indicative assuming MX-80 is the selected buffer material and are given as saturated densities.

Minimise microbial corrosion

This requirement supports the buffer safety function "protect the canister". Studies of the reduction of sulphate to sulphide in bentonite indicate that the rate decreases as saturated density increases. Based on an extensive literature review and result of on-going studies a value for a saturated density may be defined in order to minimise the viability of microorganisms in the bentonite (Stroes-Gascoyne 2011).

Resist transformation

This requirement supports the buffer safety functions "attenuate releases" and "protect the canister". Mineralogical interactions occurring over time due to elevated temperatures and chemical interactions with other components of the disposal system should not lead to significant alteration and /or loss of the buffer functions.

Suitable thermal conductivity

This requirement supports the buffer safety functions "attenuate releases" and "protect the canister". The buffer should conduct heat sufficiently well that the waste form, canister and buffer do not experience conditions detrimental to the performance of their safety functions.

1.1.2 Specific SKB and Posiva required properties – safety functions

Due to large similarities in Posiva's and SKB's concepts the required properties are very similar and will be presented together. For clarification the terminology differs between the countries and in Posiva's reports and terminology the term safety function has a different meaning than in SKB's. Posiva's term performance target corresponds to SKB's safety function.

Limit advective transport in the near-field

An important safety function (performance target in Posiva's terminology) of the buffer is to limit transport of dissolved canister corroding agents to the canister and potential radionuclide releases from the canister. The material of the buffer surrounding the canister has been chosen so as to prevent advective transport in near-field. A guideline is the hydraulic conductivity of the saturated buffer which should be sufficiently low to ensure that diffusion is the dominant transport mechanism. Depending on the concept and boundary conditions a hydraulic conductivity of 10^{-11} – 10^{-12} m/s is required to fulfil this safety function.

The buffer homogeneity is ensured partially by the fact that the buffer is made of a clay material that swells when water-saturated. A swelling pressure criterion is therefore formulated. The safety function is usually considered to be upheld if the swelling pressure is in the range of 100 kPa – 1 MPa. The swelling pressure also ensures a self-sealing capacity of the buffer.

Reduce microbial activity

The sulphide production by sulphate-reducing bacteria present initially in the buffer, in the host rock or introduced during the realisation of the near-field is, in the long-term, normally bounded to insignificant levels by their reliance on nutrients present in the groundwater. In certain transient situations, the access to nutrients could be significant, e.g. due to degradation of construction materials, stray materials in the repository, cement additives (such as super-

plastizicers), organic components present in the pore water of sedimentary host rock or even hydrogen gas produced by the anaerobic corrosion of the steel components. In such cases, the buffer has the function of reducing the activity of initially present or introduced microbes.

The microbial activity can be limited by increasing swelling pressure, which can be achieved by increasing material density. The quantitative treatment of a situation of this type would, however, depend on a number of factors, meaning that while the buffer density or swelling pressure are useful indicators for this buffer function, a strict criterion on buffer density cannot be formulated.

Damp rock shear movements

Another safety function or performance target of the buffer is to protect the canister from rock movements, in particular from the consequences of rock shear movements caused by earthquakes. The plasticity of the bentonite enables the buffer to significantly mitigate shear. This is basically only relevant for a crystalline host rock and is dependent on a number of factors: mainly the properties of the canister materials and canister design, the buffer thickness, and the expected shear movements at the given site. An increased buffer density and swelling pressure reduces the plasticity. In the Swedish case, for a maximum shear movement of 50 mm a design premise of a maximum installed density of 2'050 kg/m^3 (for a saturated buffer) has to be established.

Resist transformations (requirement on temperature)

To avoid transformation of the montmorillonite component in the buffer to non-expandable minerals a safety function or performance target for temperature can be defined. However, as the heat generation from the waste decreases relatively rapidly with time and montmorillonite alteration is a slow process any temperature criteria will always be somewhat artificial. Still, for repositories in crystalline host rock (e.g. Sweden, Finland) a temperature limit of 100 °C in order to limit chemical alterations should be achieved, while in clay environments higher temperatures can be justified, as the host rock itself is the primary barrier.

Prevent canister sinking

The swelling pressure should be sufficiently high to prevent the canister from sinking through the supporting bentonite layers thus to avoid any direct contact with the host rock (or the concrete bottom plate in the deposition hole) and any short-circuiting of the buffer.

The main determinant of the creep rate and the resulting canister sinking is the magnitude of the mobilised shear strength (shear stress divided by shear strength), which results in an increased canister sinking. The shear strength decreases with decreasing swelling pressure. Analyses of canister sinking in a deposition hole for a range of buffer densities and hence swelling pressures indicate that the total sinking will be less than 2 cm for swelling pressures down to 0.1 MPa.

Limit pressure on canister and rock

The maximum swelling pressure from the bentonite buffer must be limited in order to avoid mechanical damage of the canister and the surrounding host rock. The allowed pressure is dependent on the properties of those barriers. The swelling pressure of bentonite is generally not expected to increase as the repository evolves with time, which means that the initial condition

is the key feature. This puts strict requirements on the manufacturing and installation process, as the swelling pressure is exponentially dependent on the density. This means that a small deviation in the mass of the installed buffer may lead to a large increase in swelling pressure.

In the Swedish and Finnish case, the design premise isostatic load on the canister has been determined under the assumption that the buffer swelling pressure will not exceed 15 MPa. If the buffer freezes, development of damaging pressures due to expanding water cannot be ruled out. Therefore, the buffer temperature should not fall below the freezing temperature of a water-saturated buffer. This process is only relevant for repositories in areas where severe permafrost is expected in the future. The freezing point of bentonite is related to the swelling pressure (discussed later in this document). The swelling pressure of the buffer should therefore be sufficient to ensure that freezing never occurs. A swelling pressure of 5 MPa would yield a freezing point of ~ -4 °C, which is below the lowest temperature expected at the selected repository sites in Sweden and Finland, even for a very pessimistic assumption about the evolution of the future climate.

Other requirements

The content of canister corroding agents in the buffer should be low. Apart from unavoidable initial amounts of oxygen, the pyrite content could pose a long-term problem, as pyrite, if not oxidised by initially present or intruding oxygen, will release sulphide, a canister corroding agent. There is, however, no absolute criterion placed on this amount. However, Posiva has defined concentration limits for total sulphur and organic content, but these limits are currently being revised.

1.2 SF/HLW repository expected evolution and repository conditions in Opalinus Clay

In the following sections a brief overview is given of the expected evolution of conditions in a HLW repository in Opalinus Clay.

Nagra's repository concept

The repository concept in Opalinus Clay envisions an array of long (~ 800 m) parallel tunnels at a depth of 600 to 900 m containing SF or HLW canisters, with the region around the canisters filled with bentonite, as shown in Fig. 1-1a (Nagra 2014). The canisters would be constructed from thick-walled (12 – 14 cm) carbon steel (an alternative is copper-coated steel). The bentonite backfill is a combination of blocks beneath the canister and granular bentonite and has a reference saturated density of about 1.9 Mg/m^3. Because of the low hydraulic conductivity of the Opalinus Clay, the transport conditions after saturation of the backfill are diffusion controlled. For tunnel support, a low-pH shotcrete liner would be used, with a hydraulic seal placed between every tenth canister (Nagra 2010). The hydraulic seal would comprise bentonite of higher density than that used around the disposal canisters, constructed using a combination of blocks and pellets. In the seal zone, steel ribs would be used for support rather than a shotcrete liner. The purpose of eliminating the liner in the hydraulic seal zone is to prevent any possibility of continuous hydraulic flow through the more permeable liner, as indicated in Fig. 1-1b.

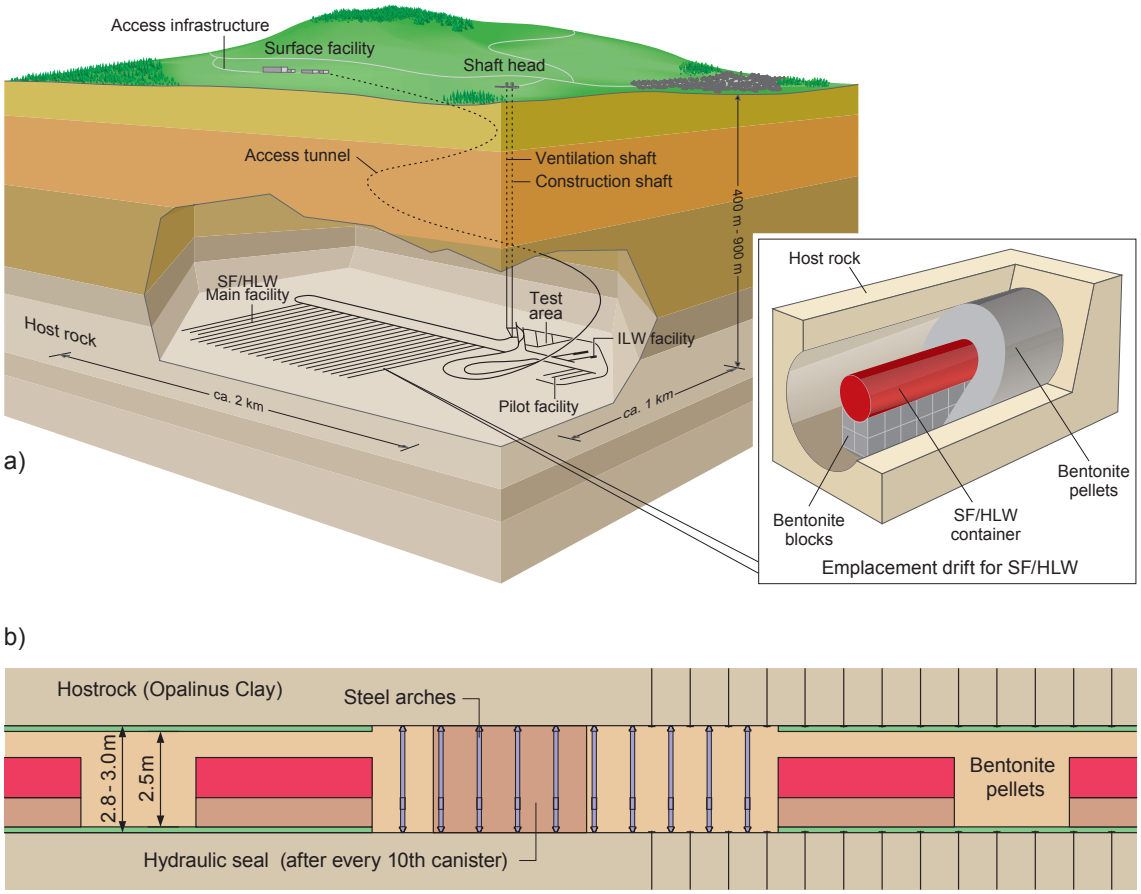

Fig. 1-1: Nagra disposal concept for SF and HLW: (a) repository layout and detail of EBS; (b) longitudinal section of emplacement tunnel showing liner and hydraulic seal.

The pre-excavation phase

The undisturbed in situ conditions of the host rock domain, geosphere and biosphere will be investigated in an extensive field campaign prior to the start of the excavation of the ramp / shafts. For the Opalinus Clay much of the understanding already exists based on studies summarized in Entsorgungsnachweis (Nagra 2002) and through ongoing field investigations and studies at the URL of Mont Terri.

Safety-relevant parameters of the undisturbed system provide a baseline for evaluating all host rock and coupled host rock/near-field processes.

During the construction of the ramp and shafts, rock parameters are continuously collected to update safety analysis models. Host rock properties are finally assessed in the underground rock laboratory. This facility allows for an extensive experimental program and for a final set of host rock parameters. The underground laboratory is also used to study aspects such as excavation damage, tunnel support techniques and interaction of backfills with the host rock.

A pilot facility is excavated and instrumented and waste canisters are emplaced followed by backfilling. Instrumentation of the pilot facility allows monitoring the evolution of the repository analogue after backfilling and sealing of the emplacement rooms.

The excavation & waste emplacement phase

The excavation phase starts with the excavation of the access to the HLW repository and is followed by the construction of operations tunnels. Waste emplacement tunnels are then constructed, including installation of the necessary tunnel support measures. Each tunnel remains open for only a short period of time until waste emplacement and backfilling occurs. A continuing sequence of excavation, waste emplacement and backfilling occurs so that a limited number of emplacement tunnels are open at any given time. This phase is characterized by excavation-related perturbations such as formation of an EDZ, desiccation of the surface region of the EDZ and cooling of the rock as a result of ventilation, the creation of a high hydraulic gradient, potential import of bacteria, oxidation of exposed minerals, mineral precipitation within the open pore space and initiation of corrosion and alteration of materials used for tunnel support etc.

The excavation phase is important with regard to long-term safety as several safety-relevant parameters are defined or can be modified during excavation, operation, placement of the waste and backfilling operations, although these changes to the host rock are restricted within a few meters of the excavation.

The thorough baseline characterization – description of the initial state of the host rock- is instrumental for understanding the evolution of safety relevant parameters and processes during the observation phase. Important aspects include:

- During excavation, breakouts and EDZ formation must be minimized in order to limit damage of the host rock.
- Tunnel support must limit further EDZ formation but should comply with long-term safety principles.
- The bentonite buffer must have a density high enough to generate a sufficient swelling pressure thus contributing to EDZ self-sealing under fully saturated conditions, ensure low hydraulic conductivity, provide sufficient sorption capacity for nuclide retention upon canister breaching and a low enough swelling pressure that gas generated by canister corrosion can migrate through the buffer.
- Seals and plugs must comply with the hydraulic requirements.

The process of waste emplacement begins with the emplacement of the first canister together with its bentonite pedestal. The granular bentonite backfill material (water content about 5 %) is emplaced around the canister. The steps are repeated. If a shotcrete liner has been installed, intermediate seals are installed between every tenth canister and the emplacement of canisters, backfilling and sealing continues until the tunnel is filled. A bentonite based sealing system is placed at the entrance to the tunnel.

The resaturation phase (0 to 100 years after emplacement)

For high level waste canisters the initial heat output is limited to 1'500 W which will result in a temperature at the canister interface with the backfill of about 130 °C within about ten years (Senger & Ewing 2008). The temperature of the rock at the tunnel boundary will reach its maximum (about 70 °C) after about 50 years. The bentonite backfill will become saturated within about 50 to 100 years, although pore water pressure within the backfill will be low. Heat transport to the far-field rock will increase the temperature to the maximum value of ~ 50 – 55 °C at a distance of 20 m above the tunnels. The pore water pressure in the rock within about

20 m of the tunnels will increase to its maximum of several MPa above the initial host rock value after 100 years as a result of the thermal expansion of pore water and rock and the low hydraulic conductivity.

Gas generation through corrosion of the steel used in tunnel support and of the canisters will begin, although most of the gas produced in the first hundred years will dissolve.

As defined here, this phase ends with the close-to-full saturation of the buffer. By then, all construction and operation tunnels are backfilled and sealed. During this phase the access ramp and shafts are kept open. The resaturation phase largely coincides with the observation phase of the pilot repository, which is thoroughly characterized to identify any deviation from the expected evolution. Only the pilot repository will be monitored.

After complete saturation of the near-field (100 to 1'000 years after emplacement)

Between 100 and 1'000 years, the canister surface temperature will decline from 80 °C to 60 °C. By about 1'000 years, the near-field rock temperature will also decline to about 60 °C. Pore water pressure will reach its maximum in the near-field of about 5 MPa above the initial formation pressure as a result of the coupled effects of gas generation (dominated by corrosion of tunnel support materials) and thermal expansion. In the far field (20 m from tunnels and beyond), pore water pressure will begin to decline and in the confining units an insignificant increase in pore pressure will have occurred. Anaerobic corrosion of the canister and steel material used for tunnel support will continue.

The end of the thermal period (1'000 to 10'000 years after emplacement)

Temperatures in the near-field will decline from about 60 °C to about 50 °C from 1'000 to 10'000 years and in the far-field rock will decrease to 10 °C above ambient rock values. Corrosion of steel materials used for tunnel support will cease after a few thousand years, although gas generation from the thick-walled disposal canisters will continue. The gas production rate is thus reduced and pore water pressure falls by several MPa in the near- and far-field rock due the combined thermal and gas production effects (both reduced).

Some compaction of the bentonite around the canister occurs and as the adjacent rock reconsolidates. The EDZ is expected to be largely self-sealed, although increased gas pressures may keep pathways open.

The cementitious liner will eventually degrade due to the resaturation with pore water and precipitates might clog pores at the interface with Opalinus Clay and bentonite. A high pH plume is expected to affect a few centimetres of the host rock and bentonite (Savage 2014).

Corrosion of the canister has produced mobile iron species that migrate through the bentonite and form iron rich clay minerals or Fe(II) precipitates around the canisters.

Canister breaching and radionuclide transport period (10'000 years and beyond)

Beyond 10'000 years, the temperatures will decline gradually from 50 °C back to ambient rock values. Though some of the canisters are now expected to be locally breached, corrosion and gas production will continue for tens of thousands of years. As a result hydrogen will continuously be transported through the backfill into the host rock and mobile (Fe(II)) will be diffusing into the bentonite. The pore water pressure in the rock will increase again in the near- and far-field slightly as the canister corrosion continues, until corrosion is complete after about 60'000 years.

Pore water will contact the waste matrix and radionuclides will diffuse through saturated buffer and into the host rock. Depending on the chemical forms and half-lives of the radionuclides, the transport distances into the rock will vary. Safety analysis calculations show that negatively charged non-sorbing long-lived nuclides (such as ^{129}I, ^{36}Cl and ^{79}Se) might migrate as far as the biosphere after several hundred thousand years.

Evolution of the pore water

Once the carbon steel canisters containing the high level waste or spent fuel have been emplaced, and the tunnels backfilled and sealed, re-saturation of the initially "dry" compacted bentonite with the pore water from the Opalinus Clay (see Tab. 1-2) formation will occur, and the components within the near-field system and the adjacent host rock, will begin to interact with one another and evolve over many hundreds of thousands of years. Opalinus Clay and bentonite pore waters (see Tab. 1-2 and 1-3) are chemically speaking very similar and consequently no negative consequences are expected through their interactions with one another.

Tab. 1-2: "Initial state" Opalinus Clay pore water chemistry.

Concentrations are given in mol L^{-1} (adapted from Bradbury et al. 2014 and originally in Mäder 2009). Saturated solids for Opalinus Clay: calcite, dolomite (ordered), quartz, siderite and pyrite.

	Opalinus Clay "initial state"
Temperature [°C]	25
pH log pCO_2 [bar] Ionic strength [mol kg^{-1}] pe Eh [mV]	7.203 -2.20 0.2299 -2.781
Dissolved constituents	
Na	1.644×10^{-1}
K	2.604×10^{-3}
Mg	9.625×10^{-3}
Ca	1.251×10^{-2}
Sr	2.106×10^{-4}
Ba	--
Al	--
Fe^{II}	5.24×10^{-5}
Fe^{III}	3.31×10^{-9}
Si	1.779×10^{-4}
Cl	1.600×10^{-1}
S^{IV}	2.472×10^{-2}
S^{-II}	1.24×10^{-8}
C^{IV}	2.506×10^{-3}

Tab. 1-3: Bentonite pore water (adapted from Bradbury et al. 2014) composition for 36 % bulk porosity obtained with the novel approach ("New model").

	"New model"
Bulk and anion accessible porosity	
ε_{bulk}	0.36
ε_{anion}	0.05
pH, ionic strength, redox potential, CO_2 partial pressure	
pH	7.75
I [m]	0.374
Eh[V]	-0.198
pE	-3.35
log pCO_2 [bar]	(-3.17) [1]
Dissolved constituents	
[Na]	3.07×10^{-1}
[Ca]	1.33×10^{-2}
[Sr]	1.14×10^{-4}
[Mg]	9.62×10^{-3}
[K]	1.54×10^{-3}
[Fe]	5.33×10^{-5}
[Al]	2.11×10^{-8}
$[C]_{inorg}$	9.20×10^{-4}
[S]	6.88×10^{-2}
[Cl]	2.17×10^{-1}
[Si]	1.82×10^{-4}

[1] In this calculation the pCO_2 was unconstrained. The reported value is the hypothetical pCO_2 a gas phase should have to be in equilibrium with this solution composition. In the other calculations, the pCO_2 was imposed as a constraint (Bradbury et al. 2014).

1.3 SF/HLW repository reference evolution and repository conditions in crystalline rock

The presentation of the analysis of the base case of the reference evolution in SR-Site (SKB 2011) is divided into four time frames:

- the excavation/operational period
- the first 1'000 years after repository closure and the initial period of temperate domain from the reference glacial cycle
- the remaining part of the glacial cycle
- subsequent glacial cycles up to one million years after repository closure

The purpose of the analysis of a reference evolution is to gain an understanding of the overall evolution of the system for the scenario selection and scenario analyses that follow later in the assessment. The ambition is to assess the impacts of processes affecting the containment safety functions and to describe a reasonable evolution of the repository system over time. The reasonable evolution is an important basis for the definition of a main scenario. Focus is on the containment capacity; consequences in terms of radionuclide releases are not analysed.

The EBS in the KBS-3 concept consists of the canister and the buffer, which are the key barriers, but there are also deposition tunnel backfill, the plugs, the backfill in the other repository areas, the bottom plate in the deposition hole and the seals in the investigation boreholes. The performance of all these components is assessed in SR-Site. However, in this document the focus will stay on the buffer.

Methodology

A thorough understanding and handling of the processes occurring over time in the repository system is a fundamental basis for the safety assessment. The basic sources of information for this are the results of decades of R&D efforts by SKB and other organisations. In a broader sense, these are based on the knowledge accumulated over centuries of scientific and technological development. The R&D efforts have led to the identification and understanding of a number of processes occurring in the engineered barriers and the natural systems relevant to long-term safety. For the purpose of the safety assessment, the relevant process knowledge for the engineered barriers and the host rock is compiled in a number of process reports which also, for each process, contain a prescription for its handling in the safety assessment.

To summarise the handling of processes in the safety assessment, a table showing the handling of each process has been produced, based on the handling documented in the process reports. The description is broken down in different time frames where relevant. Tab. 1-4 shows the prescribed handling of the buffer processes for the SR-Site.

Tab. 1-4: Process table for the buffer describing how buffer processes are handled in different time frames and for the special case of an earthquake for the SR-Site.

Green fields denote processes that are neglected or not relevant for the period of interest. Red fields denote processes that are quantified by modelling in the safety assessment. Orange fields denote processes that are neglected subject to a specified condition.

	Resaturation/ "thermal" period	**Long-term after saturation and "thermal" period**	**Earthquakes**
Intact canister			
Radiation attenuation/ heat generation	Neglected since dose rate is too low to be of importance for the buffer	Neglected since dose rate is too low to be of importance for the buffer	Not relevant
Heat transport	Thermal model	Thermal model	Not relevant
Freezing	Neglected, since this requires permafrost conditions	Neglected if buffer temperature > -4 °C; otherwise bounding consequence calculation	Not relevant
Water uptake and transport for unsaturated conditions	Buffer & backfill THM model	Not relevant by definition	Not relevant
Water transport for saturated conditions	Neglected under unsaturated conditions; for saturated conditions the treatment is the same as for "Long-term"	Neglected if hydraulic conductivity $< 10^{-12}$ m s^{-1} since diffusion would then dominate	See process "Liquefaction"
Gas transport/dissolution	Through dissolution	(Through dissolution) No gas phase is assumed to be present	(Through dissolution) No gas phase is assumed to be present
Piping/erosion	Quantitative estimate with an empirical model	Not relevant	Not relevant
Swelling/mass redistribution	Buffer & backfill THM modelling including interaction buffer/backfill and thermal expansion	Integrated evaluation of erosion, convergence, corrosion products, creep, swelling pressure changes due to ion exchange and salinity, canister sinking	Part of integrated assessment of buffer/canister/ rock

Tab. 1-4: (continued)

	Resaturation/ "thermal" period	**Long-term after saturation and "thermal" period**	**Earthquakes**
Intact canister			
Liquefaction	Not relevant	Neglected since liquefaction from a short pulse cannot occur in a high-density bentonite, due to high effective stresses	Neglected since liquefaction from a short pulse cannot occur in a high-density bentonite, due to high effective stresses
Advective transport of species	Simplified assumptions of mass transport of dissolved species during saturation	Neglected if hydraulic conductivity $< 10^{-12}$ m s^{-1}	See process "Liquefaction"
Diffusive transport of species	Chemistry model (thermal, saturated phase; unsaturated phase disregarded)	Chemistry model	Not specifically treated
Sorption (including ion-exchange)	Chemistry model (thermal, saturated phase; unsaturated phase disregarded)	Chemistry model	Not specifically treated
Alterations of impurities	Chemistry model (thermal, saturated phase; unsaturated phase disregarded)	Chemistry model	Not specifically treated
Aqueous speciation and reactions	Chemistry model (thermal, saturated phase; unsaturated phase disregarded)	Chemistry model	Not specifically treated
Osmosis	Evaluation through comparison with empirical data	Evaluation through comparison with empirical data	Not specifically treated

Tab. 1-4: (continued)

	Resaturation/ "thermal" period	**Long-term after saturation and "thermal" period**	**Earthquakes**
Intact canister			
Montmorillonite transformation	Model calculations (thermal, saturated phase; unsaturated phase disregarded)	Estimate based on evidence from nature	Part of integrated assessment of buffer/canister/ rock
Iron-bentonite interaction	Neglected since no iron will be in contact with the bentonite	Only considered for failed canister. Possible loss of buffer efficiency	Only considered for failed canister. Possible loss of buffer efficiency
Montmorillonite colloid release	Neglected if total cation charge is > 4 mM, otherwise modelled	Neglected if total cation charge is > 4 mM, otherwise modelled	Not specifically treated
Radiation-induced transformations	Neglected since dose rate outside canister is too low to have any effect	Neglected since dose rate outside canister is too low to have any effect	Neglected since dose rate outside canister is too low to have any effect
Radiolysis of pore water	Neglected since dose rate outside canister is too low to have any effect	Neglected since dose rate outside canister is too low to have any effect	Neglected since dose rate outside canister is too low to have any effect
Microbial processes	Neglected under unsaturated conditions, since the extent of aqueous reactions is limited; for saturated conditions the treatment is the same as for "Long-term"	Quantitative estimate of sulphate reduction, limited by supply of microbe nutrients in groundwater	Not specifically treated
Cementation	Discussed together with Process "Montmorillonite transformation"	Discussed together with Process "Montmorillonite transformation"	Part of integrated assessment of buffer/canister/ rock

Tab. 1-4: (continued)

	Resaturation/ "thermal" period	**Long-term after saturation and "thermal" period**	**Earthquakes**
Failed canister			
Failed canister Gas transport/dissolution	*(no failures are expected this period)*	Quantitative estimate based on empirical data	Quantitative estimate based on empirical data
Failed canister Radiation-induced transformations	Neglected since dose rate outside canister is too low to have any effect	The effect of α-radiation from nuclides from a failed canister is estimated	The effect of α-radiation from nuclides from a failed canister is estimated
Colloid transport	Neglected if density at saturation > 1'650 kg m^{-3}, otherwise bounding calculation *(no failures are expected in this period)*	Neglected if density at saturation > 1'650 kg m^{-3}, otherwise bounding calculation	Neglected if density at saturation > 1'650 kg m^{-3}, otherwise bounding calculation
Speciation of radionuclides	*(no failures are expected in this period)*	Assumptions based on empirical data	Assumptions based on empirical data
Transport of radionuclides in water phase	*(no failures are expected in this period)*	Radionuclide transport code: COMP23	Radionuclide transport code: COMP23 Reduced diffusion path
Transport of radionuclides by a gas phase	*(no failures are expected in this period)*	Quantitative estimate	Quantitative estimate

Assessment of the buffer evolution during the excavation/operational period and the first 1'000 years after repository closure and the initial period of temperate domain from the reference glacial cycle

The processes in the buffer that need to be assessed during the early evolution of the repository are identified in Tab. 1-4. These are:

1. Heat transport
2. Water uptake and transport for unsaturated conditions
3. Piping/erosion
4. Swelling/mass redistribution
5. Advective transport of species
6. Diffusive transport of species
7. Sorption (including ion-exchange)
8. Alterations of impurities
9. Aqueous speciation and reactions
10. Osmosis
11. Montmorillonite transformation
12. Cementation

The processes are treated in different modelling activities. The focus of the treatment is to evaluate how the processes can affect the safety function, either directly or indirectly.

Thermal evolution of the near-field

The heat transport in the buffer is included in the integrated assessment of the thermal evolution in the near-field. The thermal evolution of the near-field is of importance as general input information to the mechanical, chemical and hydrological processes. The direct safety-relevant thermal criterion concerns the buffer peak temperature, the safety function that requires that this temperature does not exceed 100 °C, chosen pessimistically in order to avoid, with a margin of safety, mineral transformations of the buffer.

An estimate of the distribution of peak buffer temperatures in both *dry and wet* deposition holes can be made by use of an analytical solution. In dry deposition holes the maximum buffer temperature is found at the top of the canister where the bentonite is in direct contact with the copper surface (cf. Fig. 1-2, left). Note, that the hottest point on the canister surface is located at canister mid-height. In wet deposition holes, the air-filled gap between the canister and bentonite blocks will be closed at the time of the peak temperature, and the bentonite will also be in direct thermal contact with the copper shell at points on the vertical canister surface. In this case the maximum buffer temperature will coincide with the hottest point on the canister surface, i.e. at mid-height (cf. Fig. 1-2, right).

Fig. 1-3 shows the peak temperature distribution using the canister spacing in the layout. There are two cases: with and without the temperature correction above. Without the correction there are temperature over- and underestimates for canisters associated with the low- and high conductivity parts of the distributions, respectively.

On average, less than one canister position, out of 6'000 canister positions, would have a peak buffer temperature larger than 95 °C meaning that the design requirement and the safety function Buff4 would be satisfied with a margin of 5 °C, based on this analysis.

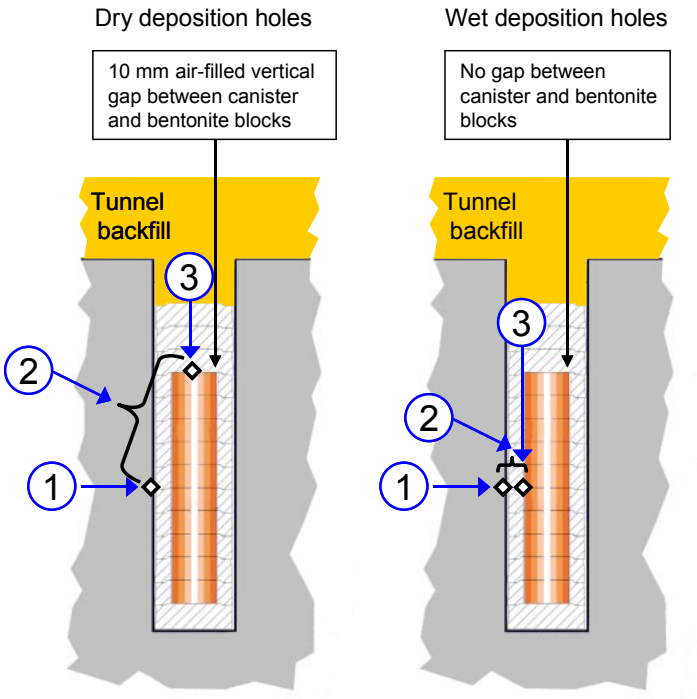

Fig. 1-2: Rock wall temperature (1), temperature drop across bentonite (2), maximum bentonite temperature (3) located at the top of the canister in dry deposition holes (left) and at canister mid-height in wet deposition holes (right).

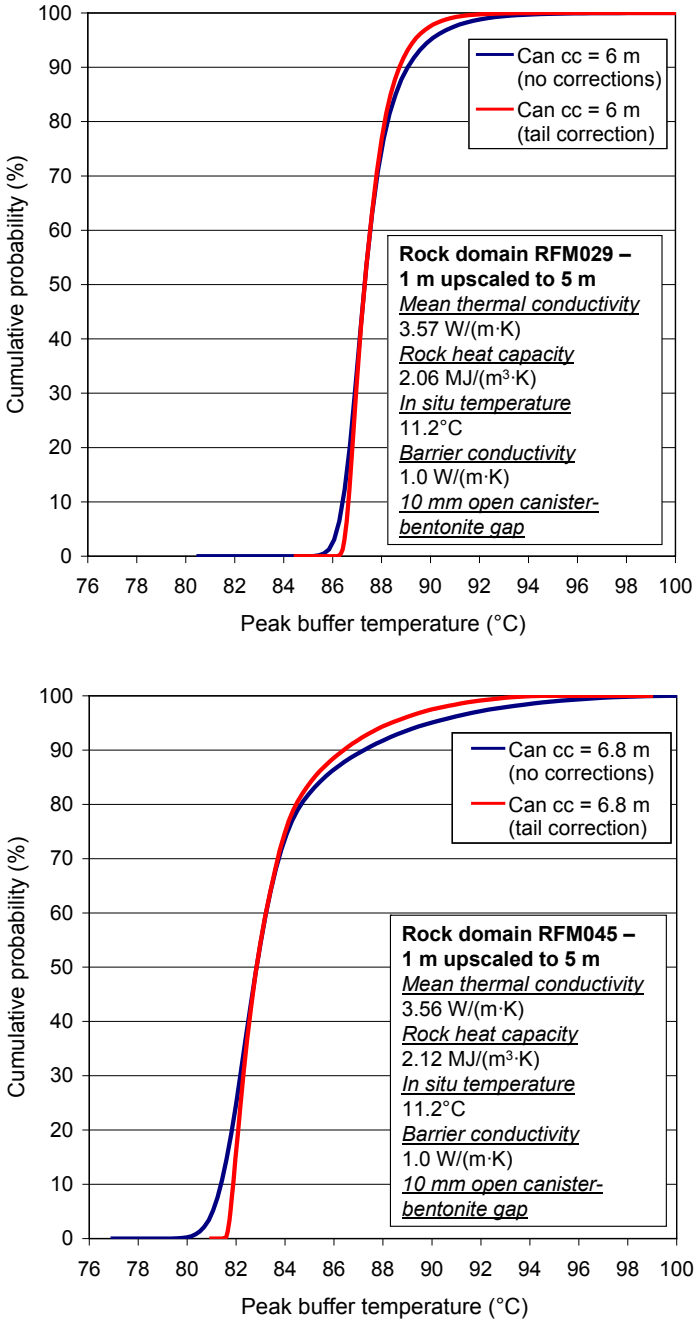

Fig. 1-3: Distribution of buffer peak temperature in two different rock domains in the Forsmark site (rock domains RFM029 above and RFM045 below), with and without correction for spatial variability.

Saturation of buffer

The process "Water uptake and transport for unsaturated conditions" is treated in the modelling of the saturation of the buffer.

The safety functions for the buffer assume a fully water-saturated state. This should mean that the buffer needs to be saturated to perform properly. However, no performance is needed from the buffer as long as the deposition hole is unsaturated, since no mass-transfer in an aqueous phase between the canister and the groundwater in the rock can take place in the unsaturated stage. The water saturation process itself has therefore no direct impact on the safety functions of the buffer and backfill. It is still important to understand the water saturation process since it defines the state of the barriers in the early evolution of the repository.

Piping/erosion

The piping process may occur in the very early evolution of the repository when strong hydraulic gradients are present. As long as the buffer and the backfill have not developed a sufficient swelling pressure there is a potential for piping and associated erosion effects in these components. Piping may lead to erosion of bentonite. Erosion is a redistribution of material within the repository. This may lead to a lowered density in certain parts of the buffer and backfill and will affect the safety functions related to buffer and backfill density.

Swelling and swelling pressure

Swelling and mass distribution in the buffer is also important after the saturation process is completed. The primary purpose of the buffer is to ensure that transport of species from the rock to the canister and from the canister to the rock is dominated by diffusion. The swelling pressure in the bentonite is expected to seal all gaps and ensures that there is a tight contact between the rock and the buffer. Therefore, it is important that the swelling pressure is maintained. The safety function indicator criterion for ensuring tightness in the buffer is a swelling pressure of 1 MPa. A high swelling pressure is needed for reducing microbial activity. The required swelling pressure for preventing canister sinking is 0.2 MPa. On the other hand, the swelling pressure must not be higher than 15 MPa in order to limit the pressure on canister and rock.

In order to verify that the intended conditions after swelling will be achieved, it is, necessary to assess more carefully the swelling process with focus on:

- buffer homogenisation
- buffer upward expansion
- movement of the canister in the deposition hole
- homogenisation after loss of bentonite mass

Buffer homogenisation

The initial state of the buffer after emplacement are unsaturated bentonite blocks and rings with much higher density than the average density for the entire hole and one empty slot at the canister surface as well as a pellet-filled slot with very low density at the rock surface. Due mainly to friction within the material, but also due to hysteresis effects, the swelling and homogenisation that comes with the wetting of the bentonite are not complete and there will remain density differences and swelling pressure differences in the buffer.

Buffer upward expansion

One of the main design requirements of the backfill is to keep the buffer in place and prevent it from swelling upwards so that the buffer will not lose too much of its density. Some upwards swelling is expected since the backfill has a lower swelling pressure than the buffer and a certain degree of compressibility.

Movement of the canister in the deposition hole

One of the safety functions for the buffer is that it should prevent the canister from sinking in the deposition hole since this would bring the canister into direct contact with the rock thus short-circuiting the buffer.

Canister settlement consists mainly of four different processes:

1. Consolidation/swelling caused by the canister weight
2. Volumetric creep caused by the canister weight
3. Deviatoric creep caused by the canister weight
4. Stress changes caused by upwards swelling of the buffer/backfill interface:
   - consolidation/swelling
   - volumetric creep
   - deviatoric creep

The fourth process can thus be divided into the same processes as the first three processes, but the consolidation and creep are caused by the swelling pressure from the buffer acting on the backfill instead of by the weight of the canister.

Homogenisation after loss of bentonite mass

Homogenisation of buffer and backfill is crucial to fulfil the safety functions related to buffer and backfill density (swelling pressure and hydraulic conductivity). The swelling properties of bentonite make the buffer and backfill material swell and close open gaps or channels to form a more homogeneous buffer. These properties are important not only for homogenising the buffer and backfill after installation of the bentonite blocks but also for limiting the potential for the long-term formation of openings in the buffer and backfill.

Buffer chemical evolution

The processes: "Advective transport of species", "Diffusive transport of species", "Sorption (including ion-exchange)", "Alterations of impurities" and "Aqueous speciation and reactions" are all components of the geochemical evolution of the buffer. After deposition, the buffer is subjected to a thermal gradient due to the heat generation from the canister. At the same time there will be a hydraulic gradient caused by the suction in the unsaturated bentonite blocks and the hydrostatic pressure in the surrounding rock. After saturation and cooling of the near-field, the interaction of groundwater with the bentonite buffer may result in an evolving distribution of some aqueous species in the bentonite pore water, as well as the redistribution of accessory minerals and the cation exchanger.

Three aspects must be considered regarding the geochemical evolution of the near-field:

1. the effect of the thermal period
2. the processes during the saturation of bentonite
3. the interaction of the water-saturated bentonite with the local groundwater

There are no buffer safety functions directly connected to this evolution, but an assessment needs to be made as to whether this evolution indirectly would violate the buffer safety functions or not.

During the period of bentonite saturation (before 10, 100, 1'000 and 2'000 years, depending on the hydrological model) advection of solutes to the bentonite pore water is the main mechanism of transport between the groundwater and the buffer. The effect of solute diffusion between the inflowing groundwater and the bentonite pore water is negligible in the cases with a high rate of water saturation (10 and 100 years). In the models with low rates of saturation (1'000 and 2'000 years), the effects of diffusion on the calculated concentrations during the period of saturation are significant. When the bentonite buffer becomes fully saturated, diffusion is the exclusive mechanism of solute transport.

During the thermal period of the repository, the initially unsaturated compacted bentonite will progressively saturate due to the hydraulic pressure of the surrounding rock (Fig. 1-4). Although the main transport mechanism in the low permeability compacted bentonite is diffusion, advective transport will be more important during the saturation stage due to the capillary pressure that is established during this stage.

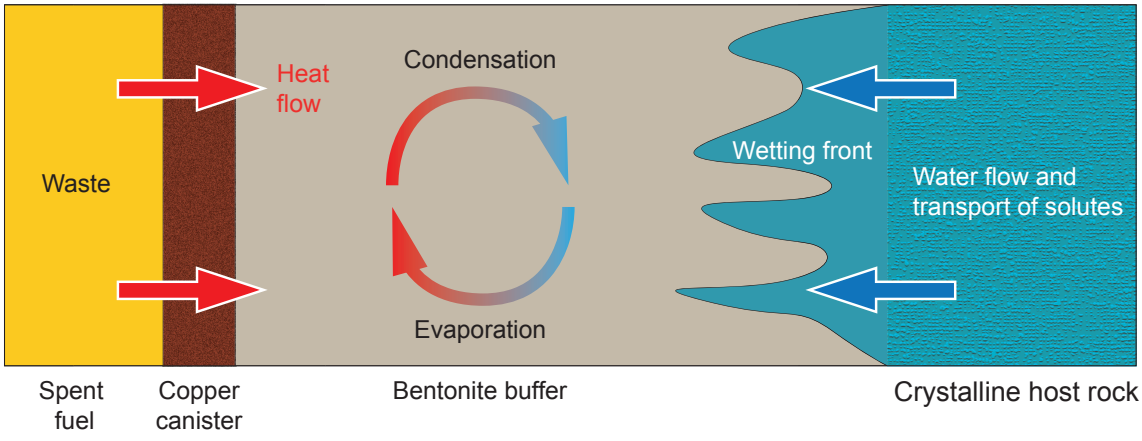

Fig. 1-4: Sketch of a vertical cross section of the near-field of a KBS-3 repository showing the thermo-hydraulic and transport processes that are believed to occur during the saturation period of the bentonite buffer (after Sena et al. 2010).

The buffer material consists of montmorillonite and accessory minerals. In the repository environment these minerals may dissolve and sometimes re-precipitate depending on the prevailing conditions. Sena et al. (2010) have calculated the redistribution of accessory minerals during the early repository evolution when a thermal gradient is present and the details about the processes and mechanisms in the modelling can be found in the reference. In the calculations the following was tested:

1. the saturation time
2. the flow rate in a fracture intersecting the deposition hole

Under a higher flow rate regime within the fracture, the effect of diffusion of solutes from the bentonite pore water to the granite or vice versa on the chemical conditions of the granite around the deposition hole will be rapidly buffered by the supply of unaffected granitic groundwater. Under these conditions, the geochemical changes induced by the chemical reactions taking place in the buffer will be limited to the buffer itself since any influence of these on the chemical conditions of the granite will be rapidly flushed due to granitic groundwater renewal. On the other hand, if the advective flow in the fracture is very low, diffusion will prevail and therefore, the chemical and diffusive processes occurring in the buffer will influence the chemical conditions of the fracture around the deposition hole.

In the calculations these parameters have been considered independently. However, a high flow rate would affect the saturation time. Therefore, no combinations of high flow and long saturation have been studied.

Ca-sulphates are originally present in the MX-80 bentonite mineralogy. At the beginning of the thermal period, anhydrite precipitates in the bentonite pores due to the increase of temperature, except close to the outer boundary of the buffer where the granitic groundwater (which is unsaturated with respect to this mineral) flows into the buffer. The dissolution of the primary anhydrite is more efficient for a situation when the saturation is rapid (10 and 100 years in Fig. 1-5).

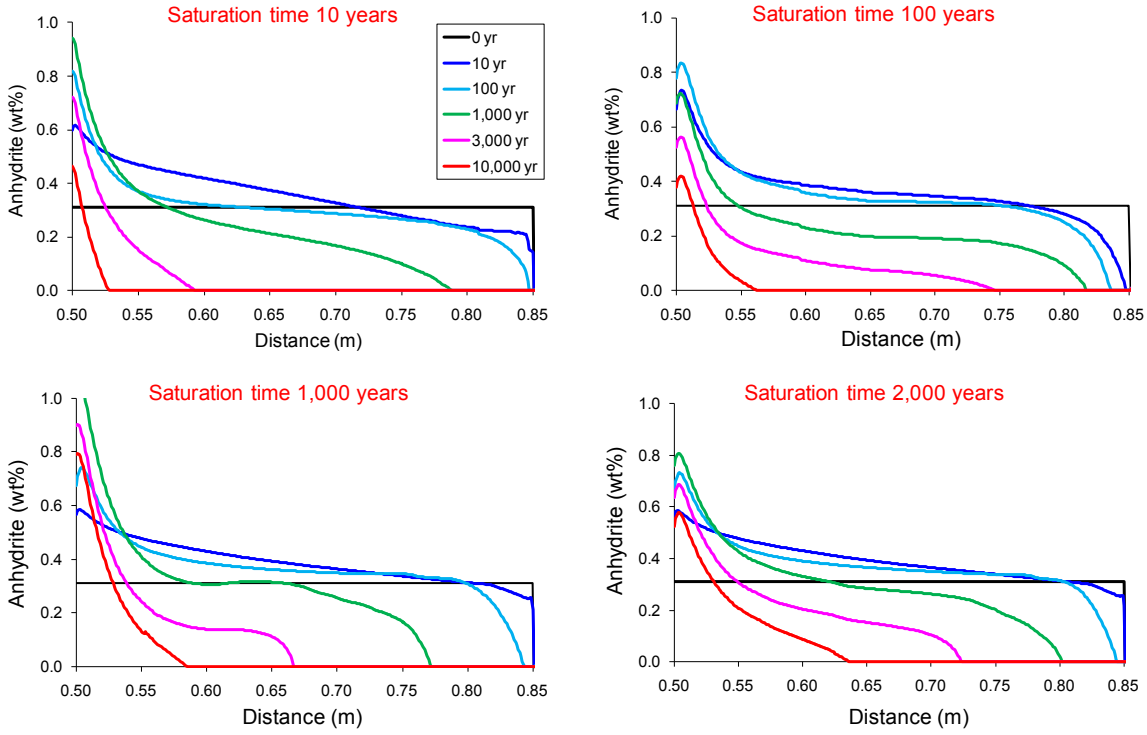

Fig. 1-5: Calculated evolution of the amount of anhydrite in the MX-80 bentonite buffer as a function of buffer saturation time (Sena et al. 2010).

SiO_2(am) is also a primary mineral of the MX-80 bentonite. The primary SiO_2(am) in the bentonite is preferentially dissolved close to the inner surface of the buffer (left side in Fig. 1-6). In the case with a relatively fast saturation (10 years), a small amount of SiO_2(am) is also dissolved during the saturation period, close to the contact with the granite. Until 10 years, the SiO_2(aq) concentration progressively increases, both in the bentonite and in the granite due to

the solute supply by SiO_2(am) dissolution close to the hot boundary of the system. After 10 years, the aqueous SiO_2 concentration decreases due to dilution provided by the inflow of the granitic groundwater, which is depleted in SiO_2(aq) compared to the initial bentonite pore water.

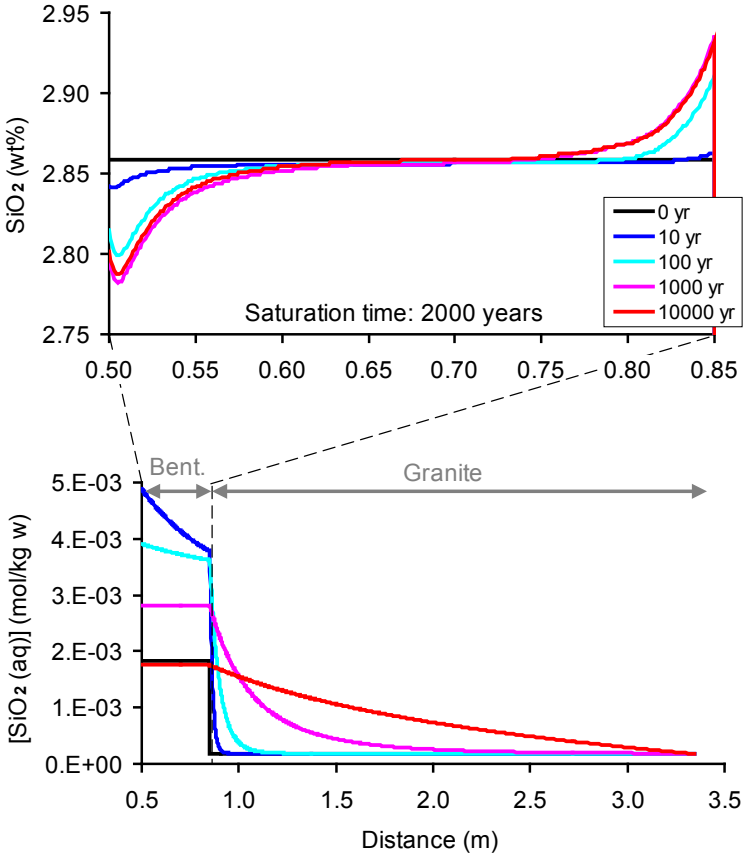

Fig. 1-6: Calculated evolution of the amount of SiO_2 in the modelled domain of MX-80 bentonite, for a saturation time of the bentonite of 10 years (Sena et al. 2010).

In general, the calculated evolution of the composition in the montmorillonite exchanger in the MX-80 bentonite indicates that the concentration of sodium decreases with time in favour of more calcium adsorbed. The concentration of potassium and magnesium also decreases in the montmorillonite exchanger. Within the same case of advective flow in the fracture intersecting the deposition hole, the calculated evolution of the composition of the exchanger is very similar for the different cases of bentonite saturation.

As a result of the numerical simulations in Sena et al. (2010), it can be concluded that the main mechanisms controlling the mineralogical changes of the bentonite during the thermal period are related to:

- the dependence of the mineral solubilities on the evolution of the temperature in the near-field
- the solute transport and mass transfer between the groundwater flowing along the fracture and the bentonite pore water

The evolution of the concentrations obtained for the bentonite pore water is a result of mixing with the local groundwater during the period of bentonite water saturation, whereas thereafter, diffusion of solutes is the dominant mechanism. The distribution of the concentration of solutes in the granitic groundwater is a consequence of the ratio between:

- the diffusion rate through the granite – bentonite interface
- the fluid flow rate along the fracture in contact with the deposition hole

In this way, the results obtained considering two regimes of groundwater flow rates along the fracture intersecting the deposition hole are substantially different.

Idiart et al. (2013) further developed this method by using 2D – axisymmetric and 3D models instead of 1D -axisymmetric model. These improvements did not affect the controlling mechanisms, only the timescales and quantity of the changes.

Effects of salinity

The process "Osmosis" basically describes how the hydromechanical properties of the buffer are affected by the ionic strength of the surrounding groundwater. The salinity of the groundwater influences the vapour pressure relation and thereby the water saturation process. However, for the groundwater at the Forsmark site the effect is negligible.

Montmorillonite transformation

The advantageous physical properties of the buffer, e.g. swelling pressure and low hydraulic conductivity, are related by the ability for water uptake between the montmorillonite mineral layers (swelling) in the bentonite. However, montmorillonite can transform into other naturally occurring minerals of the same principal atomic structure but with less or no ability to swell in contact with groundwater. The transformation processes usually involve several basic mechanisms. At the expected physico-chemical conditions in a repository, the following possible mechanisms are identified:

- congruent dissolution
- reduction/oxidation of iron in the mineral structure
- atomic substitutions in the mineral structure
- octahedral layer charge elimination by small cations
- replacement of charge compensating cations in the interlayer

Transformation from smectite (montmorillonite) to illite, which is the most common alteration observed in natural sediments, is well documented in different geological formations, and has been reproduced under laboratory conditions. The main mineralogical differences being that the illites have approximately one unit charge higher tetrahedral charge, and potassium as the main charge compensating cation.

Cementation

The term "cementation" has often been used in a broad sense to describe processes, which lead to specific changes in rheology and swelling properties of the buffer material. A number of quite different chemical/mineralogical and mechanical underlying processes could conceivably cause such cementation effects. The above sections addressing the underlying and related processes, i.e. montmorillonite stability, ion exchange, accessory minerals' alteration, diffusive transport etc. are consequently very relevant to the cementation process. There are two main concerns about the effects of cementation on the bentonite buffer; one is an increase in hydraulic conductivity, and the other is an increase of shear strength.

2 Smectite stability at increased temperatures – insights from literature

2.1 Formation conditions of smectite

Observations from hydrothermally altered rocks

Smectites are alteration products of high-temperature mineral assemblages or volcanic ash. They are formed in low-temperature environments, such as soils and diagenetic sediments. Smectites may also form from high-temperature silicates in hydrothermal systems (below 100 – 150 °C) depending on the chemical boundary conditions. This is indicated by mineral assemblages encountered in hydrothermally altered rocks (Inoue 1995) as illustrated in Fig. 2-1. Depending on the chemical composition of these rocks, two different series, the K-series and the Ca-Mg-series are distinguished. The figure underlines the importance of the original chemical and mineralogical composition affecting the thermal transformation process of smectite. For both series, Inoue (1995) proposed a smectite zone in the temperature range below about 100 °C.

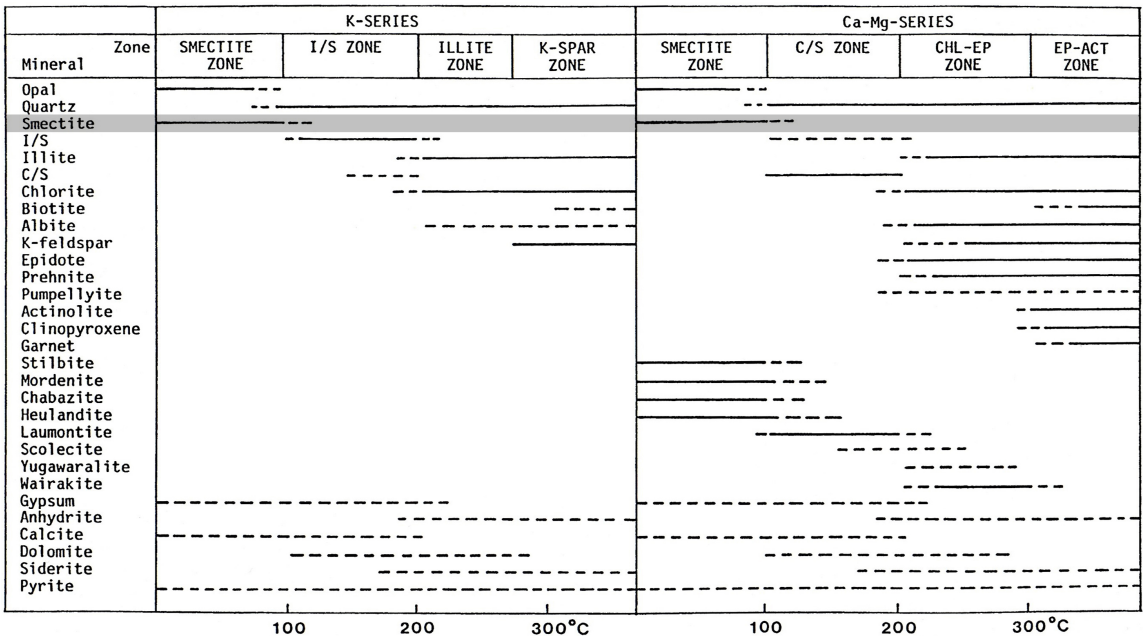

Fig. 2-1: Mineral assemblages as function of temperature in intermediate to alkaline types of hydrothermally altered rocks (from Inoue 1995).

Mineralogical composition

Smectites are chemically and structurally complex 2:1 phyllosilicate phases, whose thermodynamic properties are still not well known (see section below). In Fig. 2-2 the compositional range of smectites is shown with respect to hypothetical end member minerals, total layer charge and tetrahedral/octahedral charge (Newman & Brown 1987). The layer charge of montmorillonites ranges from 0.3 to 1.2 unit charges per $O_{20}(OH)_4$ unit, most of which is made up by octahedral charge (by substitution of Mg^{2+} and Fe^{2+} for Al^{3+}). Beidellites on the other hand, display similar layer charge but a higher contribution of the tetrahedral charge. Illites are characterised by a higher layer charge (1 – 2) with a higher tetrahedral component relative to that of montmorillonite.

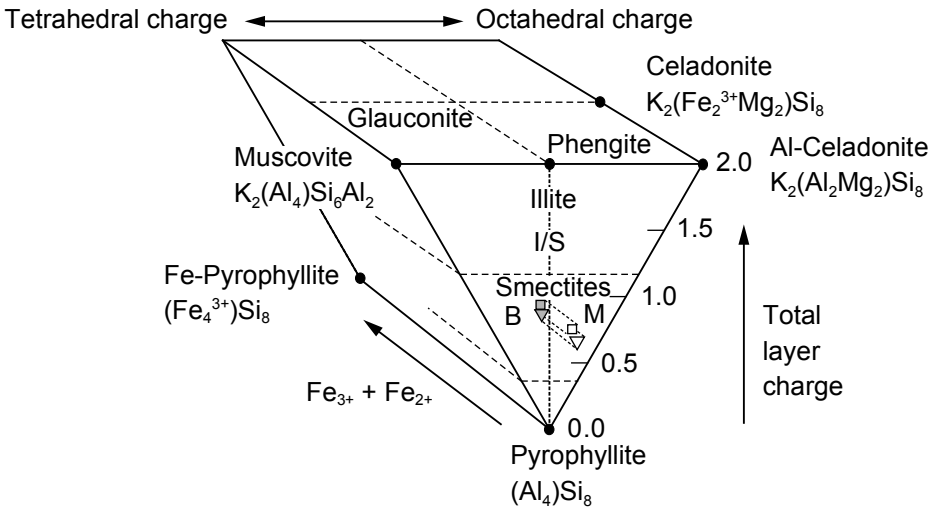

Fig. 2-2: Ideal end members in the pyrophyllite – mica series with potassium as charge compensating cation, and approximate compositional ranges for illite and smectite.

B: beidellite, M: montmorillonite (taken from Karnland & Birgersson 2006, based on Newman & Brown 1987)

Thermodynamic and kinetic considerations

A thermodynamic description of smectite minerals and even of clays in general has proven to be far from trivial. In fact, the equilibrium of clay minerals is a question still open to debate (Blanc et al. 2013) although an extensive amount of work has been performed in this area. The thermodynamic status of smectite is actually debated (see e.g. Aja & Rosenberg (1996), Essene & Peacor (1997) and references therein) and the chemical equilibrium assumption has been questioned, based both on measurements of solubilities (May et al. 1986) as well as theoretical arguments (Lippmann 1982).

The challenges met by a thermodynamic approach to smectite chemistry are several: (1) the mineral displays a large compositional range and does not have a unique stoichiometry (2) the variable amount of interlayer water may have to be considered in the thermodynamic formulation and (3) the specific set of ions which compensates the layer charge is variable and controlled by the geochemical environment. Nevertheless, there have been various attempts to describe the thermodynamic properties of smectites. Concerning the structural variability, two types of treatments have been considered: (1) phases with discrete chemical compositions (e.g.

Giggenbach 1981, Sass et al. 1987, Rai & Kittrick 1989, Vieillard 2000) and (2) solid solutions (e.g. Lippmann 1977 and 1980, Tardy et al. 1987, Aagard & Helgeson 1983). Conveniently, the stability of smectites relative to other phyllosilicates is illustrated in stability diagrams. Because of lack of adequate thermodynamic data, idealised compositions (e.g. in the Si-Al-K-H_2O system) have generally been considered. An example of a stability diagram is given by Aagard & Helgeson (1983; Fig. 2-3) who applied a solid solution model based on ideal mixing of atoms on homological sites for smectite, illite/smectite mixed layers and illite.

Unfortunately, the usefulness of such diagrams is limited due to the large uncertainty in underlying thermodynamic constants. This is particularly true for activity diagrams displaying varying Na^+, K^+ or Ca^{2+} activity since cation exchange reactions are not accounted for (Gaucher 1998). Moreover, the H_2O component respectively the hydration state in smectites is commonly neglected although shown to strongly influence thermodynamic properties (Vidal & Dubacq 2009, Dubacq et al. 2010).

Notwithstanding the drawbacks of thermodynamic considerations, activity diagrams such as that presented in Fig. 2-3 suggest the importance of SiO_2 and K^+ activities and pH in the stability of montmorillonite. Thus, higher Si activity in pore waters stabilises montmorillonite as indicated from the study of marine sediments (Abercrombie et al. 1994). Low Si and high pH, on the other hand, favour the formation of beidellite and illite. For the latter mineral to form, a sufficiently high K^+ activity is required. Fig. 2-3, which includes representative groundwater compositions at Forsmark and Olkiluoto, shows that the composition of waters with which repository bentonite is expected to interact are typically outside the stability field of montmorillonite. Particularly, the SiO_2 activity of these waters is below the expected stability limit.

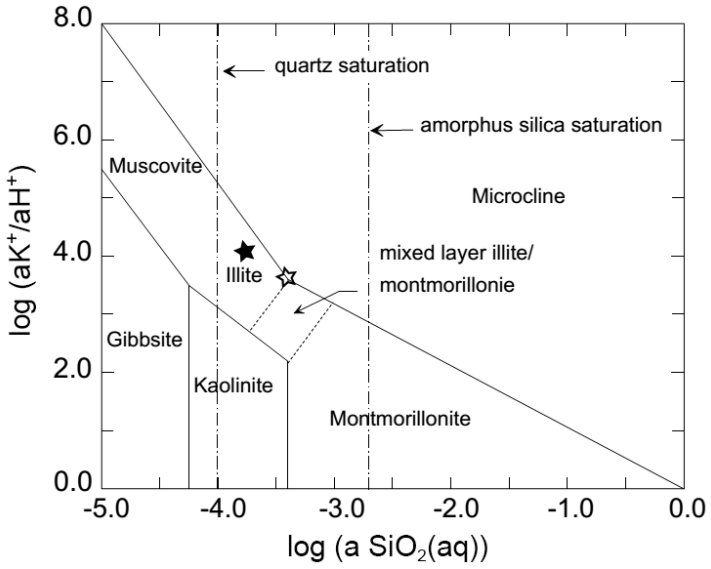

Fig. 2-3: Activity ratio diagram in the Si-Al-K-O-H_2O system at 25 °C (from Aagard & Helgeson 1983).

The filled and unfilled stars indicate representative values for present-day ground water at Forsmark (Arcos et al. 2006) and Olkiluoto (Birgersson & Wersin 2014), respectively.

On the experimental side, considerable work has been done on studying the reactivity and chemical stability of smectites.

(Eberl et al. 1978) studied hydrothermal reactivity of smectite by reacting montmorillonite and saponite with different counter-ions in pure water at a solid-to-water-ratio of 1:1 (i.e. a rather dense system) at 300 – 485 °C between 7 – 34 days. By analysing the reaction products with XRD, they found that smectite converted to mixed-layered phases under these conditions, i.e. the smectite converted to a phase with various expandable and non-expandable (mica-like) layers. Note that these mixed-layered phases are not equivalent to an illite/smectite mixed-layer, since potassium was not available in all tests. It can consequently be concluded that sub-processes which occur during the process of illitisation (the most commonly occurring process found in e.g. burial diagenesis, see Section 2.3) also occur under conditions when illite is not formed, e.g. when potassium is unavailable. One such sub-process is the substitution of Al for Si in the tetrahedral sheets of smectite, leading to an increased surface charge density. The study of the chemical stability of montmorillonite must hence be extended beyond the mere study of specific mineral transformations.

Eberl et al. (1978) also concluded that dioctahedral smectite (e.g. montmorillonite) was more reactive than trioctahedral smectite (saponite). The explanation given is that aluminium, which is a main constituent in a dioctahedral sheet, is more available for the dioctahedral smectites under the conditions of the tests. Consequently, transformation of (dioctahedral) smectite occurred in parallel with congruent dissolution of the same mineral. Finally, the authors concluded that the reactivity depended on counter-ion hydration energy; montmorillonites with counter-ions of relatively low hydration energy (K, Cs, Rb) reacted at lower temperatures than e.g. Na- Ca- and Mg-montmorillonites. This was explained as a consequence of that a higher surface charge density is required in order to "collapse" interlayers containing strongly hydrated ions (see also (Eberl 1978 and 1980). Thus, although a lower reactivity of Na- and Ca-montmorillonite as compared to e.g. K-montmorillonite was observed, it cannot be concluded that surface charge increasing processes were not occurring in the former systems. It may be so that layer charge increasing processes occurred (even to the same extent as in the collapsed systems), but that the critical layer charge density, i.e. the charge density where collapse occurs, was never reached.

Studies on the solubility of the smectite itself, where less or no attention is been paid to identifying possible alteration products, are quite vast. Such studies are typically of two kinds (1) flow through, which (ideally) gives a steady-state dissolution reaction, and (2) batch, in which equilibrium is aimed for. As dissolution/alteration of smectite is a considerably slow process at the lab scale (particularly at low temperature and near neutral pH), these processes are often studied at more extreme pH values (e.g. Zysset & Schindler 1996) and/or elevated temperature (e.g. Bauer & Berger 1998) and dissolution rates are typically reported as functions of these variables (Amram & Ganor 2005, Cama et al. 2000, Huertas et al. 2001, Köhler et al. 2003, Marty et al. 2011, Myllykylä et al. 2013, Rozalén et al. 2009 and 2008).

Dissolution rates are commonly stated in the unit of amount of dissolved smectite per time unit and reactive surface area, where the reactive surface area often is taken to be the BET surface. Looking at reported data, however, normalisation to the BET surface does not seem to give coherent results, indicating that BET surface is not a relevant measure of the reactive surface. This is indicated by (Rozalén et al. 2009) which instead normalised to mass when comparing their results with others. Their comparison, on the other hand, gives quite a coherent picture: the far from equilibrium dissolution rates for smectite is in the order of 10^{-12} mol g^{-1} s^{-1} at 50 – 70 °C and pH 4 – 10. At extreme pH (< 2, > 13) the rates are increased by approximately two orders of magnitude.

Furthermore, reported rate expressions are, in cases where more than one temperature were considered, usually expressed in terms of Arrhenius expressions, with the objective of stating activation energies for the involved reaction mechanism(s). In many cases, however, the values of such activation energies are directly correlated with the form of the proposed rate law rather than representing something physical. The rate law proposed by (Köhler et al. 2003) can be considered as an example, which states three active processes:

$$r = A_H e^{\left(-\frac{E_{A_{H^+}}}{RT}\right)} a_{H^+}^{0.6} + A_{H_2O} e^{\left(-\frac{E_{A_{H_2O}}}{RT}\right)} + A_{OH} e^{\left(-\frac{E_{A_{OH^-}}}{RT}\right)} a_{OH^-}^{0.6}$$

where a_{H^+} and a_{OH^-} is the hydrogen and hydroxyl activity, respectively, and A and E denotes the Arrhenius parameters for each process. The values of these are:

$A_H = 2.2 \times 10^{-4}$ mol m^{-2} s^{-1}, $E_H = 46$ kJ mol^{-1}, $A_{H_2O} = 2.5 \times$ 10-13 mol m^{-2} s^{-1},
$E_{H_2O} = 14$ kJ mol^{-1}, $A_{OH} = 0.27$ mol m^{-2} s^{-1}, and $E_{OH} = 67$ kJ mol^{-1}.

Note, that the A -factors differ by 12 orders of magnitude but that each term is compensated by the factor $\exp(E_A/RT)$ to result in a difference between the full Arrhenius coefficients of only 4 orders of magnitude. Such correlation is a clear indication that the expression is over-parameterised. Consequently, little physical information is given by the stated activation energies.

In tests which were aimed at reaching equilibrium via the dissolution reaction, estimations of the solubility were done. Cama et al. (2000) reported in this manner equilibrium silica concentrations of 0.5 – 0.6 mM of a high charged sodium-dominated natural smectite at pH 8.8 and 80 °C. Marty et al. (2011) reported equilibrium silica concentrations of ~ 0.8 mM and ~ 3.0 mM of a synthetic Na-smectite of lower charge at 25 °C (pH 9) and 80 °C (pH 8), respectively.

The stability of a large set of naturally occurring bentonites in various salt solutions and at elevated temperature (60 – 90 °C) was investigated with the specific aim of safety assessment for disposal of radioactive waste (Kaufhold & Dohrmann 2011, 2010, 2009). After treatment in 6.0 M NaCl solutions for 5 months at 60 °C (Kaufhold & Dohrmann 2009), the maximum silica concentrations measured was ~ 0.1 mM. Further, the only noticeable alteration was the (expected) ionic exchange towards pure sodium clays. A similar treatment in 1.0 M KCl (5 months, 60 °C) showed generally only slightly higher silica concentrations (Kaufhold & Dohrmann 2010). In those tests, however, a decrease in CEC by 10 % on average was noted. Moreover, when performing cycles of wetting and drying (short term, maximum 105 °C) of bentonites converted to basically the pure potassium-form, an average CEC decrease of 30 % was observed. The authors propose that these effects are possibly the result of illitisation. An analysis of the final material was, however, not performed. Neither was any attempt done to exchange the potassium converted clay back to some other ion, in order to check whether the potassium was really fixated. Potassium fixation in drying/wetting cycles was also reported by (Eberl et al. 1987).

Lee et al. (2010) monitored the amount of silica in solution when performing hydrothermal tests on montmorillonite extracted from a Korean bentonite in a potassium concentration of 0.5 M. At temperatures of 90 °C and 140 °C – where only minor mineral transformation occurred – the silica concentration quickly reached a constant value of ca 0.45 mM and 1.1 mM, respectively.

2.2 Modes of smectite alteration

2.2.1 Transformation to illite

The transformation of smectite to illite (illitisation) as a result of increasing temperature is a very common process observed during diagenesis and in hydrothermal environments (e.g. Meunier & Velde 2004). It requires both an increase in layer charge and the availability of K^+. The most important variables for this kinetically-controlled process are temperature, time and K^+ activity (Meunier & Velde 2004). Details of the illitisation process and its relevance to near-field conditions are presented in Section 2.3.

2.2.2 Transformation to beidellite and saponite

The heat-induced transformation of low-charge smectite (i.e. montmorillonite) to high-charge smectite (beidellitisation) is frequently observed as the first step in the illitisation process (Sato et al. 1996, Meunier et al. 1998). There is controversy whether montmorillonite and beidellite form a continuous solid solution or rather mixed layers (Meunier 2005). In the study of Beaufort et al. (2001), both low-charge smectite and purified bentonite in quartz saturated solutions were exposed to temperatures of 100 – 200 °C for a period up to 330 days. The results showed transformation to high-charge beidellitic layers whose concentration increased with time, temperature and K^+ concentration. The morphology of the high-charge smectite particles which were interstratified low-charge smectite starting material suggested a dissolution/precipitation rather than a solid transformation process. Illite/smectite mixed layer formation was only observed for samples containing K^+ at the highest experimental temperature (200 °C). The transformation from low to high charge smectite was accompanied by the formation of a Mg-rich Al-poor silicate which was interpreted as trioctahedral Mg-rich smectite. The proposed reaction scheme for the beidellitisation process was:

Low charge montmorillonite → high charge beidellitic smectite + Mg-trioctahedral smectite (1)

A similar reaction process has been observed in other experimental and field studies. Thus, thermal alteration studies of Yamada & Nawasaka (1993) and Sato et al. (1996) showed replacement of montmorillonite by a beidellite + saponite assemblage at high temperature (250 – 350 °C). In the geothermal field of Chipilapa (Salvador) beidellitic and saponitic smectites are formed in the hot fluids in volcanic rocks and then transformed to illite/smectite mixed layers and chlorite (Patrier et al. 1996). A preliminary natural analogue study (Pellegrini et al. 1999), dedicated to smectite transformation in three clay formations exposed to short periods of contact metamorphism (150 – 250 °C), indicated the transformation to trioctahedral smectite close to the contact in two of the three sites. This was interpreted as being a consequence of the limited availability of K^+ and/or the slower kinetics of the illite reaction. The third site on the other hand displayed the expected "normal" sequence with progressively higher illite content in the I/S ML towards the basaltic intrusion.

Experimental data of Eberl et al. (1978) indicate that trioctahedral smectites are stabilised relative to montmorillonite at higher temperatures. It is also noteworthy that dioctahedral and trioctahedral smectites display a very restricted range of solid solutions (Velde 1995a).

2.2.3 Transformation to chlorite

Information from sedimentary and hydrothermal system indicates that smectites may convert to smectite/chlorite mixed layers and chlorite at temperatures about 50 °C higher than those transformed to illite (Velde 1995b, Hoffman & Hower 1979). Chlorite formation often occurs concomitantly with illite upon smectite dissolution which releases Mg and Fe (Ahn & Peacor 1986, Eberl 1993) (see Fig. 2-4). Experimental data of Howard & Roy (1985) suggest the formation of Al-hydroxide complexes in the smectite interlayer at 250 °C leading to a reduction in cation exchange capacity. However, the possibility of formation of Al-hydroxide complexes in smectite interlayers at relatively low temperatures, leading to reduction in swelling capacity and cation exchange capacity was noted by Johnston & Miller (1985), based on early work of Carstea et al. (1970) and references therein. According to these authors, however, this would require conditions of significant Al solubilisation, i.e. at least mildly acidic conditions (pH < 6).

Chlorite/smectite mixed layers may occur as random or regular[1] interstratifications whereby the smectite component is trioctahedral and Mg-rich. The transformation process of dioctahedral smectite thus involves first conversion to trioctahedral smectite and illite and/or illite (see above) followed by conversion to C/S, as observed for example in Devonian lacustrine clays in Scotland (Hilliers 1993).

Chang et al. (1986) reported the transformation of trioctahedral smectite to C/S mixed layers at similar temperatures as the transformation of dioctahedral smectite to illite, i.e. 100 – 150°C in different sediment basins in Brazil. Thus, in situations where trioctahedral is the starting material, chloritisation appears to occur at lower temperatures. A rather analogous situation was reported by Son et al. (2001) for sediments in the Niagata basin (Japan) in which alternating beds containing predominantly dioctahedral and trioctahedral (saponitic) smectites occur. With increasing depth and temperature, dioctahedral smectites show transformation to I/S ML with concomitant increase of K^+ and Al^{3+} and decreasing Si. Trioctahedral smectites on the other hand transform to regular C/S ML. The results indicated that the transformation process roughly occurs at the same depth and temperature (110 – 120°C).

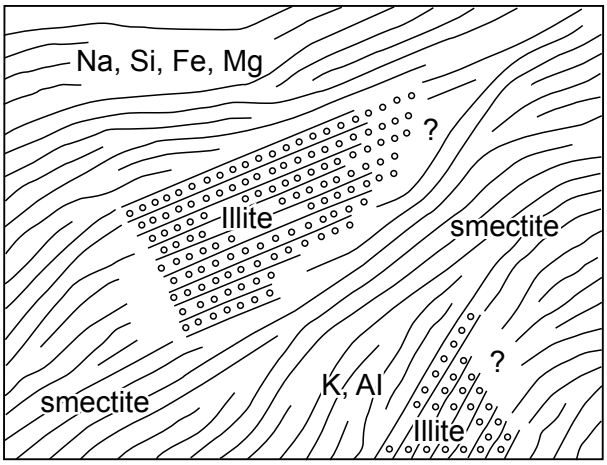

Fig. 2-4: Sketch of illitisation with a dissolution/precipitation model (from Ahn & Peacor 1986).

The released Si, Fe and Mg may further form chlorite.

[1] Regular chlorite/trioctahedral mixed layers are often termed corrensite.

2.2.4 Effects of high pH

Groundwater affected by leachates from cement tunnel supporting structures in the repository might get into contact with the buffer during the thermal period, although the probability for this is low[2].

At pH > 10 smectite becomes more soluble in parallel to the increased SiO_2 solubility. Thus, silica together with other elements is released. As suggested from experimental evidence (Bouchet et al. 2004, Karnland et al. 2007, Mosser-Ruck & Cathelineau 2004), montmorillonite dissolution in contact with high pH fluids generally is incongruent leading to an increased Al/Si ratio and increase in tetrahedral charge and the formation of beidellite. Thereby, cation exchange properties are modified and, depending on the availability of K^+, high-charge smectite is further converted to illite (Eberl et al. 1993, Bauer & Velde 1999). However, transformation to zeolites without illite formation has also been observed under alkaline conditions (Fernandez et al. 2006), even in the presence of high K^+ concentrations but at high temperatures of 150 °C (Mosser-Ruck & Cathelineau 2004). It is important to note that the vast majority of the experimental data represents highly alkaline conditions (pH > 12) and reliable data for mildly alkaline conditions (pH 10 – 11) is lacking.

As a natural analogue for interaction between alkaline water and bentonite, Alexander et al. 2013 investigated rock and ground water at sites on Cyprus, where the smectite content is in the range 20 – 50 % and where the typical ground water pH is in the range 9 – 10, with peaks up to 11. They tentatively concluded that a smectite-to-palygorskite transformation occurs under these conditions.

2.2.5 Effects of unsaturated conditions

The re-saturation of the bentonite in the deposition holes of the KBS-3 concept and in the horizontal deposition tunnels of the Nagra concept depends on hydraulic conditions in the surrounding rock. In the case of KBS-3 with an inhomogeneous fractured host rock, re-saturation times will be variable, spanning from decades to thousands of years (SKB 2011, Idiart et al. 2013). The effect of heat on buffer temperatures is calculated to last more than 10'000 years, but the duration of the main heat pulse with temperatures higher than 50 °C will be less than 1'000 years. Saturation times in the buffer will thus be either shorter or within a comparable time range as the heat period. In the Nagra case with a fairly homogenous clay rock, re-saturation times are expected to be less variable, in the range of some hundreds of years, thus in the same range as the main heat pulse. It should be noted however that for both disposal concepts peak temperatures will occur already after a few decades, where a majority of KBS-3 deposition holes and most of the bentonite in Nagra's concept are expected to be still unsaturated. Generally speaking, transport of solutes is restricted and reaction rates are slowed down compared to saturated conditions.

Under specific unsaturated conditions, loss of swelling capacity of bentonite materials at elevated temperatures has been observed. Couture (1985) reported substantial reduction in expandability upon exposure of bentonite powder to steam at 150 – 250 °C. This was confirmed by Oscarson & Dixon (1989) who noted a decrease in free swell of "loose" bentonite contacted with steam already at 110 °C. In a later study, Oscarson & Dixon (1990), however, showed that compacted bentonite heated under unsaturated conditions did not reveal any significant change in mineralogy or transport properties. A similar result was obtained by Pusch (2000), who found

[2] In Nagra's case the Opalinus Clay pore water saturating the bentonite must pass through the low pH concrete liner to minimize the impact of chemical interactions (Savage 2014).

only slight changes in swelling pressure and hydraulic conductivity of compacted dried bentonite powders, which were allowed to expand upon exposure to steam between 90 and 110 °C for 30 days. A later study by the same author performed with very dense bentonite pellet samples indicated some reduction of 125 °C and significant reduction of swelling capacity at 150 °C upon exposure to water vapour (Pusch et al. 2003). Based on microscopic analysis, the reduction of expandability was shown to be caused by cementing silica precipitates. This cementing effect was probably related to cooling upon thermal treatment.

A newly conducted study on the impact of steam treatment on swelling properties of montmorillonite and bentonite is reported in Section 5 of this report (see Section 5).

2.2.6 Effects of cementation

Thermally induced enhanced mass transfer of dissolved solids via dissolution – precipitation mechanisms and evaporation effects may affect the buffer's bulk properties, such as swelling pressure and hydraulic conductivity. In addition, smectite transformation to illite is accompanied by SiO_2 precipitation, which may add to cementation induced by dissolution and re-precipitation of accessory minerals.

The effect of cementation of the buffer via dissolution and re-precipitation during the thermal stage is considered to be small, as supported by reactive transport modelling (e.g. Idiart et al. 2013) and from long-term experiments, such as for example the large-scale LOT experiment at Äspö (Karnland et al. 2009). These data indicate small mass fluxes of dissolved and re-precipitated Si or $CaSO_4$. However, there is still a lack of knowledge on the cementing processes during the thermal phase in which thermal-hydraulic-mechanical and chemical processes are highly coupled and still not properly accounted for in the models.

Dueck (2010) conducted mechanical testing on saturated and unsaturated bentonite exposed to temperatures up to 150 °C in order to further study the effect of reduction of strain at failure observed in the A2 parcel in the LOT-test (Karnland et al. 2009). They could to a certain extent reproduce a brittle behaviour in the short term, an effect which could be reversed, however, by milling and recompacting the bentonite material.

2.2.7 Hoffmann-Klemen effect

A well-documented effect which reduces, or may even eliminate, the octahedral charge of smectites is the effect called "Hoffmann-Klemen effect" (Hoffmann & Klemen 1950) or "Greene-Kelly effect" (Greene-Kelly 1953). These researchers found that small-sized cations residing in the interlayer have the ability to irreversibly penetrate into the smectite crystal structure at high enough temperatures, thereby eliminating octahedral charge. The temperature threshold for when the effect becomes active depends on the specific ion, but is considerably larger than any conceivable repository temperature. In the case of e.g. lithium, the temperature is ~ 250 °C.

2.2.8 Possible reduction of structural Fe^{3+}

Smectites may contain structural iron of various amounts which may alter its oxidation state (between Fe(III) and Fe(II)) depending on redox conditions (Stucki et al. 1984). Although such reduction/oxidation processes should not be regarded as true mineral transformations, it should be noted that they may lead to changes in layer charge density. An increase in layer charge

density, in turn, may induce other types of processes as discussed above, e.g. potassium fixation. As the long-term repository redox conditions are expected to be reducing, it is consequently important to assess the layer charge density of any smectite component with this taken into account.

2.2.9 Summary considerations

Smectites generally form in low temperature environments, but under favourable conditions may also form at temperatures > 100 °C. The stability of smectites is still not well established because of high uncertainty of underlying thermodynamic data. Nevertheless these suggest the important role of Si, pH and K^+ in constraining smectites stability, besides temperature. As indicated from numerous observations in sediments, smectites become unstable with increase in temperature and may transform for example to illite, the most frequent reaction product of dioctahedral smectite. In general, smectite transformation processes are slow and a strong function of temperature. In some environments the formation of high charge (beidellitic) smectites together with Mg-rich trioctahedral smectites is observed as the first step of illitisation. Chloritisation of dioctahedral smectite may occur concomitantly with illite formation at relatively high temperatures upon smectite dissolution which releases Mg and Fe (Ahn & Peacor 1986). In diagenetic sediments, chloritisation is more common for trioctahedral Mg-rich smectite where it takes place at similar temperatures as illitisation of dioctahedral smectites.

At high pH, montmorillonite becomes unstable and may transform to beidellite, zeolites and at high K^+ to illite. The reaction products have mainly been observed at very high pH > 12. The stability and transformation rates at moderately elevated pH (10 – 11) are still uncertain.

Under unsaturated condition, generally less thermally-induced transformation than under saturated condition is expected although the process of K+ fixation has been observed at low temperature resulting from dry-wetting cycles. However, cementation via precipitation of new material may be enhanced under such conditions. However, the overall effect of cementation on the buffer's performance during the thermal period is probably small, as indicated from bounding calculations and reactive transport modelling as well as from experimental indications.

2.3 Illitisation

2.3.1 Introduction

As indicated in the last chapter, illitisation is by far the most frequently observed alteration process for montmorillonite and dioctahedral smectites in general. Thus, smectites become instable relative to illite with increasing temperature according to diagenetic studies along depth profiles in sedimentary basins. Experiments performed at higher temperatures document the smectite-to-illite conversion as a function of temperature, time and potassium concentration, and other variables. Some studies provide parameterised rate equations for the illitisation process, but partly with large discrepancies.

Illitisation in the buffer during the thermal phase is of concern because this may impair its safety functions, thus affecting swelling pressure, hydraulic conductivity and plasticity. The relevant time frame covers the first 500 – 1'000 years at which the buffer/canister is above 50 °C, and a few hundred years less for the buffer/rock interface.

According to literature, illitisation of smectite is an issue for deep disposal (e.g. Meunier & Velde 2004, Karnland & Birgersson 2006) but the general consensus so far is that at temperatures below 100 °C no significant degree of illitisation is to be expected (Wersin et al. 2007, SKB 2010, Section 3.5.9). This point is re-addressed in the sections below.

Microbially-induced illitisation has also been reported in the literature whereby reductive destabilisation of smectite via Fe^{3+} reduction is proposed as mechanism, in the presence of organic carbon as nutrient (Kim et al. 2004, Zhang et al. 2007, Ribeiro et al. 2009). However, the underlying data are based on experimental conditions (suspensions, high potassium and nutrient supply) which are not representative of repository conditions.

2.3.2 Process description

The overall smectite-to-illite reaction can be schematically represented as:

$$smectite + K^{+} (+ Al^{3+}) \rightarrow illite + SiO_2 + (Ca, Na) \quad (2)$$

Thus, illitisation proceeds via K^+ fixation in the interlayer and release of Si. It also requires an increase in layer charge, whereby this increase occurs mainly in the tetrahedral layer with generally little change in the octahedral layer. The released Si may precipitate as SiO_2 cement and reduce the swelling capacity and plasticity of the bentonite material.

The details of the illitisation process are complex and still under debate, but have been shown to be strongly influenced by temperature, reaction time and potassium concentration (e.g. Huang et al. 1993, Cuadros & Linares 1996, Mosser-Ruck et al. 1999). Further environmental variables affecting the reaction process include pressure (Eberl & Hower 1976, Eberl et al. 1978), the chemical composition and layer charge of the smectite (Eberl et al. 1978, Meunier & Velde 2004) and the nature of interlayer cation (Lahann & Roberson 1980, Howard & Roy 1985, Yau et al. 1987).

In diagenetic environments, such as sedimentary basins, the following sequence with increasing depth and temperature is commonly observed:

$$S \rightarrow I/S(R0) \rightarrow I/S(R1) \rightarrow I \quad (3)$$

Where R0 and R1 mean disordered (or random) and ordered I/S mixed layers (ML), respectively. This classification of I/S ML is based on XRD analysis, but their nature is still under debate (Meunier 2005, Meunier & Velde 2004). I/S ML have been described as solid solutions (e.g. Aagard & Helgeson 1983, Bethke & Altaner 1986) or as intimate associations of discrete mineral phases (Garrels 1984, Nadeau et al. 1985, Ahn & Peacor 1986). As outlined in the review of Meunier & Velde (2004), the illitisation process in diagenetic environments may often be simplified as two-step kinetic formulation (Velde & Vasseur 1992) with S → I/S (R = 0) and (2) I/S → I (R = 1). A similar sequence is observed in hydrothermally active zones (Ylagan et al. 2000, Inoue 1995). On the other hand, in most high-temperature environments, such as geothermal fields (e.g. Salton Sea) a one-step kinetic process (S → I) seems to be more appropriate (Lanson & Velde 1992, Elliot & Matisoff 1996).

As stated in the last chapter, at temperatures above 100 °C, the illitisation process is initiated by the conversion of low charge smectite to high charge (beidellitic) smectite and Mg-rich (saponitic) smectite. At higher temperatures, these reaction products may further react to I/S ML and chlorite (Beaufort et al. 2001).

Different reaction mechanisms for illitisation have been proposed, including (1) solid state transformation (Hower et al. 1976, Roberson & Lahann 1981, Inoue et al. 1988, Bell 1986), (2) dissolution and crystallisation (Nadeau et al. 1985, Whitney & Northrop 1988, Mosser-Ruck et al. 1999) without or with Ostwald ripening (Inoue et al. 1988, Ferrage et al. 2011). The reaction mechanism appears to depend on temperature and other variables (Meunier & Velde 2004).

Interpretation of illitisation rates, conventionally determined by X-ray diffraction techniques, is rendered difficult by particle size and orientation effects (Cuadros & Linares 1996) or the possible association of dehydrated K-rich smectite with illite layers which in fact often leads to an overestimation of illitisation rates (Mosser-Ruck et al. 1999, Meunier & Velde 2004).These experimental difficulties add to the different possible mechanisms and hence it is not surprising that a large variation in smectite-to-illite reaction rates and associated activation energies (< 3 – 30 kcal/mol) have been reported. As outlined in Section 2.3.4, part of this variation vanishes when potassium concentration is accounted for in the rate expression, but other factors, not well constrained or understood in the experiments, may also affect reported activation energies.

2.3.3 Influence of temperature

There is overwhelming experimental and natural analogue evidence that temperature is the main parameter affecting illitisation. So far, there is no experimental data available which would demonstrate the formation of "true" illite below 150 °C (Andra 2005).

Given sufficient time and potassium availability, as for example in diagenetic sediment basins, illitisation occurs at temperatures well below 100 °C. There, the illitisation rates show a clear dependence with the thermal gradient. Velde & Vasseur (1992) compared the rates vs. depth for low and high thermal gradient environments. For basins with low gradients (20 – 30 °C/km), a relatively constant increase of illitisation with depth can be deduced. On the other hand, for high gradient basins, illitisation generally shows faster rates with depth, but also a different shape (Fig. 2-5). This has been interpreted as a different type of reaction mechanism, where illitisation in low thermal gradient situations is described by a two-step reaction (see above), whereas in higher temperature gradients (70 – 300 °C) a single reaction better fits the data (Velde & Vasseur 1992, Velde & Lanson 1993).

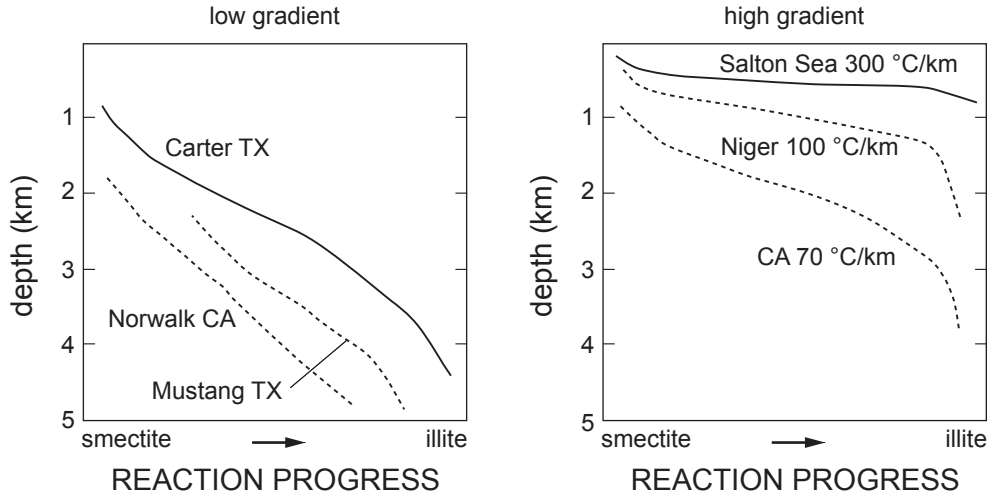

Fig. 2-5: Illitisation rates sketched for sedimentary basins with a low geothermal gradient (left) and a high gradient (right) (from Meunier & Velde 2004) (see text).

It is not clear what the lower temperature range for the smectite-to-illite reaction in diagenetic environments is. Abercrombie et al. (1994) who studied sediment cores in oceanic and sedimentary basins, suggested that illitisation is triggered by the precipitation of quartz and the concomitant lowering of silica activity (Section 3.1). The onset of the quartz precipitation reaction occurs in the temperature range of 40 – 60 °C, which, if Abercombie's hypothesis holds, would be the lower temperature range for the illitisation reaction.

2.3.4 Influence of potassium

Potassium activity exerts a large influence on illitisation rates. The difference in experimental rates obtained can be partly explained by the different potassium activities in the experiments. This has been nicely shown by Meunier & Velde (2004) who compared three well established studies (Whitney & Northrop 1988, Howard & Roy 1985, Roberson & Lahann 1981). Assuming a first order reaction rate with respect to smectite decrease (-dS/dt = kS), the rates were normalised. Fig. 2-6 (left) illustrates the strongly differing smectite decrease rates shown for 250 °C. Consequently, the reported activation energies for these three datasets also vary strongly: 4 kcal/mol (Howard & Roy 1985), 18 kcal/mol (Whitney & Northrop (1988) and 30 kcal/mol (Roberson & Lahann 1981). According to Meunier & Velde (2004) the difference in activation energy may be explained by the different K^+ in the system (K content of solids) (Fig. 2-6, right).

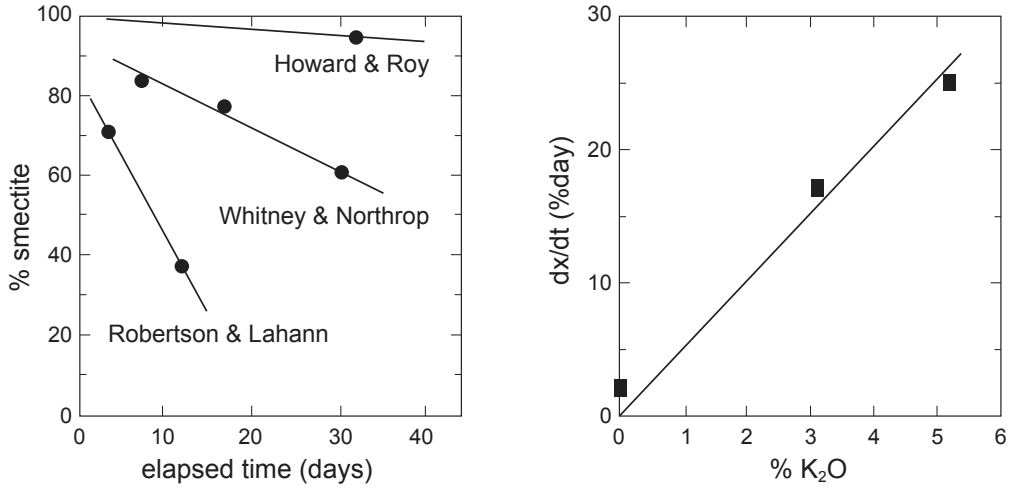

Fig. 2-6: Illitisation degree (shown as % loss smectite) in three different experimental studies at 250 °C (left) and illitisation rate (% illite per day) as function of K content (% K_2O) for the same three studies (right, from Meunier & Velde 2004).

The influence of potassium on the rate was studied by Huang et al. (1993) who described the rate law as function of K^+ concentration and smectite molar fraction in the I/S ML:

$$-\frac{dS}{dt} = k\left[K^+\right]S^2 \tag{4}$$

where S is the smectite molar fraction in %.

Note that this kinetic description assumes a one-step reaction. The activation energy (E_a) has been obtained by Huang et al. (1993) from the Arrhenius relationship with:

$$k = A \cdot \exp(E_a/RT) \quad (5)$$

yielding E_a = 28 kcal/mol and the frequency factor $A = 8.1 \times 10^{-4}$ l s^{-1} mol^{-1}. This formulation takes into account potassium concentration in solution (assumed to be constant), the temperature and time of reaction.

It is worth pointing out that recent reinvestigations of the illitisation process using XRD have shown that the amount of illite formed may be overestimated as certain "smectitic non-expandable layers" are formed which can be made "expandable" by ion exchanging to e.g. calcium (Ferrage et al. 2011). Consequently, there seems to exist a potassium fixation mechanism which should not be confused with "true" illitisation.

2.3.5 Influence of pressure

High pressures stabilise smectite. Eberl & Hower (1977) noted that dioctahedral smectites exposed to a pressure of 2 kbar and temperatures of 400 and 500 °C showed no conversion to illite at all (Na-smectite) or a reduction in conversion rate (K-smectite). Van Groos & Guggenheim (1984) confirmed the stability of Na-smectite at moderate pressures (~ 20 MPa) at 400 °C. Following from this result, the authors suggest that hydrated Na-montmorillonite should be stable if there is no supply of K^+. The results of Colten (1986) supported this hypothesis by noting that Na-smectite with two water layers is a stable complex in the range expected during diagenesis.

2.3.6 Influence of smectite mineralogy

Beidellitic smectites with a high tetrahedral charge have a structure more similar to illite than montmorillonite whose layer charge is predominantly in the octahedral layers. Therefore, transformation of beidellite to illite should be facilitated compared to montmorillonite. This hypothesis is supported mainly by indirect experimental data, where the formation of high-charge smectite as initial product in the illitisation process (e.g. Whitney & Northrop 1988, Beaufort et al. 2001). The transformation rates from glass with a simplified beidellitic composition to illite at temperatures of 260 – 390 °C were studied by Eberl & Hower (1976). The reaction products were I/S ML, kaolinite, quartz and feldspar. Describing the illitisation as first order reaction and assuming Arrhenius-type behaviour the authors deduced an activation energy of about 20 kcal/mol.

Trioctahedral smectites on the other hand appear to be more stable towards illitisation. Eberl et al. (1978), who exposed dioctahedral and trioctahedral smectites to the same alteration conditions, showed that trioctahedral phases were more stable. This was attributed to the lower availability of Al in the lattice compared to dioctahedral smectite. On the other hand, trioctahedral smectites are more prone to chloritisation (see above).

2.3.7 Influence of cations in the interlayer and in solution

As outlined in Section 2.3.2, high K^+ activity enhances illtisation rates. This has been attributed to the lower hydration energy of K^+ compared to other common interlayer cations. In fact, as already stated in Section 2.1, there is correlation between the hydration energy and the required layer charge for dehydrating the cation (Eberl et al. 1978). Hence, the layer charge for dehydrating and fixing K^+ is estimated to be -0.77 (per half-cell) whereas -0.86 is estimated for Na^+.

Lahann & Roberson (1980) postulated that K^+ fixation precedes and favours layer charge increase and that the presence of cations with larger hydration energies (Na^+, Ca^{2+}, Mg^{2+}) slows down this process. On the other hand, Howard & Roy (1985) argue that layer charge increase can occur also in the absence of potassium and is only dependent on temperature. This argument complies with the findings reported in Section 4 of this report.

The illitisation process during burial diagenesis in sandstones and mudstones which occurs in an interbedded sequence in the Niigata basin (Japan) was studied by Niu et al. (2000). The faster rate in mudstone compared that in sandstone was explained by the higher K^+ content of the original smectite material in the mudstone.

It has been shown that divalent cations Ca^{2+} and Mg^{2+} have a stabilising effect. For example, experimental data of Roberson & Lahann (1981) indicate that Ca^{2+} and Mg^{2+} slowed down the conversion of smectite to I/S mixed layers in K^+ rich solutions at temperatures of 270 and 350 °C. The reason thereof was not discussed, but may be related to the preferred selectivity of these cations over K^+. This type of explanation was given by Inoue (1983) for the observed decreased K^+ fixation in the presence of Ca montmorillonite compared to the K variant under hydrothermal conditions (150 and 300 °C). Yau et al. (1987) noted the stabilising effect of $CaCO_3$ preventing the alteration of bentonite at temperatures of 200 and 300 °C for 537 days.

2.3.8 Influence of water activity and transport

Almost all experimental data refer to saturated conditions and low solid/liquid ratios, thus with an easy supply of solutes for the reaction process. Under unsaturated conditions, smectite-to-illite transformation rates are considerably slowed down depending on the saturation state. This was shown by the experimental study of Whitney (1990) indicating retardation of illitisation under unsaturated conditions. The main reason for this result was attributed to the restricted transport of solutes.

The importance of solute (in particular of K^+) transport in affecting illitisation rates is indicated from a number of examples in sediments. Altaner et al. (1984) studied K-rich bentonite beds surrounded by K-rich shales. The contact zones were systematically found to be more illitic and K-rich then the centre of the bentonites. This was explained by slow diffusion of K^+ which limited the transformation (Altaner 1989). Sucha et al. (1993) studied the illitisation reaction in shale and bentonite layers in the eastern part of the Slovac basin. They showed that the I/S series is almost identical in both types of rock, but that for a given depth the illite content is higher in shales than in bentonite, hence pointing to a slower illitisation rate in bentonites.

2.3.9 Compilation of activation energies

Experimental data

Given the large variety in experimental conditions and the aspects discussed above, it is not surprising that the reported activation energies for the smectite-to-illite reaction vary considerably. These are compiled in Tab. 2-1 for selected experimental studies which assumed a one-step reaction process and an Arrhenius-type relationship (see e.g. eq. (5)). It is worth noting that the derived activation energies depend on assumed frequency factors, but these unfortunately are generally not reported in the original references. In spite of this deficiency, interesting features can be deduced from this compilation.

Tab. 2-1: Selected data of smectite-to-illite reaction experiments.

Starting material	**Temperatures** [°C]	**Activation energy** [kcal/mol]	**Authors**
I/S (random) purified from Spanish bentonite	60 – 200	7	Cuadros & Linares (1996)
K-saturated Wyoming montmorillonite	250 – 400	6	Ferrage et al. (2011)
K-saturated purified Wyoming bentonite	150 – 250	4	Howard & Roy (1985)
K-saturated purified Wyoming bentonite	250 – 450	18	Whitney & Northrop (1988) (calc. Meunier & Velde 2004)
Montmorillonite	270 – 350	30	Roberson & Lahann (1981)
Na-montmorillonite (SWy-1)	250 – 325	28	Huang et al. (1993)
Smectite purified from claystone	180 – 350	33	Roaldset et al. (1998)
Synthetic beidellite	152 – 393	20	Eberl & Hower (1976)

The activation energies vary between 4 and 33 kcal/mol, about one order of magnitude. Inspection of the starting materials suggests that lower values are partly related to high K^+ activities (Ferrage et al. 2011, Howard & Roy 1985) or intermediate values (Whitney & Northrop 1988), as proposed by Meunier & Velde (2004) (see above). The low activation energy obtained by Cuadros & Linares (1996) on the other hand cannot be explained by this, because variable K^+ concentrations were used in those experiments and accounted for in the rate equation. It might be due to the different starting material (I/S ML with about 15 % illite) relative to the other studies. Also, it should be pointed out that the reliability of the determined illitisation rates, obtained indirectly by Si release measurements, has been questioned (Karnland & Birgersson 2006).

The experimental data with higher activation energies (28 – 33 kcal/mol) refer to low potassium systems (Lahann & Roberson 1981, Roaldset et al. 1998) or to variable K^+ content (Huang et al. 1993). The latter study in fact indicated a linear dependence of the K^+ concentration on illitisation rates. It has been proposed that activation energies of ~ 30 kcal/mol represent energies necessary for breaking Si-O and Al-O bonds (Meunier 2005). The value of 20 kcal/mol for synthetic beidellite is somewhere between the high and low activation energies.

Modelling of natural smectite/illite systems

Smectite transformation rates in natural sediments have been modelled using Arrhenius-type rate expressions by a number of authors (Bethke & Altaner 1986, Pytte & Reynolds 1989, Velde & Vasseur 1992, Elliot et al. 1991, Pusch & Madsen 1995, Esposito & Whitney 1995, Kamei et al. 2005). The activation energies derived from these modelling studies and listed in Tab. 2-2 are rather high, in the range of roughly 20 – 30 kcal/mol. Note that the studies of Velde & Vasseur (1992) and Esposito & Whitney (1995) assume a two-step reaction progress contrary to the others with a one-step reaction.

Tab. 2-2: Activation energies applied in modelling studies to simulate illitisation.

Type of rock/environment	**Max. temperatures** [°C]	**Activation energy** [kcal/mol]	**Authors**
K-bentonites (Kinnekule bentonites, Ordovician)	140	25 – 27	Pusch & Madsen (1995)
Shales, mudstones & sanstones in contact metamorphic zone (SW Washington)	Not given	27 & 7	Esposito & Whitney (1995)
Shales in contact metamorphic zone (Pierre Shale)	250	33	Pytte & Reynolds (1989)
Shales in geothermal field (Salton Sea)	200	28	Velde & Lanson (1993) (reported in Meunier & Velde 2004)
Diagenetic mudstones (Paris Basin)	~ 150	27 & 9	Velde & Vasseur (1992)
Diagenetic mudstones	~ 150	18 – 24	Bethke & Altaner (1986)
Bentonites (Mowry and Niobrara)	150 – 200	30	Elliot et al. (1991)
Tertiary argillaceous rock/quaternary intrusive rock	270	25.6	Kamei et al. (2005)

$$\frac{dS}{dt} = -k_1 S \text{ with } \log k_1 = \log A_1 - \frac{E_{a1}}{RT} \tag{6}$$

And second reaction involving the formation of regular I/S (R1) with 50 – 100 % illite:

$$\frac{dM}{dt} = -k_1 S - k_2 M \text{ with } \log k_2 = \log A_2 - \frac{E_{a2}}{RT} \tag{7}$$

where M is the content of illite in %. Note that this kinetic model does not account for K^+ activity.

Most of the modelling studies shown in Tab. 2-2 (Pusch & Madsen 1995, Pytte & Reynolds 1989, Bethke & Altaner 1986, Elliot et al. 1991) are based on the multi-parameter kinetic models of Pytte (1982):

$$\frac{dS}{dt} = -kS^a \frac{[K^+]^b}{[Na^+]}$$

$$\text{with } k = A\exp(\frac{-E_a}{RT}) \tag{8}$$

Generally, the best fits were obtained assuming a = 4 – 6 and b = 1.

Altaner (1989) extended Pytte's model by including K^+ diffusion and applied it to thin beds of K-bentonites of Western Montana. He could simulate the zonation within the bentonite beds which display an increasing illite content towards the rims reasonably well. The results indicated that diffusion of K^+ derived from the surrounding shales was an important constraint for illitisation rates. Furthermore, results suggested times of 7 – 9 million years at temperatures of about 80 – 90 °C.

The kinetic models of Huang et al. (1993), Pytte (1982) and Velde & Vasseur (1992) were applied by Elliot & Matisoff (1996) to four different geologic settings (Denver Basin, Gulf Coast, the Salton Sea Geothermal System, and Paris Basin). The model results were compared with measured illite contents and K/Ar ages. None of the models was successful in simulating the data in all four basins. With the Huang model, the Salton Sea and to lesser extent, the Gulf Coast data could be adequately described. The two other models yielded satisfactory results only for the Denver basin. In general, the model of Huang which is the only one based on experimental data, appears to be promising for simulating basins exposed to high temperature gradients and smectites exposed short thermal pulses (Meunier & Velde 2004).

In summary, modelling studies on natural sediments suggest that illitisation is a slow process and more adequately described by high activation energies (20 – 30 kcal/mol) rather than by lower values reported in literature.

2.4 Implications for the bentonite buffer

2.4.1 Summary considerations based on literature data

First the main points drawn from the above section are summarised:

- The transformation of smectite-to-illite is induced by increasing temperature. The conversion process is complex and still not completely understood. It displays slow kinetics over a wide range of environmental conditions.
- Besides temperature and time, potassium activity strongly affects kinetic rates of the smectite-to-illite reaction. Further relevant variables are the composition of the smectite, the concentrations of cations, pressure, water saturation state and mass transfer constraints.
- Experimentally determined illitisation rates span a large range which is also manifested by differences in activation energies. Part of these differences may be explained by difference in K^+ activities in the experiments.
- Systematic studies which include variations of K^+ activities are rare. Exceptions are the studies of Huang et al. (1993) and Cuadros & Linares (1996). The data from these two studies show contrasting rates and activation energies. The reasons for these differences are not obvious, but might be related to the different composition of the starting smecite materials. Moreover, the data of the Cuadros & Linares study appear to somewhat doubtful because illitisation rates are entirely based on Si release data (see above).
- Modelling studies of natural smectitic sediments (including bentonites) in a variety of environmental settings generally lend support to slow kinetic rates with large activation energies. Thus, this indirectly supports experimentally determined rates pointing to high activation energies (20 – 30 kcal/mol), such as that derived by Huang et al. (1993).
- Modelling of natural thin bentonitic beds surrounded by rocks with higher permeability indicate the importance of K^+ diffusion limiting illitisation. This is in contrast to large sedimentary basins which can be approximated as "closed" systems (Meunier & Velde 2004).

What does this mean for buffer exposed to the initial thermal period? As indicated by Meunier & Velde (2004), geological settings in which smectitic sediments are exposed to "short" thermal periods, illitisation can be probably described by a single step process, rather than a two-step one. Such environments include for example sediments contacting hydrothermal veins, or sedimentary basins with a large geothermal gradient (e.g. Salton Sea). These have been modelled a single type reaction process and activation energies > 20 kcal/mol. The kinetic data of Huang et al. (1993) appears to yield fairly consistent results for such environments contrary to the data of Cuadros & Linares (1996) which would predict too fast illitisation rates.

It should be pointed out that applying Huang's model or that of Pytte to the repository conditions in the KBS-3 concept yields negligible illitisation, as shown for example by Karnland & Birgersson (2006). This is because of the low temperatures (< 100 °C) and short duration of the thermal pulse (< 1'000 years). Moreover, in such considerations the supply of K^+ is assumed to be instantaneous, thus the diffusional constraint is neglected. In addition, saturated conditions are implicitly assumed, although many deposition holes are expected to experience unsaturated conditions for hundreds of years. Thus, kinetic reaction models, such as that of Huang & Pytte can be considered to be based on conservative assumptions with regard to the near-field situation.

The down side of above models (and also analogues exposed to a thermal event) is that they are based on high temperature data far beyond those expected in the near-field. This raises the question of the appropriateness of extrapolating reaction mechanism(s) (Meunier et al. 1998). The problem is that there do not seem to be any adequate experimental data or natural analogues representing similar conditions as those experiences by the buffer. Hence, calculations based on high temperature data can be regarded at best as bounding estimates rather than as quantitative predictions. Given the boundary conditions (low mass transfer constrained by diffusion, partly saturated conditions) in the buffer, such estimates on illitisation or smectite loss rates should be on the safe side. On the other hand, uncertainty remains concerning the initial process of illitisation, such as potential increase in layer charge with or without montmorillonite dissolution.

2.4.2 Transport limitation

Recently an assessment was performed where the transport aspect of possible mineral transformation in a KBS-3 buffer was investigated (Birgersson *in prep.*). Disregarding thermodynamic (chemical stability) and kinetic (rate) limitations of transformation, a KBS-3 buffer still needs to exchange substantial amounts of matter with the ground water in order to be transformed. Thus, since the KBS-3 buffer is so dense that diffusive processes dominate mass transfer, and since the interaction with the ground water (at most) only occurs in a limited set of thin fractures, possible transformation processes may be strongly restricted. This is particularly true for montmorillonite transformation as the solubilities certainly are small, thus limiting diffusive flux (in addition to the lowered diffusivity in the buffer). This notion was confirmed in the modelling performed by Birgersson (*in prep.*) – a simplified chemical model was defined and solved numerically which, however, treated the transport part of the process rather realistically (i.e. it included the transport restrictions described above). The resulting mineral transformations of the base case defined in Birgersson (*in prep.*) are shown in Fig. 2-7.

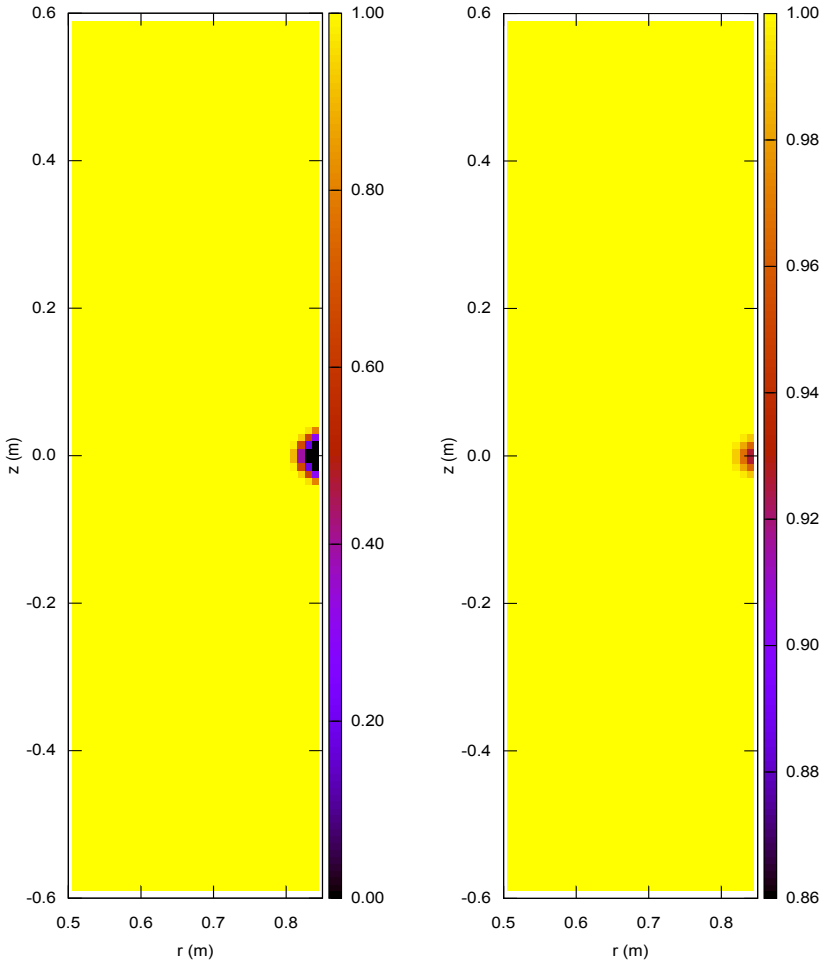

Fig. 2-7: The extent of transformation of the bentonite buffer in a KBS-3 deposition hole after 100'000 years of interaction with the ground water as modelled in (Birgersson *in prep.*).

The model assumes that the buffer is intersected by a single fracture of width 0.1 mm at mid height (z = 0 m), a diffusivity of 10^{-11} m^2/s in the buffer, a solubility of the (generic) buffer material of 2 mM, and that 30 % of the buffer material is soluble. The left plot shows the extent of soluble material left (1 corresponds to unchanged buffer, 0 corresponds to 30 % dissolved), the right plot shows the corresponding pore water concentration (1 corresponds to 2 mM, 0 to 0 mM).

This modelling exercise thus shows that montmorillonite transformation in a KBS-3 environment may be assessed without considering details regarding the actual chemical processes (basically only the equilibrium solubility is used as input); the transport restriction constituted by thin fractures in contact with the buffer leads in itself to rather limited transformation of the bentonite, as shown in Fig. 2-7. Note, however, that this study does not cover the scenario where transformation is assumed to occur internally in the buffer, i.e. when there is no need for interaction with the ground water.

3 Smectite-to-illite conversion: hydrothermal experiments with MX-80 bentonite at 270 °C and variable potassium activity conditions

3.1 Objectives and design of experiments

Objectives

The principle objective of this study was to perform hydrothermal "illitisation" experiments at temperature conditions where previous studies did observe some degree of smectite-to-illite conversion under certain chemical conditions close to 300 ºC, and to see if these findings can be better constrained in terms of different chemical conditions and experimental duration. A further objective is to use state-of-the-art X-ray analytical procedures in order to confirm either the absence or presence of significant formation of illite in the experiments.

MX-80 bentonite

MX-80 bentonite ("Wyoming bentonite") was used for all experiments. There have been several studies on MX-80 raw material (e.g. Karnland et al. 2006) and thus the composition is rather well known. Karnland et al. (2006) quantified mineral content by the Rietveld method using powder XRD, and the composition and stoichiometry of montmorillonite was determined with a structural formula of a 2:1 clay and data obtained by acid digestion and ICP/AES analysis. According to Karnland et al. (2006) the most abundant mineral phases in MX-80 are: montmorillonite (> 80 %), plagioclase (~ 3 %), quartz (~ 2.8 %), and minor muscovite, illite, tridymite, cristobalite. The MX-80 bentonite is blended in order to obtain a constant quality. Other reported accessory minerals include microcline, orthoclase, calcite, gypsum, pyrite, goethite, lepidocrocite and anatase in quantities of up to one or two percent.

Smectite-to-illite conversion

Different mechanisms may contribute to illitisation of smectite, namely solid-state transformation (layer-by-layer replacement) and dissolution-precipitation mechanisms. Solid-state transformation preserves the overall clay content but requires Al and K and releases Si and the exchanger cations. In a closed system, the Al and K may be derived from accessory phases (K-feldspar), and the release of Si will lead to silica formation. For dissolution-precipitation, the Al and also some K may be supplied by consuming primary clay. Formation of silica is also a feature of this process.

The following equation is approximately balanced on a montmorillonite clay formula (mont), conserving Al in solids, using K-feldspar (Kfsp) as source for potassium, and it is for the case of a solid-state transformation (gib = gibbsite):

$$1\ \text{mont} + 2\ \text{Kfsp} + 0.93\ H^+ = 1\ \text{illite} + 1\ \text{gib} + 4\ SiO_2 + 0.85\ Na^+ + 0.04\ Ca^{2+}$$

This equation shows that the process may be limited by the availability of a potassium source (e.g. K-feldspar) and substantial amounts of silica will precipitate. One may also derive from the above relationship that illitisation most likely proceeds at silica-saturated conditions (quartz, cristobalite, amorphous silica), and likely also at saturation with respect to an Al-bearing phase (gibbsite, K-feldspar, smectite). The potassium activity would be buffered in this case near mutual equilibrium with K-feldspar and illite. Remaining variables are pH and the activities of Na and Ca.

Design of the experiments

Different pore water compositions, varying in potassium concentration among other differences, were equilibrated with aliquots of MX-80 bentonite, and batch experiments were performed with these materials at 270 °C for variable lengths of time. One of the pore water compositions was that of typical "granite" pore water specified by Posiva and this served as a reference case. Bentonite starting materials were either fine grained raw MX-80 bentonite, or sodium homo-ionised and partly purified MX-80 bentonite. K-feldspar powder was added to some charges to provide a solid source for potassium.

This design included an unrealistic case in the presence of 0.1 m KCl solution with Na-exchanged bentonite pre-equilibrated with the KCl solution. It included a "realistic" case with raw MX-80 bentonite pre-equilibrated with a synthetic "granite" pore water solution and reacted in this solution. It also included a case with purified MX-80 bentonite (removal of most accessory minerals) with added powdered K-feldspar as a solid source for potassium and reacted in a "granite" solution. The latter was also a "realistic" case but with better defined geo-chemical boundary conditions.

The reacted bentonite was examined by XRD methods. NEWMOD was used (Reynolds & Reynolds 1995) to model a series of illite/smectite X-ray patterns with variable I/S ratios. The degree of illitisation was then quantified by applying a calibration to the computed patterns using the peak distance method of Reynolds & Moore (1989).

3.2 Materials and methods

3.2.1 Overview of the experimental procedures

The details of sample preparation are explained in this section. The following helps to keep an overview of the procedures.

- Two different starting materials were used: raw MX-80 bentonite and Na-exchanged partially purified MX-80 bentonite.
- Two different solutions were used: a synthetic "granite" groundwater and a 0.1 m KCl solution to provide an elevated potassium activity.
- Combining the above, three different starting conditions were used: raw MX-80 and Na-exchanged MX-80 pre-equilibrated with a granite-type solution, and Na-exchanged MX-80 pre-equilibrated with a 0.1 m KCl solution.
- The pre-equilibrated starting materials were reacted in their respective solutions, with liquid/solid ratio near 20.
- All experiments were performed at 270 °C and continuously agitated (end-over-end rotation).
- Four different experimental durations were used: 10, 25, 45 and 137 days.
- Two experimental series were carried out: a test series with 4 titanium autoclaves for 25 days (experiment labels S2-S5), and a main series with 10 autoclaves (experiment labels K1-K8, GA, GB).
- Preparation for XRD analysis included a number of procedures, including fine fraction separation and ion exchange with Ca (test series only), Mg and Sr (main series).

3.2.2 Equipment

All experiments were carried out in thick-walled titanium autoclaves with titanium closures and a titanium sealing ring (Fig. 3-1). The standard containers have an internal volume of 40 ml, and two longer autoclaves have a volume of 100 ml. The containers and sealing system were all fabricated in-house.

The autoclaves were mounted onto a rotary system inside a standard laboratory furnace built for operation at 300 °C (Fig. 3-1). The rotary system was built in-house, and is driven by a gear motor mounted externally. The rotation axis is mounted horizontally held by high-temperature bearings. The autoclaves are mounted radially to the rotation axis, four per segment to balance the load, and up to 16 autoclaves can be accommodated. The slow rotation motion (10 – 20 s per turn) induces an end-over-end agitation and ensures thorough mixing conditions.

Fig. 3-1: Details of titanium autoclaves (left), mounting arrangement of autoclaves in the oven (middle), and oven with external motor drive for the rotation system (right).

3.2.3 Methods

Preparation of MX-80 bentonite starting material

Industrially prepared MX-80 was used as initial material. It was dried at 50 °C for two days and afterwards mechanically ground to a maximum particle size of 1 mm. Larger hard grains were removed, softer grains were gently crushed to a smaller size.

This starting material was used for all differently prepared fractions used for the experiments as detailed below.

Preparation of MX-80 Na-saturated homo-ionic clay

MX-80 bentonite starting material was further processed in such a way that all interlayer cations were replaced by Na^+. This was done by applying a series of treatments to 12 sub-samples in parallel as outlined below, that yielded a total of ca. 90 g of dry material:

- MX-80 starting material was dispersed in 500 ml 1 M NaCl-solution and stirred with a glass rod (called *saturation*). The suspension was left to settle and the supernatant was removed. The addition of 1 M NaCl-solution, stirring, settling and decanting was repeated three times.

- Thereafter, the material was washed by adding de-ionised water followed by centrifugation for 10 minutes at 4'500 rpm and decanting (called *washing*). Addition of water, centrifugation and decanting was repeated three times.
- The remaining slurry except for the sedimented coarsest material was transferred into dialysis membranes (ZelluTrans/Roth Dialysiermembranen T3: MWCO 12'000 – 14'000) which were placed in 5-liter plastic containers with de-ionised water. The water outside the membrane was changed daily until the electrical conductivity had stabilised below 10 µS/cm (called *dialysis*).
- Thereafter, the sample was dispersed by three times four minutes of ultrasonic treatment. It was transferred to an Atterberg cylinder for 16.5 hours in order to separate the clay fraction > 2 µm. The sedimentation height was 22.5 cm at a temperature of 22 °C. The remaining fraction at the bottom of the cylinder was removed.

Hydrochloric acid for coagulation was added in some samples when needed.

The process of *Saturation*, *Washing* and *Dialysis* was repeated a second time for most samples. A second Atterberg separation was only applied to one of the sub-sample, and this one was not used was (not added to the bulk). All samples were dried in an oven at 50 °C afterwards (*Drying*). The merged sample was called "*MX-80 Na-sat*".

Composition and preparation of solutions

The composition of the synthetic pore water had been specified by Posiva. It was meant to represent a typical pore water in a granite host rock relevant for the planned Finnish repository. A recipe was calculated based on the given specifications (Tab. 3-1). The solution was made from *pro analysi* grade chemicals, combining sub-solutions of Ca-Cl, Mg-Cl and the Alkali salts.

Tab. 3-1: Recipe for the synthetic "granite" pore water.

Chemical component	**Amount** [g/kg_{H2O}]
NaCl	6.735
KCl	0.021
$CaCl_2 \cdot 2H_2O$	4.794
$MgCl_2 \cdot 6H_2O$	0.524
Na_2SO_4	0.03
$NaHCO_3$	0.029

The second solution used was a 0.1 normal KCl solution prepared from *pro analysi* grade KCl. The concentration in this solution is 3.91 g/l of K^+ or 7.46 g/l of KCl. It is 355 times more concentrated in K^+ compared to the "granite" pore water.

Preparation of bentonite starting materials

Three types of bentonite starting materials were prepared that represent a *realistic* case, another *solid-source-potassium* case with a solid source for potassium added, and a *high-potassium* case. Potassium content in the interlayer space and its concentration in the associated solution is known to be an important controlling factor for the reaction progress of the montmorillonite-to-illite conversion:

1. *Realistic case* (potassium in equilibrium with the synthetic pore water): MX-80 bentonite saturated with the synthetic "granite" pore water. This brings an inventory of potassium on the exchanger in equilibrium with the synthetic pore water. In addition, there will be minor accessory minerals present that contain potassium, such as K-feldspar and muscovite/illite. This starting material is called *I3* or referenced as "*MX-80 raw*".
2. *Solid-source-potassium case:* Na-exchanged MX-80 saturated with synthetic pore water. There will be an inventory of potassium on the exchanger in equilibrium with the synthetic pore water. Accessory minerals such as K-feldspar were largely removed during the homo-ionisation process and clay separation. Ground K-feldspar will be added later (see below). This starting material is called *I2* or referenced as "*Na-Bent*".
3. *High-potassium case:* Na-exchanged MX-80 saturated with potassium chloride solution (KCl 0.1 N). This represents an unrealistic condition meant to force the illitisation processes. This staring material is called *I5* or referenced as "*K-Bent*".

Saturation was done by adding the dry bentonite (*MX-80* and *MX-80 Na-sat*) to 500 ml of solution (synthetic "granite" pore water or = 0.1 N KCl) while stirring with a glass rod. The material was left settling for 30 minutes. Afterwards, the bentonite was centrifuged to accumulate the bentonite at the bottom of the vials. The supernatant solution was then poured off. Saturation and centrifugation was repeated three times.

Thereafter the bentonite was washed by filling the vials with de-ionised water followed by centrifugation and decanting. Washing was also repeated three times. The materials were again dried at 50 °C in order to obtain a dry reference mass for the experimental charges produced later on.

It should be noted that this pre-equilibration step ensures a known amount of potassium to be on the exchanger. It also ensures that when experimental charges are prepared with synthetic solutions the exchanger and the solution do not react to an unknown distribution of potassium between the exchanger and the solution, and thus uncertain initial conditions.

Preparation of experimental charges

Starting materials (see above) and dry MX-80 bentonite were used to prepare starting mixes to be filled into the titanium autoclaves. The autoclaves can hold up to 40 ml of sample. The mixes were prepared as follows.

- "MX-80 raw" bentonite (I3) was combined with synthetic pore water at a solid-liquid ratio of ca. 1/20.
- "Na-Bent" (I2) was combined with synthetic pore water at a solid-liquid ratio of 1/20. Additionally, 0.3 grams of pure and ground potassium feldspar was added to the charges to provide a solid source for potassium.
- "K-Bent" (I5) was combined with potassium chloride solution (KCl 0.1 N) at a solid-liquid ratio of 1/20.

- An additional charge was prepared consisting of dry MX-80 bentonite as a test case.
- Two titanium autoclaves are larger (100 ml), and more sample mix was prepared for these, accordingly.

The prepared mixes were transferred into titanium autoclaves which were closed and sealed by a titanium sealing ring. A list of all experiments and their charges and conditions is provided in Tab. 3-2.

Tab. 3-2: List of experiments, charges and conditions, all at 270 °C.

Note: (1) Samples S2 – S5 belong to the test series, others to the main series of experiments; (2) the bentonite types are explained above; (3) ground K-feldspar was added as solid source to the experiments with Na-bentonite; (4) the solutions are detailed in Tab. 3-1.

Run (1)	**Bentonite type** (2)	**Additives** (3)	**Solution** (4)	**S/L** [g/g]	**Duration** [days]
S2	Na-Bent	0.3 g Kfsp	"granite"	1/20	24.9
S3	MX-80-raw		"granite"	1/20	24.9
S4	MX-80		dry		24.9
S5	K-Bent		KCl 0.1 N	1/20	24.9
K1	K-Bent		KCl 0.1 N	1/20	10
K2	K-Bent		KCl 0.1 N	1/20	45
K3	MX-80-raw		"granite"	1/20	10
K4	MX-80-raw		"granite"	1/20	137
K5	MX-80-raw		"granite"	1/20	45
GA	MX-80-raw		"granite"	1/20	137
K6	Na-Bent	0.3 g Kfsp	"granite"	1/20	10
K7	Na-Bent	0.3 g Kfsp	"granite"	1/20	137
K8	Na-Bent	0.3 g Kfsp	"granite"	1/20	45
GB	Na-Bent	0.3 g Kfsp	"granite"	1/20	137

Physical conditions for the hydrothermal experiments

The titanium autoclaves were installed in an oven containing a horizontal rotation axis. The autoclaves are mounted radially, with the lids towards the rotation axis. An external motor drive kept the bucket autoclaves in constant motion like in an end-over-end shaker. Selected autoclaves were removed after the desired run times and opened. Any supernatant solution was decanted and filtered, and the charges were removed, centrifuged, decanted and the supernatant filtered. The solid material was saved for further processing as detailed below.

A test run (*Test*) was performed with 4 autoclaves at 270 °C and 24.9 days duration. These experiments were named S2, S3, S4 and S5.

The main run (*Series 1*) was done with 10 autoclaves for 10, 45 and 137 days. These experiments were named K1, ..., K8, GA and GB (see also Fig. 3-1).

The experimental charges contained initially a small volume of air. This ensured that the experiments developed a pressure along the saturated steam curve that also depended to a minor extent on the salinity of the system. This also ensured that no uncontrolled overpressures could develop that would result in a leaky system.

Preparation of ion-exchanged (Ca, Mg, Sr) samples for XRD analysis

Bentonite samples extracted from the autoclaves were saturated with Ca^{2+}, Mg^{2+} or Sr^{2+} before oriented mounts were produced for XRD analysis.

A sample was added to a 40 ml vial, topped with 2N ammonia solution, followed by ultrasonic treatment for three minutes for dispersion. 250 ml of $CaCl_2$ (2N), $MgCl_2$ (0.5N) or $SrCl_2$ (0.5N) was added, respectively. The solution was left for 30 minutes and was occasionally stirred with a glass rod. Afterwards, it was centrifuged and the supernatant solution was decanted. Filling with 250 ml of solution and centrifugation was applied three times. Finally the bentonite was washed. Washing was done with de-ionised water and centrifugation afterwards, again repeated three times.

Preparation of oriented mounts for XRD analysis

The saturated (homo-ionic) sample was transferred into a 40 ml vial and filled with distilled water. Ultrasonic treatment was applied for two minutes. The solution was then pipetted onto two sample mounts (labeled x and z) and left for air-drying.

The oriented mounts were then X-ray scanned with a step size of 0.02° from 2 to 40 °2θ. A fixed divergence slit was used with a copper (Cu) anode. The generator setting was 40 mA at 30 kV. Air dried mounts (x-samples) were scanned at a room temperature of 23 °C. Ethylene glycolated (EG) mounts were produced by using the x-samples which were left in an EG-environment over night at 50 °C. They were scanned immediately after removing from this environment. Z-samples were heat treated in a furnace for 1.5 hours at 550 °C before scanning.

3.2.4 Mixed-layer clay quantification by computed XRD patterns

Introduction: montmorillonite properties and XRD patterns

A clay mineral is named by listing the species with the smallest d (001) first and additional names separated with a slash (for example I/S). A reflection pair of this mineral that is made up of the illite 002 and smectite 003 peaks is labelled 002/003 (meaning the peaks of I002 and S003). For EG solvated conditions the reflection near 16 °2Θ is designated as the illite/EG-smectite 002/003 reflection. This is illustrated in Fig. 3-2, where computed XRD patterns for illite and smectite are shown.

The coefficient of variation (CV) is an index for the stacking sequence of two mineral structures. A value below 0.75 % means that the stacking sequence is very regular and that the mineral qualifies for a name of its own (for example corrensite which is made up of 50/50 layers of chlorite and smectite).

For measuring absolute peak positions one needs to normalise the positions. One may use the position of the quartz peak to shift a pattern in order to obtain positions that are directly comparable. To counteract the problem of pattern shift one may also measure the distance between two diffraction peaks (recommended is 002/003 – 001/002).

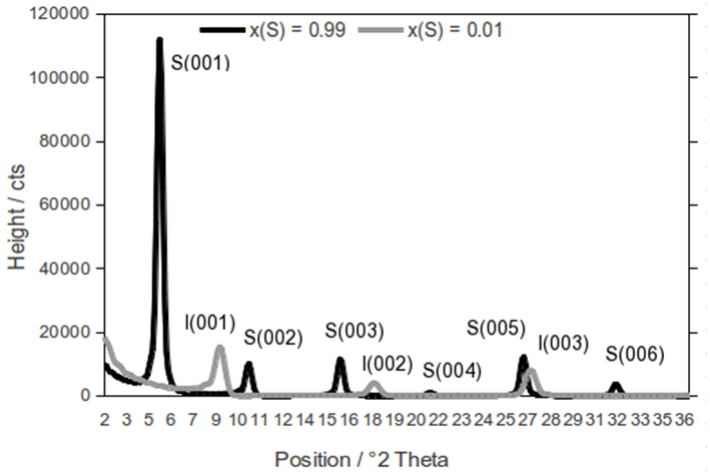

Fig. 3-2: XRD pattern of an illite and smectite clay mixture computed with NEWMOD (Reynolds & Reynolds 1995).

x(S) = 0.99 is pure smectite (black curve), and x(S) = 0.01 is illite (grey curve).

A good way to approach quantification by peak position is to use air-dried and EG-solvated sample preparation. For patterns from air-dried condition it is assumed that a smectite interlayer contains two layers of water molecules coordinated around the exchangeable cations. Note that the basal spacing is fairly sensitive to ambient humidity variations and the type of exchangeable cation. One should therefore control humidity for air-dried preparation.

If one wants to work with a single reflection, the peak near 17 °2Θ is best suited (I002, S003), correcting for pattern shift as discussed above. The peak near 9° is more sensitive to shifts caused by the presence of small crystallites.

The Reichweite factor R is determined by the position of the (001) reflection between 5 and 9 °2Θ. A reflection located at 5° indicates a random inter-stratification (R0) and one near 6.5 ° indicates R1 ordering. To make it easier to estimate R, one may consider the results from Blanc et al. (1997). These authors specify the following ordering types: R0 = disordered type, R1 = first neighbour ordered type, R2 = second neighbour ordered type and R3 = third neighbour ordered type. A transition from R0 to R1 occurs when the illite fraction reaches about 0.6. It is not certain if an ordering of type R2 really exists in natural samples. It is observed that the ordering type changes to R3 at a ratio of 0.85 illite.

Spacing between basal peaks and calibration

The distance between the positions of basal reflections 001/002 and 002/003 was used. XRD patterns of mixtures with several different illite proportions were computed with NEWMOD (Reynolds & Reynolds 1995). The distance between the designated two peaks were then measured at the positions of highest intensity. Peak positions were identified manually and this introduces an uncertainty of ± 0.01 °2Θ. A reference table was assembled in this manner for Sr-saturated I/S mixed layer minerals (Tab. 3-3). The Reichweite factor (R) has been set according to Reynolds & Moore (1989). A DISMECTITE-2GLY (meaning ethylene glycolated dioctahedral smectite) was taken as substitute for saturated montmorillonite. Illite was represented by DIMICA (meaning dioctahedral mica). The ratio of iron was set to 0.1 (for smectite as well as for illite) and the ratio of potassium in DIMICA was set to 0.7.

Tab. 3-3: Reference table for quantifying illite content in glycolated illite/smectite.

Note: Data were generated with NEWMOD (see text). Uncertainty in peak position is ± 0.01 °2Θ.

%-Illite	**R**	**001/002** [2Θ]	**002/003** [2Θ]	**°Δ2θ**
0	0	10.45	15.74	5.29
1	0	10.44	15.74	5.30
5	0	10.42	15.78	5.36
10	0	10.37	15.82	5.45
15	0	10.32	15.87	5.55
20	0	10.27	15.91	5.64
30	0	10.17	16.02	5.85
40	0	10.03	16.16	6.13
50	0	9.86	16.33	6.47
60	1	9.69	16.64	6.95
70	1	9.51	16.83	7.32
80	1	9.28	17.11	7.83
90	3	9.05	17.42	8.37

Tab. 3-3 shows the position and d-spacing between the basal peaks 001/002 and 002/003. Karnland et al. (2006) estimated the illite ratio by means of ICP/AES analysis of digested purified samples. They calculated the ratio of illite in the 2:1 clay mineral of Wyoming MX-80 raw material to 0.01. Results from the current study show a mean peak distance of 5.30 °Δ2Θ for raw MX-80 in its initial state. We assumed that this mean distance corresponds to the calculated ratio of 0.01 illite and calibrated the NEWMOD patterns to this value. Optimisation had been done by varying the layer thicknesses of the 2:1 clay aggregates. Best fits have been obtained by using evenly dispersed aggregates with a thickness between 3 and 24 N (layers).

XRD patterns were also generated for Ca, Sr as well as Mg saturated 2:1 clay minerals. They all showed the same distances between peaks at a certain illite content. The identity of the inter-layer cation does not affect the distance between the 001/002 and 002/003 peaks, but it does affect their intensities. An additional calibration curve has been calculated for evenly dispersed aggregates with a thickness of 3 – 14 N (layers). The resulting curve displays the same shape as the curve calculated for thicknesses between 3 – 24 N. The difference between the two calibrations is a shift of +0.03 °2Θ for the curve with smaller aggregate thicknesses (3 – 14 N). Data and the calibration curve for 3 – 24 N are shown in Fig. 3-3.

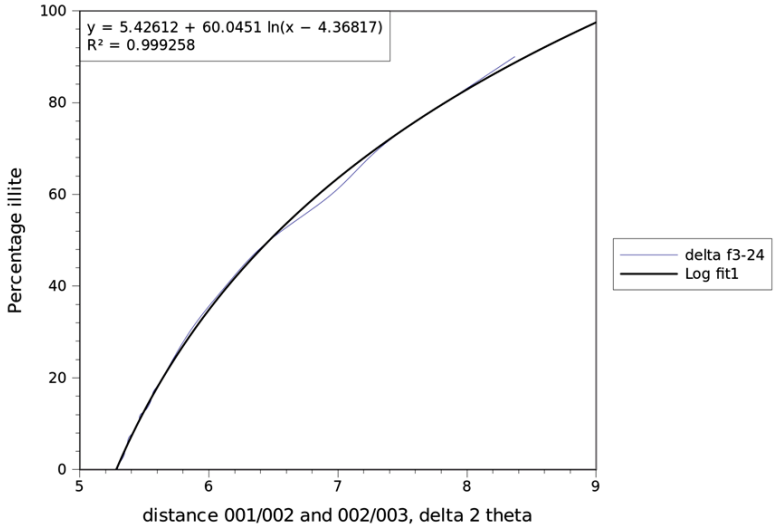

Fig. 3-3: Calibration curve for illite content in I/S using computed XRD patterns and data from Tab. 3-3.

Curve "delta f3-24" connects data points computed for layer thicknesses of 3 – 24 N. Curve "Log fit1" is a logarithmic fit to the data using the equation displayed on the upper left corner. The irregularity visible at 60 – 70 % illite content is due to a change in the R factor (Tab. 3-3).

Discussion

We assessed that an exchange of interlayer cations affects the peak intensities only but not the difference in d-spacing between 001/002 and 002/003 peaks. The calculated calibration curve (Fig. 3-3) for peak distances can therefore be used independent of the substituted interlayer cation. We also conclude that it is precarious to use a possible alternative method of peak area for 2:1 clays due to the substantial variation in peak intensity depending on the interlayer cation.

The variation of aggregate thicknesses and their distribution has an impact on °Δ2Θ. Thin aggregates produce larger °Δ2Θ values compared to thicker layer aggregates. A typical X-Ray pattern for thin aggregates shows peaks with broad shoulders and low maximum intensities, whereas thick-layer aggregates cause peaks with narrow shoulders and relatively high intensities. Nevertheless, the evolution of °Δ2Θ for thin-layer and thick-layer aggregates with increasing illite content are very similar. The curve constructed from Tab. 3-3 and shown in Fig. 3-3 has the same shape, but it is shifted to the left along the x-axis for thick-layer aggregates (lower °Δ2Θ values). Hence, one does not need to re-compute the calibration curve for different aggregate thicknesses.

In order to adapt the curve to a given type of 2:1 clay sample, one needs to know the initial illite content of the clay independently. The calibration curve is simply shifted along the x-axis until it crosses the calculated °Δ2Θ at the given illite content. This shift may even be used as an indicator for the composition of the clay aggregates. The calibration curve in Fig. 3-3 is adjusted to the 2:1 clay of raw MX-80 bentonite with an aggregate fraction < 2 µm. We assumed an illite content of 1 % for raw MX-80, adopted from analytical data of Karnland et al. (2006).

3.3 Results

3.3.1 XRD peak distance quantification of homo-ionised samples

The X'Pert Data Viewer was used for distance measurements. Peak positions were identified on raw XRD-patterns by using automatic peak recognition of the software. Mean values were taken for samples that were scanned several times. The method of peak distance was applied to ethylene glycolated samples only. The I/S peaks 001/002 and 002/003 were used and measured distances in 2- theta between these pairs of peaks (°Δ2Θ). Measurement uncertainty is estimated to ± 0.03 °2Θ. This value is based on measurements from Series 1 samples by comparing individual values to mean values. The results are summarised in Tab. 3-4.

Tab. 3-4: Peak distances between 001/002 and 002/003 peaks in °Δ2Θ.

Note: (1) Samples I2-I5 represent starting materials, samples S1 – S2 belong to the test series, K1 – K8 and GA to the main series of experiments, BentA and BentB are starting materials additionally processed by Atterberg (10 days and 2 days); (2) The bentonite types are explained in a previous section.

Run (1)	**Bentonite type** (2)	**Duration** [days]	**Ca-sat**	**Mg-sat**	**Mg-sat**	**Sr-sat**	**Mean distance** [°Δ2Θ]
I2	Na-Bent	0	5.28	5.33	5.31		5.31
I3	MX-80-raw	0	--	5.30	5.29		5.30
I5	K-Bent	0	5.28	--	5.33		5.31
S2	Na-Bent	24.9	5.28	5.31			5.30
S3	MX-80-raw	24.9	5.31	5.31			5.31
S4	MX-80	24.9	5.28	5.30			5.29
S5	K-Bent	24.9	**7.12**	**6.24**			**6.68**
BentA	MX-80 (Att 10d)	0			**5.25**		5.25
BentB	MX-80 (Att 2d)	0			5.29		5.29
K1	K-Bent	10				**5.44**	**5.44**
K2	K-Bent	45				**5.53**	**5.53**
K3	MX-80-raw	10			5.29	5.3	5.30
K4	MX-80-raw	137			5.30	5.3	5.30
K5	MX-80-raw	45			5.29		5.29
GA	MX-80-raw	137			5.29	5.30	5.30
K6	Na-Bent	10			5.31	5.28	5.30
K7	Na-Bent	137			5.31	5.31	5.31
K8	Na-Bent	45			5.31	5.32	5.32
Mean distance (without values in bold)			5.29	5.31	5.30	5.30	5.30

Results for Mg-saturated and Sr-saturated bentonites are comparable. Test runs with Ca-saturated samples show systematically somewhat smaller values. Differences in measurement conditions may also have an influence (e.g., air humidity, delay time after removing samples from the ethylene glycol environment). The variations are small and within the range of expected uncertainty. Sample BentA_AT10d displays the smallest peak-to-peak distances. We suggest that this strong decrease is an effect of the 2:1 clay aggregate fractionation caused by the long additional Atterberg application treatment (10 days).

Atterberg separation (14 days) was again applied to Sr-saturated samples from Series 1 before XRD. X-Ray scanning was applied separately on Atterberg top (AT) and Atterberg bottom suspended (AB) fractions. Resulting °Δ2θ distances from the AT-fractions (top) showed distinct peaks and consistent results, whereas measurements on AB-fractions (bottom) showed a broad scatter. K5AB, for example, displayed a value which was distinctly too low (5.24 °Δ2θ) and K3AB had a value which was clearly too high (5.38 °Δ2θ). Peaks in the X-ray patterns of the AB samples often had asymmetric shapes and high backgrounds disturbed the determination. This is due to other mineral phases that overlap the 2:1 clay peaks. The content of sedimented clay was probably considerably lower in the AB samples compared to the AT samples. A repeated sedimentation of the fraction > 2 μm improved the peak patterns for AT samples by removing the relative amounts of accessory minerals.

XRD patterns of selected samples

The XRD pattern of sample K4 (MX-80 raw), top fraction after Atterberg separation (Fig. 3-4) shows six distinct peaks, which are all due to the 2:1 clay mineral structure. No or just traces of accessory minerals are present. The second pattern was made for the same bentonite sample K4, but this time it represents the bottom fraction after Atterberg separation. Identified mineral phases are discrete illite, quartz and feldspar. There is less intensity from this sample and background is relatively elevated. Some clay mineral peaks in this pattern are disturbed additionally by accessory minerals, making it more uncertain to quantify illite layers in such patterns.

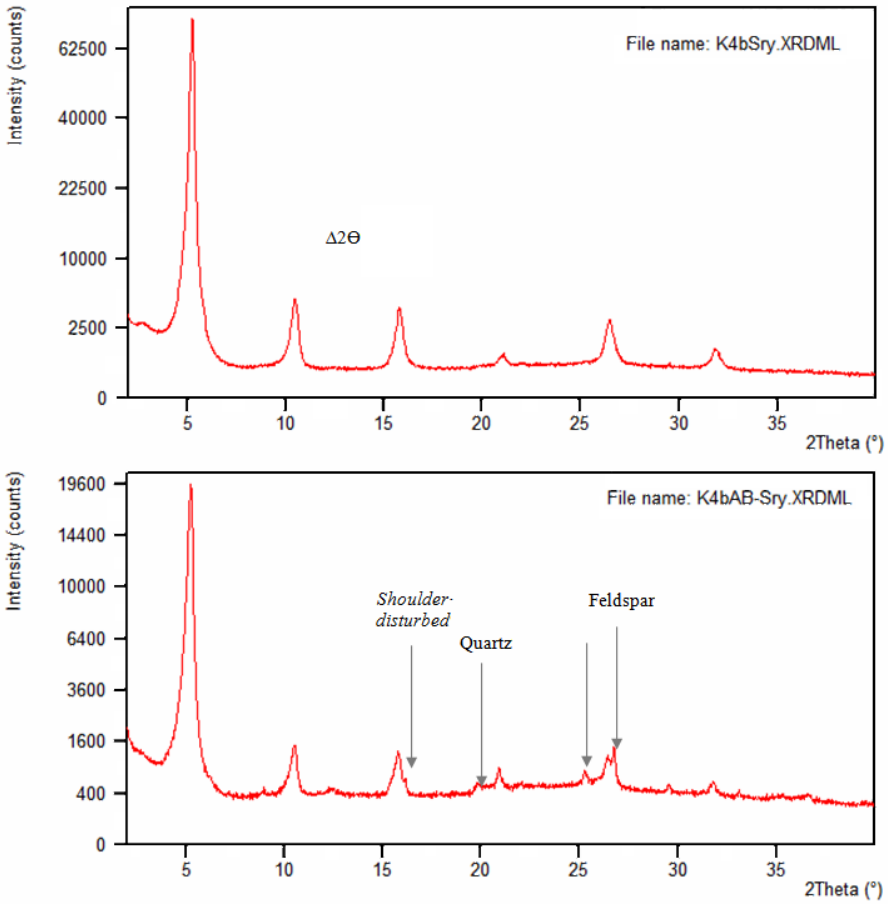

Fig. 3-4: XRD patterns of oriented clay samples.

Top: sample K4, top fraction, after Sr saturation and Atterberg separation, and ethylene glycol treated. The peak distance measured between peaks is indicated by "°Δ2θ" (2Theta (°)). Bottom: XRD pattern of K4, bottom fraction. Some peaks of accessory minerals are marked, and some of these may disturb the peak shape and position of the 2:1 layer structure.

Discussion

It was observed that most XRD patterns made from MX-80 bentonite – either reacted or non-reacted – did display a small discreet illite (or muscovite) peak, but some did not. In view of the possibly small degrees of illite formation it was thought important to rationalise this observation. This difference could be traced to sample preparation. To get rid of discrete illite one can remove the fraction > 2 µm by Atterberg separation. It appears that discrete illite/muscovite is associated with the coarser fraction. By doing so, one will also lose some 2:1 clay. Peak distances (°Δ2θ) did not respond detectably to a removal of the fraction > 2 µm, however. It appears that there are two types of illitic material present – one revealed by measurements of peak differences, and one by a discrete peak that is associated mostly with the coarser fraction.

The 2:1 clays of the bottom fraction after Atterberg separation (AB) (> 2 µm) show broad scattering in °Δ2θ. Therefore, it is not possible to use this fraction to determine illite content according to the method of °Δ2θ from Reynolds & Moore (1989). We propose that this irregularity is due to the fractionation of the 2:1 clay (variation in thicknesses of clay aggregates). Peak distances (°Δ2θ) of bottom-fraction samples were smaller in four out of six cases.

But two samples displayed °Δ2θ-values which were obviously too large. Both were samples which have been in the oven for 10 days (namely K3AB and K6AB). We can think of two explanations for the occurrence of such irregularities: firstly, the 2:1 clay peaks in AB overlap with other mineral intensities (discrete illite, feldspar or quartz) and therefore they are distorted in the measurement. Secondly, it is possible that the thickest 2:1 clays did not build up the largest aggregates (over 2 μm). It may be the thinnest clays instead. The latter case would explain the high values of observed in K3AB and K6AB and it this may also be the reason for the low °Δ2θ value of BentA_AT (Tab. 3-4).

3.3.2 Illite content of thermally reacted samples

The results of the quantification of illite are shown in Tab. 3-5. Data was calculated from the measured XRD peak distances between 001/002 and 002/003 peaks, and with the calibration shown in Fig. 3-3. Starting materials (I5, I3 and I2) were processed and all reacted samples from the series 1 of experiments. Data from samples where multiple sub-samples were available (different homo-ionisations, see Tab. 3-4) were averaged. The so obtained %-illite content was rounded to the nearest percentage.

Tab. 3-5: Percentage of illite in reacted samples (270 °C) and starting materials.

Note: (1) Samples I2 – I5 represent starting materials, samples K1-K8 and GA represent the main series of experiments, BentA and Bent B are starting materials additionally processed by Atterberg (10 days and 2 days); (2) The bentonite types are explained in a previous section. The uncertainty based on d-spacing uncertainty of the calibration is ca. ± 2 % illite.

Run (1)	**Bentonite type** (2)	**Duration** [days]	**Mean distance** [°Δ2Θ]	**%-Illite**
I5	K-Bent	0	5.31	2
K1	K-Bent	10	5.44	10
K2	K-Bent	45	5.53	14
BentA	MX-80 (Att 10d)	0	5.25	−.
BentB	MX-80 (Att 2d)	0	5.29	1
I3	MX-80-raw	0	5.30	1
K3	MX-80-raw	10	5.30	1
K4	MX-80-raw	137	5.30	1
K5	MX-80-raw	45	5.30	1
GA	MX-80-raw	137	5.29	1
I2	Na-Bent	0	5.31	2
K6	Na-Bent	10	5.30	1
K7	Na-Bent	137	5.32	2
K8	Na-Bent	45	5.31	2

There is no evidence of illitisation in reacted samples from "MX-80 raw" or "Na-Bent" regardless of the presence of added K-fsp or the more abundant accessory mineral content in MX-80 raw (see Tab. 3-2 for details of experimental conditions). If any reaction progress did occur, it was below the detection limit of the X-ray peak position quantification method. The only distinct increase in illite content occurred in the samples based on "K-Bent" and the 0.1 N KCl solution. It appears that the much higher potassium activity in these samples did promote illitisation because other experimental parameters were comparable. The smectite-to-illite conversion appears to have been faster in the beginning (10 % after 10 days) and decreased afterwards, reaching a value 14 % after 45 days. There was no experiment available with duration of 137 days for the high-potassium case.

3.4 Summary and conclusions

The principle objective was to perform hydrothermal "illitisation" experiments with MX-80 (Wyoming) bentonite at temperature conditions where previous studies did observe some degree of smectite-to-illite conversion under certain chemical conditions close to 300 ºC, and to see if these findings can be better constrained in terms of different chemical conditions and experimental duration.

The experimental design included 3 different geochemical conditions, (1) an unrealistic "high-potassium" case in the presence of 0.1 m KCl solution with Na-exchanged bentonite pre-equilibrated with the KCl solution. It included a "realistic" case (2) with raw MX-80 bentonite pre-equilibrated with synthetic "granite-type" pore water and reacted in this solution. It also included a case (3) with Na-exchanged partially purified and MX-80 bentonite (removal of most accessory minerals) and with added powdered K-feldspar as a solid source for potassium, and this mix was reacted in a "granite-type" solution. The latter is also a "realistic" case but with better defined geochemical boundary conditions. All experiments were performed at 270 °C in titanium autoclaves mounted on a rotary system in an oven, for durations of 10, 45 and 137 days for the main series of 10 experiments.

The different clay preparation procedures included:

- Two different starting materials: raw MX-80 bentonite and Na-exchanged partially purified MX-80 bentonite.
- Two different solutions: a synthetic "granite-type" groundwater and a 0.1 m KCl solution to provide an elevated potassium activity.
- Combining the above, three different starting conditions were used: raw MX-80 and Na-exchanged MX-80 pre-equilibrated with a granite-type solution, and Na-exchanged MX-80 pre-equilibrated with a 0.1 m KCl solution.
- The pre-equilibrated starting materials were reacted in their respective solutions, with liquid/solid ratios near 20.
- Preparation for XRD analysis included a number of procedures, including fine fraction separation and ion exchange with Mg and Sr.

State-of-the-art X-ray analytical procedures were used in order to confirm either the absence or presence of significant formation of illite in the experiments. The illite content was quantified with the method of difference in peak position between the I/S 001/002 peak and the 002/003 peak. A calibration was generated with calculated patterns for mixtures, assuming plausible parameters and end-members, and it was linked to an independently known illite content of 1 % for the starting material MX-80 bentonite. Preparation for XRD analysis included a number of procedures, including fine fraction separation and homo-ionisation with Mg and Sr.

There was no evidence of illitisation in reacted samples from MX-80 raw bentonite or Na-exchanged bentonite reacted in "granite-type" solution regardless of the presence of added K-feldspar or the more abundant accessory mineral content in raw MX-80. If any reaction progress did occur, it was below the detection limit of the X-ray peak position quantification method. The only distinct increase in illite content occurred in the samples based on K-bentonite reacted in a 0.1 N KCl solution. It appears that the much higher potassium activity in these samples did promote illitisation because other experimental parameters were comparable. The smectite-to-illite conversion appears to have been faster in the beginning (10 % after 10 days) and decreased afterwards, reaching a value 14 % after 45 days.

These findings are consistent with previous hydrothermal experiments where at these temperatures only charges with rather elevated potassium concentrations showed significant conversion of smectite to illite. No reaction progress was observed in our experiments after 137 days for more realistic potassium concentrations, namely those present in a "granite-type" pore water (here 21 mg/l KCl, or 0.28 mN), approximately 360 times more dilute compared to the 0.1 N solution in our "high-potassium" experiments. The potassium activity may be buffered by K-feldspar over extended periods of time (as presumably was the case in at least one of our chemical conditions with K-fsp added) or illite itself, but also much below our "high-potassium" experiments.

Although we do not know the exact nature of the reactions involved during illitisation, nor how they may change with decreasing temperature, one may expect a decrease in reaction rates of many orders of magnitude when extrapolating from 270 °C to repository-relevant maximum temperatures of 80 – 100 °C, lasting for hundreds to a few thousands of years. In this context, an experimental duration of a significant fraction of a year (137 days) is appropriate to gauge if illitisation may be a significant issue in the context of performance assessment for a deep repository with an MX-80 based engineered barrier system. This work supports the general view that the thermal effect alone is unlikely to induce significant smectite-to-illite conversion in a repository situation.

4 Experiments on thermal stability of montmorillonite at 90 – 150 °C

4.1 Introduction

Transformation of montmorillonite to non-swelling phases seems to be governed by the sub-processes of either congruent or incongruent dissolution. Congruent dissolution is obviously a sub-process in dissolution/precipitation transformation, while incongruent dissolution is basically equivalent with the layer charge increasing sub-process occurring in solid-state transformation ("beidellitisation") (e.g. Eberl 1978, Sato et al. 1996). Thus, the study of montmorillonite dissolution is fundamental for understanding its mineral transformation. Also the stability range of smectite may be studied in dissolution tests by allowing the mineral to equilibrate with its solution.

Quite a lot of studies of smectite dissolution have focused on the kinetics at very high or very low pH (e.g. Amram & Ganor 2005, Bauer & Berger 1998, Metz et al. 2005, Zysset & Schindler 1996), while a smaller number of studies have allowed the smectite to reach (near) equilibrium at more neutral pH (Cama et al. 2000, Marty et al. 2011). Dissolution tests have furthermore basically always been performed at a high water-to-solid ratio. Consequently there is a need for performing these types of test under conditions more relevant for the KBS-3 concept.

There is also a need to further investigate the process of potassium fixation without an accompanied layer charge increase, which has been reported to occur under certain conditions (Eberl et al. 1987, Kaufhold & Dohrmann 2010).

The idea behind the tests presented in this chapter is thereby to study the montmorillonite (congruent and/or incongruent) dissolution process and possible potassium fixation under KBS-3 relevant conditions:

- Moderate temperature (90 °C)
- Near neutral pH (self-regulating)
- Compacted state (very low water-to-solid ratio)
- Comparison of the dissolution behaviour between natural bentonite (MX-80) and the purified montmorillonite (Wyoming type)

In addition, there was a need for accelerated tests in order to verify or disprove trends found at the repository conditions. The present study consequently contains two experimentally quite different main series, one run at 90 °C and the other at 150 °C.

4.1.1 General experimental principles

The testing principle was to expose typical low charged montmorillonite to various chloride test solutions of Na^+, K^+, Ca^{2+}, and Mg^{2+} at increased temperatures. Subsequent analyses of the clay and solutions aimed at quantifying montmorillonite dissolution rates, equilibrium conditions, extent of potassium fixation, and other possible alteration of the montmorillonite as a result of the various test conditions.

Fixation of potassium was specifically studied by high concentration of KCl solutions in some tests. Ion exchange against potassium chloride solution was further performed after the heating phase for all test samples in order to admit potassium fixation also in tests where no potassium was present during the heating phase.

4.2 Test material

All test material in both the performed test series was based on Wyoming sodium bentonite produced by American Colloid Company under the brand name Volclay MX-80. The material was used as delivered, after Na-exchange and removal of the size fraction larger than 2 µm, and after Na-exchange and removal of the size fraction larger than 0.5 µm in different tests. The latter material is referred to as Na-montmorillonite in the following text.

The fractioning and conversion to sodium state was made according to the following procedure. 10 grams of MX-80 material was dispersed in 1 L de-ionised water, and the size fraction larger than 2 µm was removed by centrifugation. The remaining material was place in 1 L of 1 M NaCl solution and left with circulation for 24 h. The solid material was separated by centrifugation and the supernatant was replaced by a new 1 L of 1 M NaCl solution. After a third exposure to NaCl solution the centrifuged material was placed into a dialyze membrane (Spectrapore 3, 3'500 MWCO), which was placed in Plexiglas tubes containing stirred de-ionised water. The electrical conductivity was measured in the external water, which was changed when the conductivity had risen above 10 µS/cm. Dialysis was terminated when the conductivity remained below this value. A part of the dialyzed material was again dispersed in 1 L de-ionised water and the material coarser than 0.5 µm was removed by centrifugation. Water was removed from the solids by drying at 60 °C, and the materials ($d < 2$ µm and $d < 0.5$ µm) was milled to a lump grain size similar to that of the original MX80 material.

4.2.1 Equipment and test method in the 90 °C test series

The testing method was to expose the clay materials to external chloride test solutions of Na^+, K^+, Ca^{2+}, and Mg^{2+}, respectively, at 90 °C. Subsequent analyses aimed at quantifying the release of substances, especially of silica, into the external test solutions, and of structural mineralogical changes in the montmorillonite.

Six test samples were compacted into titanium/PEEK (Polyether-ether-ketone) test cells with a diameter of 35 mm and height of 5 mm (Fig. 4-1). The solid mass was adjusted to give a density of 1'850 kg/m^3 after full water saturation, corresponding to a calculated dry density of 1'336 kg/m^3. MX-80 bentonite was used as delivered in one test cell (sample MmS-A1), Na-exchanged material with a maximum grain size of 2 µm in one test cell (MmS-A2) and Na-exchanged material with a maximum grains size of 0.5 µm in four test cells (MmS-A3 to MmS-A6). The samples were supported on both sides by titanium filters, and a piston on top of the upper filter transferred the swelling force to a transducer connected to a data acquisition system.

All samples were water saturated by a slow circulation of de-ionised water below the bottom filters in order to let air out of the upper filters. After approximately one week, the de-ionised water was replaced by 250 mL 0.2 M NaCl solutions in the tests MmS-A1 to A3, 0.2 M KCl in test MmS-A4, 0.1 M $CaCl_2$ in test MmS-A5 and 0.1 M $MgCl_2$ in test MmS-A6. The solutions were slowly circulated from plastic bottles and PEEK and Tygon tubing through both the bottom and top filters by use of a peristaltic pump. After an additional week the concentrations were lowered by a factor of 4 to the actual test concentrations. The ion-exchange from the

original Na^+-form to K^+, Mg^{2+} or Ca^{2+}-forms was consequently made successively in situ in the test cells. The rationales for this choice of materials and test sequence was to enable detection of effects from accessory minerals by initial differences in samples MmS-A1 to MmS-A3, which was exposed to the same kind of test solution, respectively, and to detect mineralogical changes in the montmorillonite as an effect of the various test solutions in the tests MmS-A3 to MmS-A6. The temperature was increased to 60 °C after 2 weeks and to 90 °C three weeks after the first contact with the chloride test solutions, and the temperature was kept at 90 °C for 280 days. Swelling pressure was measured during the saturation and initial heating phase in order to determine when conditions close to equilibrium were reached. Drift of the force transducers at the relatively high temperature over time ruled out reliable continuous measurement over the whole test period. Before test termination, the transducers were removed, recalibrated and replaced and the pressures were measured at room temperature for the respective test solutions. Water sampling by extraction of 30 mL from the circulating solutions was made repeatedly at different time intervals during the test period. The six test solutions were changed to new solutions after 70 and 170 days of the thermal exposure. The extracted and replaced solutions were analysed by use of ICP/AES with respect to major cations. In order to avoid heating/ drying artefacts, the water-to-solid ratio (w) was measured at termination of the tests by drying at low vapor pressure at room temperature in a freeze-drying apparatus. The technique was tested on parallel samples and found to give results equal to drying by heating with respect to water-to-solid ratio and to cation exchange capacity. Drying by low total pressure was therefor used wherever suited in all of the performed analyses.

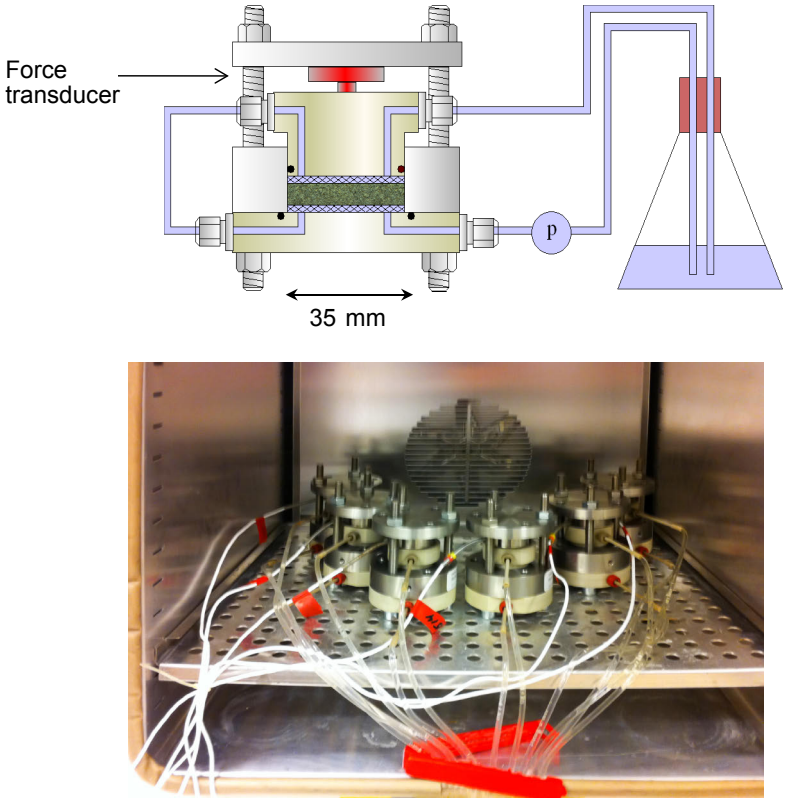

Fig. 4-1: Principle drawing of the test setup for the 90 °C test series (top) and a photo of the 6 test cells placed in the laboratory oven (bottom).

4.2.2 Equipment and test method in the 150 °C test series

The testing method involved exposing Na-montmorillonite to a large volume (100 mL) of relatively high concentration chloride test solutions of Na^+, K^+, Ca^{2+}, and Mg^{2+}, respectively, at 150 °C. The initial concentrations were 0.25 M in the Na and K solutions, and 0.125 M in the Ca and Mg solutions. The concentrations were successively increased in order to test the significance of concentration to twice the initial concentration in K, Ca and Mg solutions and to four times in the Na solution. The test conditions were expected to lead to an early, and almost complete, ion exchange of the Na-montmorillonite with the respective cations in the chloride solutions. The rationale for starting with material from the same Na-montmorillonite batch in all tests, and not use pre-exchanged material, was to guarantee that possible differences after the thermal treatment were related only to the applied test conditions. Subsequent analyses of the supernatants aimed at quantifying the release of substances, especially of silica, and analyses of the montmorillonite aimed at quantifying structural mineralogical changes.

Six cylindrical PEEK test cells with an inner height of 70 mm and an inner diameter of 50 mm were used. The cells were filled with 100 mL of the different test solution, respectively, and 3 grams of Na^+-montmorillonite was placed in each solution. The tubes were sealed with a top lid equipped with FPM O-rings (Viton), which were kept in place by 8 bolts, respectively (Fig. 4-2). Heating was made in a standard laboratory oven with a measured temperature variation of a few degrees centigrade in the oven air.

The two samples MmS-B5 and MmS-B6 were kept in the oven for a period of 27 days, and no replacement of the supernatants were made before sampling. Four of the tests cells MmS-B1 to MmS-B4 were repeatedly taken out of the oven after approximately 14 days and allowed to cool down to room temperature. The upper lids were removed and the suspensions were transferred to centrifuge bottles and centrifuged. Approximately 80 mL of the supernatants were sampled and the solids and new test solutions were replaced in the test cells for the next 14 days of heating. The concentration was doubled after two exchange rounds in order to study possible effects of the salt concentration, and also to facilitate the settlement of the montmorillonite. After totally 7 test solutions (91 days), the solids were separated for the subsequent analyses.

Fig. 4-2: Test equipment for the 150 °C series.

PEEK test cell, centrifuge bottles and test material for one test sample.

4.3 Analyses

4.3.1 Water content and density

Water-to-solid ratio (w), defined as:

$$w = \frac{m_w}{m_s}$$

where m_w is the mass of water and m_s is the mass of solids, was determined by drying the samples under low vapor pressure at room temperature in a freeze dryer. The sample dry densities were calculated according to:

$$\rho_d = \frac{\rho_s \cdot \rho_w}{\rho_s \cdot w + \rho_w}$$

where ρ_s is the density of solids (2'750 kg/m^3) and ρ_w is the density of water (1'000 kg/m^3).

4.3.2 Water analyses

The concentrations of Al^{3+}, Fe^{3+}, Na^+, K^+, Ca^{2+} Mg^{2+} and silica in the extracted, changed and final solutions were determined by ICP-AES technique at the Department of Ecology, Lund University. The test solutions from the 90 °C tests series were analysed shortly after sampling, while the solutions from the 150 °C test series were stored in a refrigerator and analysed at the end of the experiment. The charge balance was checked with analyses of Cl^- in some analyses, and the maximum charge divergence was 12 %.

4.3.3 Cation exchange capacity

The cation exchange capacity (CEC) was determined by exchange with copper(II)triethylenetetramine following the procedure of Meier & Kahr (1999) slightly modified. The ground samples (400 mg) were dried at low vapour pressure, dispersed in 50 ml deionised water by ultrasonic treatment and shaken overnight. 20 ml of 15 mM Cu(II)-triethylene-tetramine solution was added to the suspension, which was left to react for 30 minutes on a vibrating table. After centrifugation the absorbance at 620 nm of the supernatant was measured using a double-beam spectrophotometer (Perkin Elmer Lambda 3). CEC was calculated on the basis of the uptake of Cu by the clay and is expressed in milliequivalents per 100 g (meq/100 g). CEC was also calculated on the basis of the ICP/AES analyses performed to determine the ion distribution in the samples (next paragraph) in the 90 °C-series. All CEC determinations were duplicated.

All samples were analysed with the existing charge compensation ions after each test, and after ion exchange against K^+ in order to enable possible potassium fixation, and subsequently ion exchanged against Na^+ in order to get comparative conditions. All samples were consequently dispersion in 1 L of 1 M KCl solutions and kept overnight under circulation in order to enable fixation. The suspensions were thereafter placed to settle and the solids were separated from solution as much as possible by centrifugation. Finally, the solids were ion-exchanged against Na^+ by the same procedure as used in the preparation of the Na^+-montmorillonite.

4.3.4 Exchangeable cations

Since all tests started with the same Na-montmorillonite material, which successively was ion exchanged in the various tests, it was of crucial importance to check the extent of the exchange. Analyses were specifically made in the 90 °C series, in which the concentrations of the solutions were much lower than in the conditions in the 150 °C test series, and in which the ion-exchange was limited by transport through filters and through the compacted clay itself. The Cu-trien solutions used for the CEC determination were consequently analysed by ICP/AES with respect to major cations (EC). Ideally, i.e. when the content of easily soluble salts such as chlorides and carbonates of alkali metals is low, the sum of cations extracted should be equivalent to the CEC of the sample. In the present materials, in which accessory minerals were removed, only a negligible amount of access salt from the test solutions was expected. The concentration of the potential charge-compensating cations Ca, Mg, Na and K in the extracts was determined by use of an ICP-AES equipment at the Department of Ecology, Lund University.

4.3.5 SEM/EDX element analyses of the solids

The mean chemical compositions of the test samples were determined by use of a scanning electron microscope equipped with an energy dispersive X-ray analyser (SEM/EDX), instead of more traditionally ICP/AES, due to the limited amount of test material. Approximately 0.5 g of each sample was dispersed in de-ionised water and dried in a plastic jar under low air pressure (< 2 kPa) in order to produce a specimen without water and with a flat and smooth surface. Approximately a square cm of material from each sample was mounted on a slide by use of carbon tape, and placed in a SEM Hitachi S-3400N microscope. The specimens were studied in low vacuum mode (80 Pa) by use of a quad-type semiconductor backscattered electron detector, and elemental analyses were performed with an Oxford energy dispersive spectrometer with a Si detector (Inka X-sight mod 7021 EDX). An acceleration voltage of 15 kV, a sample current about 1 nA and a counting live-time of 50 s were used. The setup was calibrated against standards for the elements of interest and cobalt was used to monitor drift of the instrument.

Generally, there may be some scatter in the SEM/EDX analyses due to true local variation in the element distribution in bulk material, and to uneven surfaces. In order to minimise such artefacts, area analyses of 25 × 25 μm and 100 × 100 μm were used, and the mean of the two area analyses were used.

The results were used to calculate the structural formulas of the materials. The calculation was based on the structure of 2:1 layer silicate, and on the following assumptions and simplifications:

- an ideal structure based on 24 oxygen,
- all iron was assumed to be trivalent,
- potassium in the Na-converted clay was considered non-exchangeable and was allocated to illite,
- any calcium that may exist after the dialysis of the Na-converted clay was assigned to the pool of interlayer cations,
- all magnesium was assigned to the octahedral sheet except for in the magnesium exchanged sample, in which the magnesium content corresponding to the measured CEC was assigned to the cation pool and the remaining amount to the octahedral sheet.

4.4 Results and discussion

4.4.1 90 °C test series

The water content results were used to calculate the density of the samples at test termination assuming full water saturation and a grain density of 2'750 kg/m^3 and the results are shown in the compilation Tab. 4-1. The swelling pressure evolution during the water saturation and initial heating phase is shown as a function of time in Fig. 4-3. The initial rather large scatter in measured swelling pressure between the equally prepared Na^+-montmorillonite samples is typically a result of the small sample size and likely represents small variations in sample density. The results are in line with previous tests with respect to the responses to exchangeable ion and solution concentrations (Karnland et al. 2006). The final swelling pressures after recalibration of the transducers were in line with expected values for the measured sample densities and did not indicate any material alteration except for the ion-exchange (Tab. 4-1).

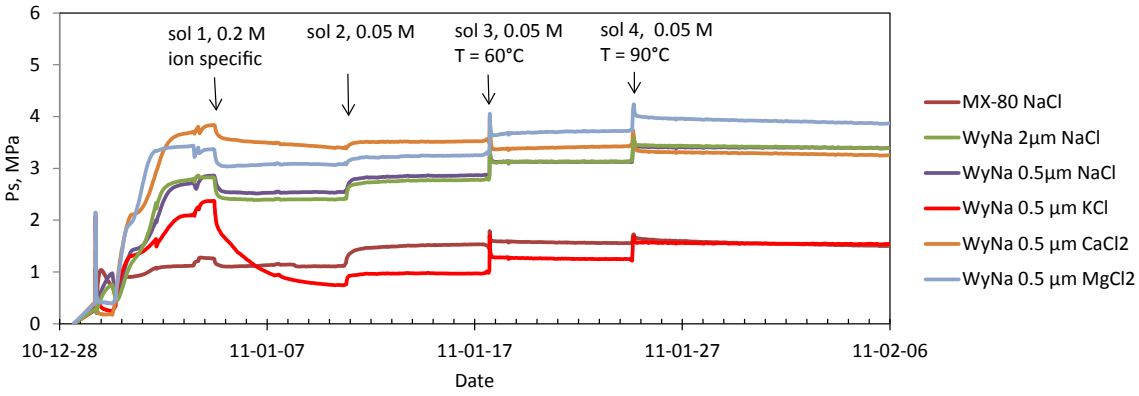

Fig. 4-3: Swelling pressure evolution during water saturation and initial heating phases.

Tab. 4-1: Results from test series MmS-A concerning water content (w), saturated density (ρ_m), pore ratio e, porosity (n), dry density (ρ_d), initial swelling pressure ($P_{s,\,ini}$) and final swelling pressure($P_{s,\,fin}$).

Test ID	**Material**	**W** [--]	**ρ_m** [kg/m^3]	**E** [--]	**n** [--]	**ρ_d** [kg/m^3]	**$P_{s,\,ini}$** [MPa]	**$P_{s,\,fin}$** [MPa]
MmS-A1	MX-80	0.430	1'802	1.18	0.54	1'261	1.53	1.57
MmS-A2	WyNa d < 2 µm	0.443	1'789	1.22	0.55	1'240	2.78	2.53
MmS-A3	WyNa d < 0.5 µm	0.445	1'787	1.22	0.55	1'237	2.87	2.35
MmS-A4	WyK d < 0.5 µm	0.406	1'826	1.12	0.53	1'299	0.97	1.22
MmS-A5	WyCa d < 0.5 µm	0.388	1'847	1.07	0.52	1'331	3.52	2.97
MmS-A6	WyMg d < 0.5 µm	0.389	1'846	1.07	0.52	1'330	3.25	2.97

Water analyses

The six test solutions were changed 3 times at the test temperature 90 °C, with relatively frequent sampling and analyses during the first set of solutions, and only one final sampling during the last set (Fig. 4-4). In addition to the original chloride solutions, silica dominated the content in all analysed solutions. The very low content of aluminum, iron and magnesium showed that the silica content was not related to release of colloidal montmorillonite particles, but to dissolved or precipitated colloidal silica. Evaporation from the solutions in the present tests contributed significantly to the measured increase in silica concentration, in addition to the release from the test samples (Fig. 4-4, left). Taking the individual solution volume changes into account, the calculated silica release were initially relatively large, but decreased successively and ceased at silica concentrations between 2 and 3 mmoles/L (Fig. 4-4, right, Tab. 4-2) in all tests regardless of the charge-compensating cation. The evaluated release rates based on the individual sampling results are shown in Tab. 4-2. At 20 °C the initial mean rate was 2.8×10^{-12} mole Si/g clay/s, at 60 °C 8.7×10^{-12} mole Si g clay/s, and at 90° 1.9×10^{-11} mole/g clay/s.

The dissolution rates are presented as moles of matter per time and mass (moles/s/g) instead of more traditionally moles per time and surface area. The reason for this is the uncertainty concerning what area to use. Taking the approach of Cama et al. (2000) as an example, they used the BET surface area, which was measured before and after the tests. Recalculating their results to matter Si per time and mass reduced the scatter in evaluated dissolution rates by approximately a factor of three. A typical mean result from their high water-to-solid experiments performed at 80 °C at pH 8.8 was thereby 7.5×10^{-11} mole Si/g clay/s, which is similar to what was found in the present study, indicating that the degree of compaction does not influence the dissolution rates dramatically.

The low release of silica from MX-80 material (Tab. 4-3) shows that the bulk part of accessory minerals is not the major source of silica, and there is a tendency of increasing release with decreasing particle size. However, based on these data alone, a silica rich phase with a particle size less than 0.5 µm, such as cristobalite or obsidian, could have contributed to the release of silica.

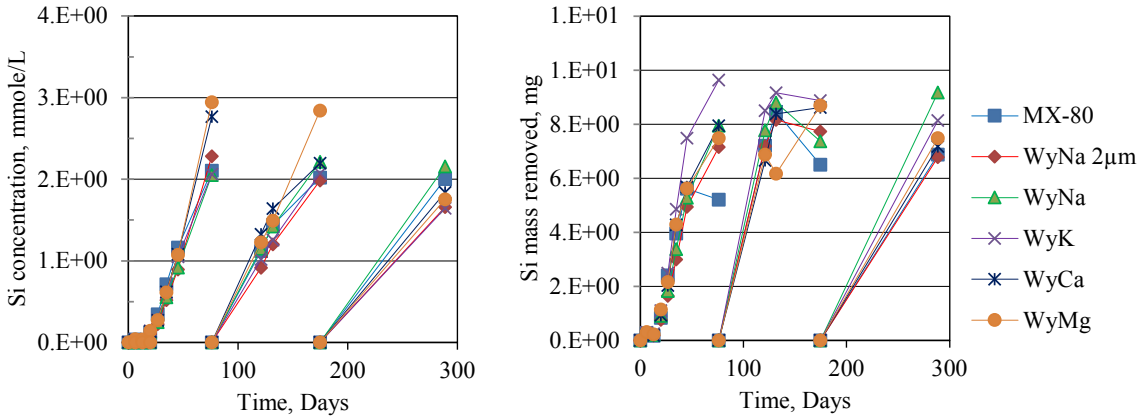

Fig. 4-4: Concentration in external solutions (left) and released silica mass (right) versus time in the six tests.

Tab. 4-2: Silica dissolution rates evaluated for all sampled solutions.

Duration [days]		**T** [°C]	**Dissolution rate** [mole Si/g clay/s]					
			MX-80	**WyNa 2µm**	**WyNa**	**WyK**	**WyCa**	**WyMg**
6	New sol	20	2.9E-12	2.4E-12	2.8E-12	3.2E-12	2.3E-12	3.3E-12
13		20	1.6E-12	1.7E-12	1.9E-12	2.3E-12	1.8E-12	2.2E-12
20	New sol	60	7.7E-12	7.0E-12	8.4E-12	1.0E-11	8.5E-12	1.0E-11
27	New sol	90	2.2E-11	1.5E-11	1.7E-11	2.3E-11	1.9E-11	2.0E-11
35		90	1.3E-11	1.1E-11	1.3E-11	1.9E-11	1.8E-11	1.7E-11
45		90	1.0E-11	1.2E-11	1.2E-11	1.6E-11	8.7E-12	8.3E-12
76		90		4.6E-12	5.5E-12	4.5E-12	4.7E-12	3.9E-12
121	New sol	90	1.0E-11	1.0E-11	1.1E-11	1.2E-11	9.5E-12	9.8E-12
132		90	7.4E-12	5.8E-12	6.1E-12	3.9E-12	1.0E-11	
175		90					3.6E-13	3.8E-12
289	New sol	90	3.9E-12	3.8E-12	5.2E-12	4.6E-12	4.0E-12	4.2E-12

Tab. 4-3: Total amount of released silica into the external water solutions according to ICP/AES analyses.

Test ID	**MmS-A1**	**MmS-A2**	**MmS-A3**	**MmS-A4**	**MmS-A5**	**MmS-A6**
Material	MX-80	WyNa 2µm	WyNa	WyK	WyCa	WyMg
Removed Si mass [mg]	22	24	27	30	27	27
Removed Si/total Si	0.012	0.013	0.015	0.016	0.014	0.014
Removed SiO_2/total mass	0.006	0.009	0.009	0.011	0.009	0.009

CEC and EC

The results from the ICP/AES analyses of exchanged cations in the CEC analyses clearly showed that an extensive exchange had taken place in the samples exposed to KCl, $CaCl_2$ and $MgCl_2$ solutions (Fig. 4-5). The three samples MmS-A4 (K), MmS-A5 (Ca) and MmS-A6 (Mg) were dominated to more than 90 % by the intended ion. The results in this study may consequently be considered representative for montmorillonite dominated by these charge-compensating ions, respectively.

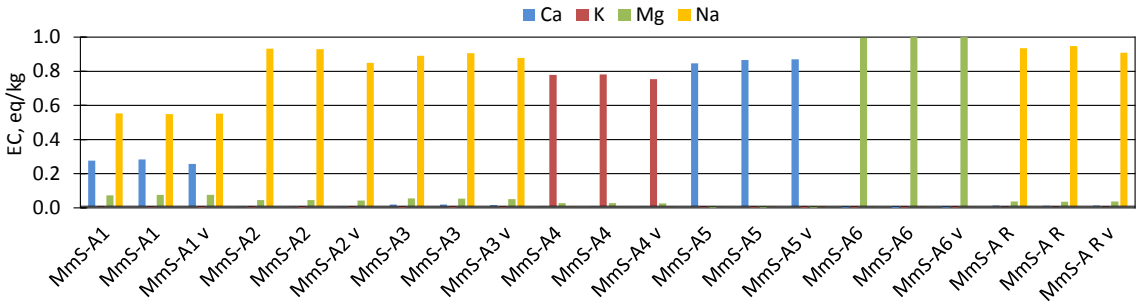

Fig. 4-5: Ion distribution in the reference material and in the test samples after the heating phase.

"v" indicates results from samples, which were dried ahead of the analyses by means of low pressure at room temperature instead of at high temperature.

The cation exchange capacity (CEC) of reference and test samples was determined by use of traditional drying at 70 °C and from samples dried at low vapour pressure at room temperature (Fig. 4-6). No significant changes compared to reference were noticed in CEC as a result of the thermal treatment in the samples exposed to NaCl (MmS-A1, MmS-A2 and MmS-A3), $CaCl_2$ (MmS-A5) and $MgCl_2$ (MmS-A6) solutions. The slightly lower CEC in sample (MmS-A4) exposed to KCl solution may be explained by the potassium ions, and there was no significant difference left after the ion-exchange to K^+-form and subsequently to Na^+-form for all samples (Fig. 4-7).The results consequently imply that the mass loss of silica of 1.1 % of the total initial mass did not result in a significant permanent change in CEC regardless of the dominating charge-compensating cation.

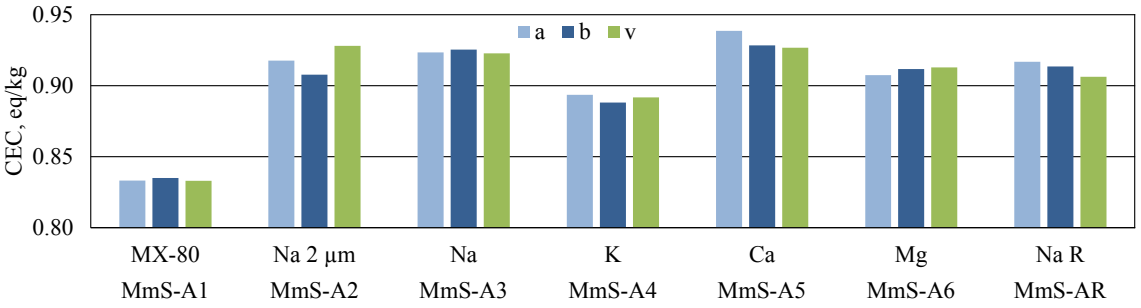

Fig. 4-6: First set of CEC results from reference and test samples in the 90 °C-series after the heating phase but before ion exchange to K^+- and subsequently Na^+-form.

"v" indicates results from the samples, which was dried ahead of the analyses by means of low pressure at room temperature instead of drying at high temperature.

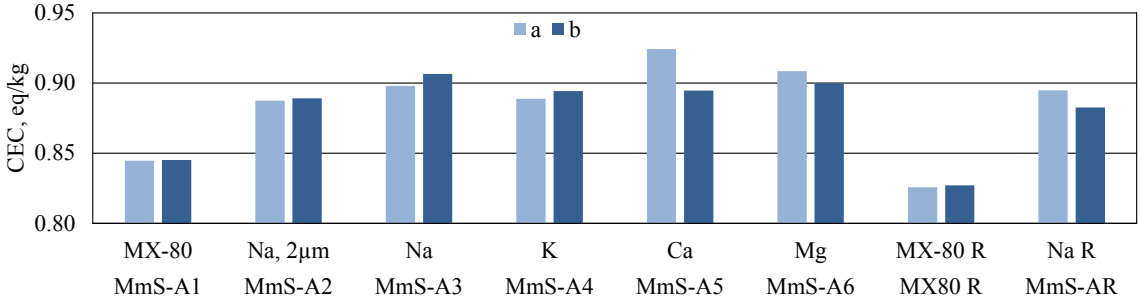

Fig. 4-7: Second set of CEC results from reference and test samples in the 90 °C-series after the heating phase after ion exchange to K^+- and subsequently Na^+-form.

a and b indicate doublets.

Elemental analyses of solids

The results from the SEM/EDX element analyses were used to calculate the structural formulas of the test material (Tab. 4-4). The results show a tendency of lower Si content, which is in qualitative agreement with the silica release revealed by the ICP/AES analyses of the water solutions. Fixation of potassium was found neither in sample MmS-A4, which was ion exchanged during the heating period, nor in any of the other samples which were exchanged for potassium after the heating period and thereafter exchanged back to sodium.

Tab. 4-4: Structural formula based on SEM/EDX element analyses of all samples in the 90 °C test series.

MmS-AR represents the reference material, which is completed with duplicates (MmS-BR1 and MmS-BR2) of the reference material in series MmS-B, since both series used the same bentonite batch.

Test ID	Material	Structural formula
MmS-A1	MX-80	$Si_{7.84}Al_{0.16}Al_{3.16}Ti_{0.00}Fe_{0.35}Mg_{0.45}Ca_{0.02}Mg_{0.00}K_{0.01}Na_{0.66}$
MmS-A2	Na, 2 µm	$Si_{7.89}Al_{0.11}Al_{3.18}Ti_{0.01}Fe_{0.36}Mg_{0.38}Ca_{0.02}Mg_{0.00}K_{0.00}Na_{0.63}$
MmS-A3	Na	$Si_{7.88}Al_{0.12}Al_{3.16}Ti_{0.02}Fe_{0.35}Mg_{0.41}Ca_{0.02}Mg_{0.00}K_{0.01}Na_{0.66}$
MmS-A4	K	$Si_{7.82}Al_{0.18}Al_{3.14}Ti_{0.01}Fe_{0.40}Mg_{0.41}Ca_{0.01}Mg_{0.00}K_{0.01}Na_{0.66}$
MmS-A5	Ca	$Si_{7.84}Al_{0.16}Al_{3.20}Ti_{0.01}Fe_{0.33}Mg_{0.41}Ca_{0.00}Mg_{0.00}K_{0.00}Na_{0.71}$
MmS-A6	Mg	$Si_{7.99}Al_{0.01}Al_{3.15}Ti_{0.01}Fe_{0.35}Mg_{0.39}Ca_{0.03}Mg_{0.02}K_{0.00}Na_{0.57}$
MmS-AR	Na	$Si_{7.95}Al_{0.05}Al_{3.14}Ti_{0.00}Fe_{0.37}Mg_{0.41}Ca_{0.03}Mg_{0.00}K_{0.00}Na_{0.65}$
MmS-BR1	Na R	$Si_{7.91}Al_{0.09}Al_{3.11}Ti_{0.01}Fe_{0.36}Mg_{0.46}Ca_{0.06}Mg_{0.00}K_{0.00}Na_{0.59}$
MmS-BR2	Na R	$Si_{7.95}Al_{0.05}Al_{3.12}Ti_{0.02}Fe_{0.36}Mg_{0.44}Ca_{0.06}Mg_{0.00}K_{0.00}Na_{0.56}$

4.4.2 150 °C test series

Water analyses

The total mass of Al^{+}, Ca^{2+}, K^{+}, Mg^{2+}, Na^{+} and silicon in all solutions from the six tests are shown in Tab. 4-5. The results from the four tests MmS-B1 to MmS-B4 represent the sum of ions in all seven solutions, which were exchanged approximately every fortnight. The results from tests MmS-B7 and MmS-B6 represent the solution, which were in contact with the samples for the entire test period of 29 days. In addition to the initial chloride salts, silica and sodium dominated the content of the solutions. The very low aluminum content shows that the solutions were not contaminated by released colloidal montmorillonite particles, i.e. the measured silica content consequently corresponds to dissolved or precipitated colloidal silica.

The results for aluminum and magnesium, which are present in the montmorillonite layer structure, were quite different. The released content of aluminum was very low and constant in the successive solutions, indicating that aluminum either did not dissolve from the montmorillonite, or alternatively precipitated within the clay. In contrast, the content of magnesium, which also is contained in the montmorillonite structure, was initially higher and showed a decreasing trend with the number of solution exchanges (Tab. 4-7). The relationship between total amount of released magnesium and total amount of released silica is similar to that in the montmorillonite layer structure, which may indicate congruent dissolution. However, the marked successive decrease in magnesium and the relatively low total amount (0.08 eq/kg) may rather be an effect of ion exchange with remnants of magnesium in the original Na-montmorillonite.

The relatively large amount of sodium in the solutions of samples MmS-B2, MmS-B3, MmS-B4 and MmS-B6 is explained by ion exchange of the initial material from pure sodium to a state dominated by the cation of the test specific chloride solution (Tab. 4-6). The total exchanged charge equivalent per mass shows the scope of ion-exchange, which was almost complete in the samples MmS-B2 to MmS-B4 since the original CEC was 88 ± 2 eq/kg. The exchange in sample MmS-B6 was not complete since only one test solution was used, and the measured extent of exchange thereby represents equilibrium conditions with the initial Na^{+}.

Tab. 4-5: Total mass of ions in the solutions.

All values in milligram, which may be related to the initial 3 gram of mass in each sample. Values in italics indicate the cation of the test-specific chloride solutions. The denomination "91/7" indicate 91 days of duration and 7 solutions.

Test ID	**Chloride**	**Duration**	**Element mass** [mg]					
	Solution	Days/sol.	Al	Ca	K	Mg	Na	Si
MmS-B1	Na	91/7	0.08	0.87	21.2	3.06	*9'209*	30.7
MmS-B2	K	91/7	0.02	1.74	*7'959*	2.56	56.13	40.3
MmS-B3	Ca	91/7	0.01	*5'923*	4.36	2.84	51.57	41.7
MmS-B4	Mg	91/7	0.12	3.15	2.28	*2'810*	54.35	40.0
MmS-B5	Na	27/1	0.01	0.61	3.71	1.24	*2'130*	9.2
MmS-B6	K	27/1	0.05	1.19	*1'734*	1.67	50.30	14.3

Tab. 4-6: Sum of exchanged cation equivalents from all test solutions.

Results from the initial chloride solutions are consequently not included. The denomination "91/7" indicate 91 days of duration and 7 solutions.

Test ID	**Chloride**	**Duration**	**Equivalents**					**Eq./mass**
	Solution	Days	Ca	K	Mg	Na	Sum	[eq/kg]
MmS-B1	Na	91/7	0.04	0.54	0.25	--	0.84	0.28
MmS-B2	K	91/7	0.09	--	0.21	2.44	2.74	0.91
MmS-B3	Ca	91/7	--	0.11	0.23	2.24	2.59	0.86
MmS-B4	Mg	91/7	0.16	0.06	--	2.36	2.58	0.86
MmS-B5	Na	27/1	0.03	0.09	0.10	--	0.23	0.08
MmS-B6	K	27/1	0.06	--	0.14	2.19	2.38	0.79

Tab. 4-7: Measured magnesium mass, and total magnesium equivalents per mass, in relevant test solutions.

Results in mg, and on the last row in eq/kg.

Test ID	**Duration**	**MmS-B1**	**MmS-B2**	**MmS-B3**	**MmS-B4**	**MmS-B5**	**MmS-B6**
Solution no.	[Days]	Na	K	Ca	Mg	Na, 1s	K, 1s
1	14	0.59	0.68	0.85			
2	14	0.58	0.72	1.03			
3	10	0.64	0.20	0.12			
4	14	0.48	0.38	0.32			
5	12	0.38	0.22	0.21			
6	12	0.24	0.14	0.14			
7	15	0.15	0.22	0.17			
1	27					1.24	1.67
Sum	--	3.06	2.56	2.84	--	1.24	1.67
Sum [eq/kg]		0.08	0.07	0.08	--	0.03	0.05

The total amount of released silica was approximately proportional to the reaction time, indicating far from equilibrium conditions (Tab. 4-8). The approximately doubled reaction time in samples MmS-B5 and B6 did consequently not change the evaluated release rates significantly (Tab. 4-9). There was no trend in dissolution rates with the number of exchange cycles in any of the tests, indicating that the source for dissolution was relatively constant. The increase in test solution concentration after the first exchange, also by a factor of two, did not change the release rates significantly in any of the tests. The differences in mean dissolution rates between materials dominated by different ions were small and in the same range as the differences within the individual tests.

Tab. 4-8: Total release of Si (and as SiO_2) from all samples according to the ICP/AES water analyses.

Tests MmS-B1 to MmS-B4 were 91 days tests, and the MmS-B5 and MmS-B6 were 27 days tests.

Test ID	**MmS-B1**	**MmS-B2**	**MmS-B3**	**MmS-B4**	**MmS-B5**	**MmS-B6**
Chloride solution	Na	K	Ca	Mg	Na	K
Si release [mg]	31	40	42	40	9	14
Si release/total Si [g/g]	0.035	0.046	0.048	0.046	0.010	0.016
SiO_2 release/sample mass [g/g]	0.022	0.029	0.030	0.029	0.007	0.010

Tab. 4-9: Silicon release rates (mole Si/g clay/s) for each exchange period of the water solutions.

Tests MmS-B1 to MmS-B4 were 91 days tests, and the MmS-B5 and MmS-B6 were 27 days tests.

Solution	**Test ID**	**MmS-B1**	**MmS-B2**	**MmS-B3**	**MmS-B4**	**MmS-B5**	**MmS-B6**
No.	[Days]	Na	K	Ca	Mg	Na	K
1	14	5.6E-11	6.3E-11	6.3E-11	6.6E-11		
2	14	4.5E-11	6.5E-11	5.8E-11	6.9E-11		
3	10	5.4E-11	5.5E-11	7.5E-11	4.7E-11		
4	14	3.4E-11	6.9E-11	5.8E-11	7.2E-11		
5	12	4.7E-11	6.7E-11	7.8E-11	6.1E-11		
6	12	5.1E-11	5.3E-11	7.3E-11	-		
7	15	4.1E-11	5.3E-11	4.5E-11	4.6E-11		
	mean	4.6E-11	6.1E-11	6.3E-11	5.9E-11		
1	27					4.7E-11	7.3E-11

CEC and EC

Cation exchange analyses were performed both after termination of the heating tests, and after the K/Na exchange procedure (Fig. 4-8). The latter analyses were made in order to eliminate possible ion-specific effects, and to admit potential potassium fixation. All CEC values from the heated samples, both measured before and after the K/Na exchange procedure, were significantly higher than in the reference material. The CEC values were generally slightly higher after the K/Na exchange procedure likely due to analytical artefacts and thereby illustrate the accuracy of the technique rather than real changes in the materials. Comparative measurements should consequently preferably be made in one and the same set of analyses. The increase in CEC as an effect of the heat treatment was, however, clearly shown in both the measurements (last column in Tab. 4-10 and 4-11). The mean increase of the material exposed to 150 °C for 91 days was approximately 10 % compared to the reference material. The difference can be

concluded to be a consequence of the heat exposure alone, since the reference material was pretreated together with the test material before the heating, and went through the same ion-exchange sequence afterwards. The CEC increase was largest in the Ca-saturated sample in all analyses, both before and after the K/Na exchange procedure.

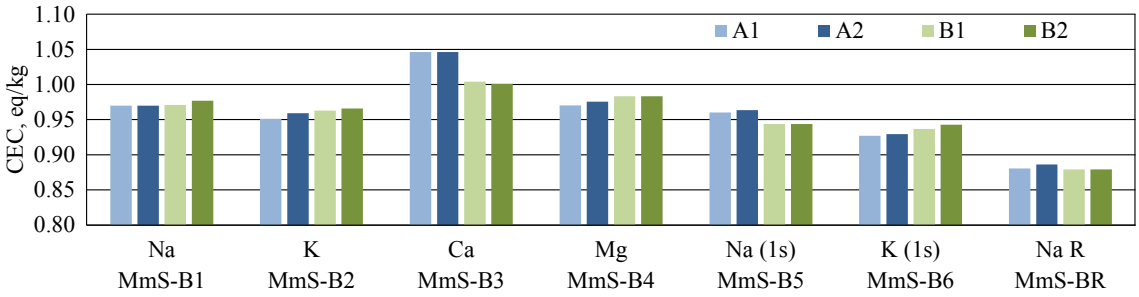

Fig. 4-8: Measured CEC after heating tests, and after exchange to K- and subsequent exchange to Na-state.

MmS-BR represent reference material. A and B represents two samples from the same test material and 1 and 2 separate measurements of absorbance.

It should be noted that the mass loss of silica in the present tests was equal to or less than 3 % of the total mass (Tab. 4-8). This value is approximately three times too low to explain the CEC increase as simply an effect of dissolution of a separate silica phase, e.g. amorphous silica.

Tab. 4-10: Measured CEC after heating tests, but before the K/Na exchange procedure.

MmS-BR1 and 2 represent montmorillonite reference material and MX-80 R represent MX-80 reference material. The denomination "91/7" indicate 91 days of duration and 7 solutions. A and B represent doublet analyses from one test material. S-DEV represents standard deviation and d-CEC-ref indicates the difference between the actual sample mean and reference mean.

Test ID	**Material**	**Duration**	**A**	**B**	**Mean CEC**	**S-DEV**	**d-CEC-ref**
	Type	Days/sol.	Mole charges/kg				
MmS-B1	Na	91/7	0.94	0.94	0.94	0.000	0.07
MmS-B2	K	91/7	0.93	0.93	0.93	0.003	0.06
MmS-B3	Ca	91/7	1.00	0.99	0.99	0.003	0.12
MmS-B4	Mg	91/7	--	0.95	0.95	--	0.09
MmS-B5	Na	27/1	0.93	0.92	0.93	0.010	0.06
MmS-B6	K	27/1	0.91	0.91	0.91	0.003	0.04
MmS-BR1	Na, R1	--	0.87	0.87	0.87	0.003	0.00
MmS-BR2	Na, R2	--	0.87	0.86	0.86	0.003	0.00
MX-80 R	MX-80, R	--	0.83	0.83	0.83	0.001	--

Tab. 4-11: Measured CEC after heating tests, and after exchange to K- and subsequent exchange to Na-state. MmS-BR represents reference material.

The denomination "91/7" indicate 91 days of duration and 7 solutions. A and B represent doublet analyses from one test material. S-DEV represents standard deviation and d-CEC-ref indicates the difference between the actual sample mean and reference mean.

Test ID	**Material**	**Duration**	**A1**	**A2**	**B1**	**B2**	**mean**	**S-DEV**	**d-CEC-ref**
	Type	Days/sol.	Mole charge/kg						
MmS-B1	Na	91/7	0.97	0.97	0.97	0.98	0.97	0.003	0.09
MmS-B2	K	91/7	0.95	0.96	0.96	0.97	0.96	0.005	0.08
MmS-B3	Ca	91/7	1.05	1.05	1.00	1.00	1.02	0.022	0.14
MmS-B4	Mg	91/7	0.97	0.98	0.98	0.98	0.98	0.006	0.10
MmS-B5	Na	27/1	0.96	0.96	0.94	0.94	0.95	0.009	0.07
MmS-B6	K	27/1	0.93	0.93	0.94	0.94	0.93	0.006	0.05
MmS-BR	Na, R	-	0.88	0.89	0.88	0.88	0.88	0.003	0.000

Element analyses of the solids

Structural formulas based on the SEM/EDX elemental analyses are shown in Tab. 4-12. Fixation of potassium was found neither in samples MmS-B2 or MmS-B6, which were ion exchanged during the heating period, nor in any of the other samples which were exchanged for potassium after the heating period and thereafter exchanged back to sodium. The total charge increases in the three long-term tests (MmS-B1 to 3) are 0.07, 0.05, 0.11, which corresponds to an increase in calculated CEC of 0.09, 0.07, and 0.15 eq/kg clay. Comparison with the measured CEC increase of 0.09, 0.08, and 0.14 eq/kg clay shows the consistency of the SEM/EDX and CEC measurements for these three samples. The magnesium sample was left out in this comparison due to the difficulty to distribute the measured magnesium between interlayer and octahedral positions in the evaluation procedure for the structural formula.

Tab. 4-12: Structural formula based on SEM/EDX element analyses of all samples in the 150 °C test series.

Tests MmS-B1 to MmS-B4 were 91 days tests, and the MmS-B5 and MmS-B6 were 27 days tests. MmS-BR1 and MmS-BR2 represents duplicates of the reference material.

Test ID	**Material**	**Structural formula**
MmS-B1	Na	$Si_{7.83}\ Al_{0.17}\ Al_{3.10}\ Ti_{0.02}\ Fe_{0.36}\ Mg_{0.46}\ Ca_{0.02}\ Mg_{0.00}\ K_{0.03}\ Na_{0.71}$
MmS-B2	K	$Si_{7.87}\ Al_{0.13}\ Al_{3.13}\ Ti_{0.01}\ Fe_{0.35}\ Mg_{0.47}\ Ca_{0.03}\ Mg_{0.00}\ K_{0.02}\ Na_{0.69}$
MmS-B3	Ca	$Si_{7.76}\ Al_{0.24}\ Al_{3.09}\ Ti_{0.02}\ Fe_{0.39}\ Mg_{0.46}\ Ca_{0.12}\ Mg_{0.00}\ K_{0.00}\ Na_{0.57}$
MmS-B4	Mg	$Si_{7.79}\ Al_{0.21}\ Al_{3.11}\ Ti_{0.02}\ Fe_{0.38}\ Mg_{0.48}\ Ca_{0.03}\ Mg_{0.00}\ K_{0.00}\ Na_{0.66}$
MmS-B5	Na	$Si_{7.92}\ Al_{0.08}\ Al_{3.12}\ Ti_{0.02}\ Fe_{0.35}\ Mg_{0.45}\ Ca_{0.11}\ Mg_{0.00}\ K_{0.00}\ Na_{0.51}$
MmS-B6	K	$Si_{7.93}\ Al_{0.07}\ Al_{3.14}\ Ti_{0.01}\ Fe_{0.32}\ Mg_{0.44}\ Ca_{0.05}\ Mg_{0.00}\ K_{0.01}\ Na_{0.66}$
MmS-BR1	Na R1	$Si_{7.91}\ Al_{0.09}\ Al_{3.10}\ Ti_{0.01}\ Fe_{0.36}\ Mg_{0.46}\ Ca_{0.06}\ Mg_{0.00}\ K_{0.02}\ Na_{0.59}$
MmS-BR2	Na R2	$Si_{7.95}\ Al_{0.05}\ Al_{3.11}\ Ti_{0.02}\ Fe_{0.36}\ Mg_{0.44}\ Ca_{0.06}\ Mg_{0.00}\ K_{0.02}\ Na_{0.56}$

The relative content of Si was significantly lowered in the four samples MmS-B1 to MmS-B4 as compared to the reference samples. In parallel, the relative content of other elements were increased in the montmorillonite in a corresponding way. The mean decrease in Si content was 0.12 unit charges, which corresponds to approximately 1.5 % of the original Si content. This may be compared to the mean Si release into the external water solution, which corresponds to approximately 4.4 % of the original Si content in the clay (Tab. 4-8). This apparent mass balance discrepancy of Si cannot be explained by dissolution of other minerals, since the calculated structural formulas are based on the total amount of elements in the material, i.e. all elements are allocated to a montmorillonite structure. A plausible explanation for the apparent discrepancy is instead described in the following section.

A simplified mean reaction for the replacement of Si by Al from the reference material to the altered material in samples MmS-1 to MmS-4 in the 91 days tests is:

$$Si_{7.93}\,Al_{3.18}\,Ti_{0.02}\,Fe_{0.36}\,Mg_{0.45}\,Ca_{0.06}\,K_{0.02}\,Na_{0.58}\,O_{24.00}\,H_{4.00} + 0.12\,Al^{3+} + 0.09\,X^{+} \rightarrow$$
$$Si_{7.81}\,Al_{3.30}\,Ti_{0.02}\,Fe_{0.37}\,Mg_{0.47}\,Ca_{0.05}\,K_{0.01}\,Na_{0.66}\,O_{24.00}\,H_{4.00} + 0.12\,Si$$

Where X is a general monovalent ion, which may be replaced by an appropriate amount of cations of different valence. Assuming no other aluminum-bearing minerals, then the only source for the aluminum is the montmorillonite itself. Congruent dissolution of the present montmorillonite results in a release of 7.93/3.18 = 2.49 Si for each Al. Replacement in the remaining montmorillonite of 0.12 Si by 0.12 Al will thereby result in total release of Si of 0.12 + 2.49 × 0.12 = 0.42, which corresponds to 5.3 % of the total initial Si content.

This approach implies two coupled processes; dissolution and thereby reduction of the total amount of montmorillonite, and a parallel alteration of the remaining montmorillonite in the direction towards beidellite. The aluminum mass will thereby be conserved, but the relative aluminum content will increase due to silica release.

The total mean mass loss of silica in the four samples as calculated from replacement of 0.12 Al then corresponds to a total mass loss of 0.10 gram per sample, which represents 3.4 % of the initial clay mass, which in turn corresponds fairly well with the measured total mean silica mass in the external solutions (Tab. 4-8).

4.5 Conclusions

A crucial question for the interpretation of all the present results is to what extent the measured material changes are related to the montmorillonite, or in other words, whether or not small amounts of accessory minerals also play an important role. Comparison of the total dissolved mass in the external solutions with the results concerning CEC and element distribution in the solids show that possible accessory minerals did not play a dominant role in the observed processes. All results are therefore attributed to the montmorillonite alone although this may lead to minor overestimations in some cases. The main findings are summarised in the following items:

- Montmorillonite dissolves and releases silica under the present experimental conditions if the silica activity is under a critical value. At 90 °C the evaluated equilibrium concentration is in the range of 2 to 3 mM. The results are in line with other relevant studies, e.g. Cama et al. (2000).
- Well below the equilibrium silica activity, the dissolution rates were evaluated to be 2.5×10^{-12}, 8×10^{-12} and 2×10^{-11} mole Si/g clay /s at 20, 60 and 90 °C, respectively, in the compacted samples. Comparing these results with those reported by Cama et al. (2000) indicates that the degree of compaction does not have a major influence on the dissolution rates.

- In batch tests at 150 °C the evaluated mean dissolution rate was 5×10^{-11} mole Si/g clay/s.
- Dissolution rates of MX-80 bentonite and of the corresponding purified montmorillonites were similar, which show that presence of accessory minerals in the bentonite did not significantly influence the process. Montmorillonite dissolution consequently dominated in all examined materials.

No significant difference in dissolution rates or equilibrium concentrations were observed, regardless of dominating cations, in the purified montmorillonites.

- The dissolution process resulted in an increase in layer charge density located in the tetrahedral sheets. The montmorillonite was consequently altered in the direction towards beidellite.
- The aluminum required for the beidellitisation process seems to be provided by parallel congruent dissolution of the montmorillonite.
- Fixation of potassium was not observed, either in the K^+-montmorillonite, or in any of the other samples, although all were potassium exchanged post-heating.

5 Effect of steam on the swelling capacity of bentonite

5.1 Introduction

Couture (1985) presented data on the effects of steam on bentonite at temperatures between 150 and 250 °C. The reaction was studied experimentally by varying the water-to-solid ratio in a systematic way in a closed system, and subsequently measure the clay/water volume after mixing with water, dispersion and settlement. A rapid irreversible reduction of the volume of the bentonite was claimed to be the result after only 7 days of exposure to steam. The reduction was reported to be temperature dependent, but the clay/water volume was reduced also at 150 °C to approximately one third of the volume of unreacted reference clay. The largest reduction was found at relatively low water-to-solid ratios during heating, and no or only minor effects were found if the clay was completely dry, or if the water-to-solid ratio was high enough during heating. The reduced volume was further claimed to be related to a maximum basal spacing of the montmorillonite of 19 Å, corresponding to only three layers of water molecules between the montmorillonite layers. A minor mineralogical examination of the reacted clays was performed, but no alteration was found either with respect to exchangeable ions or to the montmorillonite layer itself. The cause of the reduction in clay/water volume was thereby left open.

Since a repository may be partially water saturated during a substantial period of time, the results have led to persisting uncertainty for the safety assessment, because swelling ability of montmorillonite is fundamental for a bentonite buffer with respect to almost all of the buffer functions. As a consequence, some additional studies have been performed concerning the effects of steam on bentonite and possible implications for a repository (Oscarson & Dixon 1990, Haas et al. 1999). Fortunately, these studies have not shown the dramatic changes reported by Couture (1985), especially with respect to the irreversibility.

The present work, therefore had the basic ambition to repeat the experiments by Couture and expand the tests and analyses enough to understand the discrepancy between the available studies, and thereby remove, or at least reduce, the uncertainty concerning the effects steam on bentonite.

5.2 Test materials

Totally nine different commercial bentonites were used in the experiments representing a broad range of different qualities with respect to exchangeable ion, accessory minerals and production techniques. The materials were;

- MX-80 Volclay, a Wyoming sodium bentonite produced by American Colloid Company
- Deponit CA-N, a natural calcium bentonite mined by S&B Industrial Minerals S.A. in the north-eastern part of the island of Milos, Greece
- Asha 505, a natural Na-bentonite quarried in the Kutch area (north-west India) by Ashapura Minechem Co.
- Calcigel, a natural Ca-bentonite produced by Süd-Chemie AG, quarried in the Landshut area in Bavaria, Germany
- Tixoton, a natural Ca-bentonite which has been sodium activated. The product was delivered by Süd-Chemie AG
- SPV 200, a Wyoming sodium bentonite produced by American Colloid Company milled to a fine powder while the similar MX-80 product is milled to mm-sized granules

- FEBEX bentonite, a Mg-Ca bentonite extracted from the Cortijo de Archidona deposit in the southern part of Serrata de Nijar in Almería, Spain. The deposit has been exploited by the major Spanish bentonite producer, Minas de Gádor S.A (now Süd-Chemie, Espana)
- Ikosorb Ca White (actual commercial name: IBECO RWC White) is a Ca, Mg, Na bentonite mined in Morocco in the Mount Tidienit area
- Kunigel V1, a sodium bentonite produced by Kunimine Industries Co., Ltd., Japan. The bentonite is quarried in under-ground mines in the Tsukinuno district, northern part of Japan
- Saponite CDA, a natural saponite from the Madrid area, Spain

Further information about the materials may be found in Karnland et al. (2006) and Svensson et al. (2011) and in product sheets from the producers. The materials were used as delivered, and in the case of MX-80, Febex, Asha 505 and Deponite CaN also after purification and exchange to Na^+-form. The purified Volclay MX-80 material was further used after exchanged to K^+ and Ca^{2+}-forms, respectively. In addition to the basically commercial products, the Clay Mineralogical Society standard bentonite SWy-1 was used, which was of special interest since this material was also used in the study by Couture (1985).

The purified materials are referred to as montmorillonites in the following text, and the preparation of them is described in Section 4 in this report.

5.3 Equipment and test technique

The basic testing principle was to expose the various clay materials to 150 or 200 °C at different water-to-solid ratios for one week, and thereafter measure the water containing capacity initially after passive water uptake and secondly after active dispersion and settlement. Small clay samples were confined in containers made of PEEK and titanium in series of five individual samples (Fig. 5-1). Also stainless steel end pieces were tested in order to copy the tests performed by Couture (1985). Standard laboratory ovens were used to keep the temperature.

The water-to-liquid ratio in each sample was controlled by mixing in water before heating, or by controlling the water pressure through a titanium filter in contact with the clay. In the latter case, the pressure was chosen to give a defined relative humidity, corresponding to a specific water-to-solid ratio in the clay. This technique was claimed by Couture to guarantee that only vapour, and no liquid water, was present, as the system was open and the applied water pressure was below the boiling point for the temperature in question.

After the heating phase, the clay samples were allowed to cool in the test cells, and the water-to-solid ratios were determined by drying at low pressure at room temperature. The samples were grinded to a similar grain size as the specific reference material, and 0.1 gram of dry material was placed in 5 mL sized test tubes, and deionised water was added. The tubes were sealed and placed to rest for several weeks until no further change in clay volume was observed. In most cases, the upper surface of the clay was distinct and the clay/water volume was determined. The tubes were thereafter shaken and the clay samples were dispersed ultrasonically for 15 minutes, and the clay was allowed to settle and the clay/water volume was again measured.

The various test materials, conditions and results are summarised in Tab. 4-1. MX-80 bentonite was used as delivered at different initial water-to-solid ratios in test Series MmS-300, -400 and -500. MX-80 bentonite was further used as delivered and after purification and exchange to pure sodium (WyNa) and calcium (WyCa) montmorillonites in test series MmS-600 and -700. In series MmS-800, montmorillonite purified from Deponit CaN (MiNa), Asha 505 (KuNa) and

Febex (FeNa) were used in sodium form, montmorillonite from MX-80 in potassium form (WyK) and finally SWy-1 was used in its natural form. Test series MmS-900 and MmS-1000 contained bentonites as delivered, which were exposed to water pressure of 446 kPa intended to give a water-to-solid ratio of maximum 0.25 based on water retention curves (Dueck 2004). Series MmS-1100 encountered some unintended drying and was not examined further. Series MmS-1200 included SWy-1 material at different water-to-solid ratios, and finally series 1300 used a 50/50 mixture of pure Na- and Ca-montmorillonite produced from MX-80 bentonite.

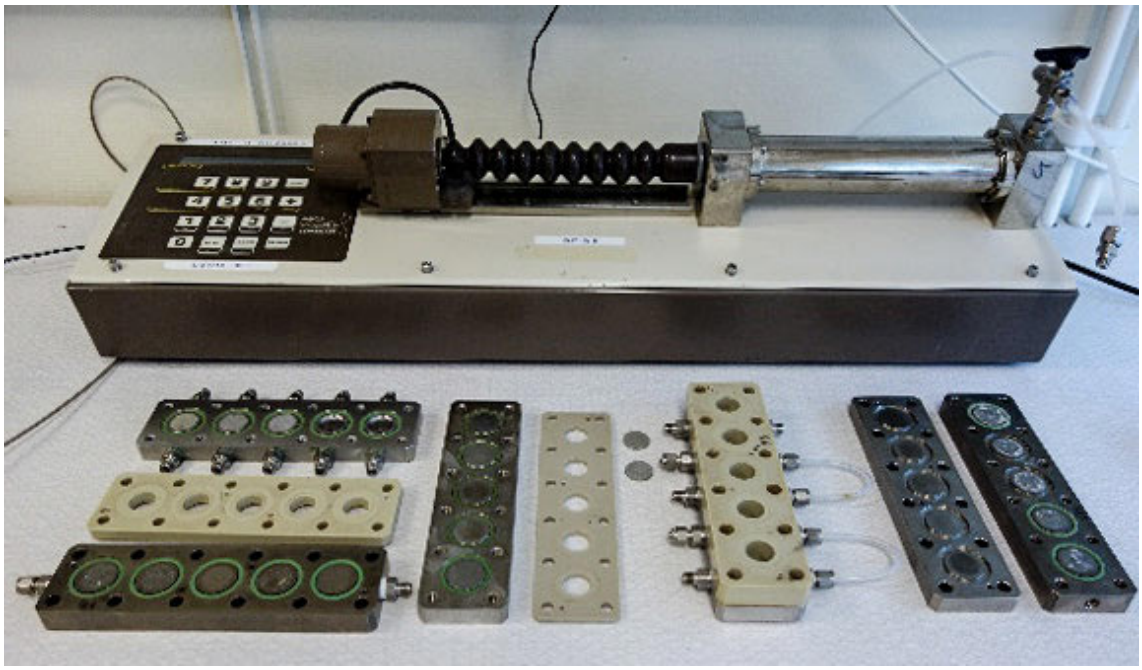

Fig. 5-1: Test equipment showing the pressure controlling device and the various parts used for steam exposure of the clay.

The clay samples were placed in the central PEEK holders and were confined either by solid titanium (or steel) plates, or by a titanium filter for water pressure supply. The system was bolted together and sealed by use of Viton O-rings.

5.4 Results and discussion

The main results are compiled in Tab. 5-1. The most important general result was the small differences in the extent of passive water uptake (swelling capacity) from dry state, between reference and steam exposed material. On the other hand, there were rather complex results and large differences in final volume in some cases after dispersion and settlement of the same clays. The results may be illustrated by Series MmS-1000 in which the largest difference in unconfined swelling, for all samples, was found for the Tixoton material (Fig. 5-2). Still, this difference between reference and steam exposed samples was small compared to what was the case for the volumes after the active dispersion and settlement. Noteworthy are also the results for the Kunigel samples, which all were similar regardless of the exposure to steam and to active dispersion.

Tab. 5-1: Layout and major results from all steam tests.

Pw indicate water (vapor) pressure, w indicate the water-to-solid ratio, sed = sediment in the bottom, grad = an obvious gradient in clay density due to gravity, homo = almost a homogeneous structure, gel = gelformation, V(r swell) shows the volume of the reference material after unconfined swelling from dry state, V(r disp) shows the volume of reference material after active dispersion and settlement. The columns V(s swell) and V(s disp) indicate the corresponding results for the steam exposed materials.

Test ID	**Clay**	**V(cell)** [cm^3]	**m(s)** [g]	**T** [°C]	**Pw** [kPa]	**w(int)** [g/g]	**w(meas)** [g/g]	**V(r swell)** [cm^3/g]	**V(r disp)** [cm^3/g]	**V(s swell)** [cm^3/g]	**V(s disp)** [cm^3/g]
MmS 301	MX-80	3.14	5.12	150	480	0.25		15	sed+ grad	16	grad
MmS 302	MX-80	3.14	5.12	150	480	0.25				15	grad
MmS 303	MX-80	3.14	2.30	150	480	1.00				16	grad
MmS 304	MX-80	3.14	2.30	150	480	1.00				17	grad
MmS 305	MX-80	3.14	0.30	150	480	10.00				16	grad
MmS 401	MX-80	6.28	10.24	150	480	0.25		17	sed+ grad	16	grad
MmS 402	MX-80	6.28	10.24	150	480	0.25				15	grad
MmS 403	MX-80	6.28	4.61	150	480	1.00				16	grad
MmS 404	MX-80	6.28	4.61	150	480	1.00				17	grad
MmS 405	MX-80	6.28	0.61	150	480	10.00				15	grad
MmS 501	MX-80	6.28	1.00	150	480	0.00	0.04	19	sed+ grad	19	35+grad
MmS 502	MX-80	6.28	1.00	150	480	0.50	0.41			17	40+grad
MmS 503	MX-80	6.28	1.00	150	480	1.00	0.90			19	50
MmS 504	MX-80	6.28	1.00	150	480	2.00	2.06			19	50
MmS 505	MX-80	6.28	1.00	150	480	3.00	2.94			18	50
MmS 601	MX-80	6.28	3.00	150	480	0.25	0.26	17	sed+grad	19	sed+grad
MmS 602	Wy-Na	6.28	3.00	150	480	0.00	0.01	27	grad	27	grad
MmS 603	Wy-Na	6.28	3.00	150	480	0.25	0.27			27	grad
MmS 604	Wy-Ca	6.28	3.00	150	480	0.00	0.02	5	18	8	10+grad
MmS 605	Wy-Ca	6.28	3.00	150	480	0.25	0.29			9	10+grad
MmS 701	MX-80	6.28	1.00	200	1'600	0.25	0.14	17	sed+grad	18	18
MmS 702	Wy-Na	6.28	1.00	200	1'600	0.00	0.03	32	grad	27	grad
MmS 703	Wy-Na	6.28	1.00	200	1'600	0.25	0.16			27	grad
MmS 704	Wy-Ca	6.28	1.00	200	1'600	0.00	0.05	7	11	5	9
MmS 705	Wy-Ca	6.28	1.00	200	1'600	0.25	0.22			5	8
MmS 801	MiNa	3.14	5.12	150	480	0.25	0.19	39	homo	36	homo
MmS 802	KuNa	3.14	5.12	150	480	0.25	0.18	33	homo	31	homo
MmS 803	FeNa	3.14	5.12	150	480	0.25	0.21	33	homo	31	homo
MmS 804	WyK	3.14	5.12	150	480	0.25	0.21	22	sed+grad	21	sed+grad
MmS 805	SWY-1	3.14	5.12	150	480	0.25	0.22	25	sed+grad	27	sed+grad
MmS 901	MX80	6.28	4.00	150	446	< 0.25	0.24	17	sed+grad	16	sed+grad
MmS 902	Deponit	6.28	4.00	150	446	< 0.25	0.20	7	21	7	8
MmS 903	ASHA	6.28	4.00	150	446	< 0.25	0.18	16	sed+grad	18	sed+grad
MmS 904	SWY-1	6.28	4.00	150	446	< 0.25	0.19	25	sed+grad	25	sed+grad
MmS 905	SWY-1	6.28	4.00	150	446	< 0.25	0.20			25	sed+grad
MmS 1001	SPV200	6.28	4.00	150	446	< 0.25	0.19	12	32	13	15
MmS 1002	Ikosorb	6.28	4.00	150	446	< 0.25	0.21	11	43	8	9
MmS 1003	Kunigel	6.28	4.00	150	446	< 0.25	0.14	10	10	11	9

Tab. 5-1: (continued)

Test ID	Clay	V(cell) [cm^3]	m(s) [g]	T [°C]	Pw [kPa]	w(int) [g/g]	w(meas) [g/g]	V(r swell) [cm^3/g]	V(r disp) [cm^3/g]	V(s swell) [cm^3/g]	V(s disp) [cm^3/g]
MmS 1004	Tixoton	6.28	4.00	150	446	< 0.25	0.24	16	44	10	7
MmS 1005	Saponite	6.28	4.00	150	446	< 0.25	0.22	3	5	2	5
MmS 1201	SWy-1	3.14	1.00	150	480	0.00	0.02	24	48 gel	25	46 gel
MmS 1202	SWy-1	3.14	1.00	150	480	0.20	0.23		48 gel	26	42 gel
MmS 1203	SWy-1	3.14	1.00	150	480	0.30	0.30		48 gel	25	grad
MmS 1204	SWy-1	3.14	1.00	150	480	0.40	0.42		48 gel	27	grad
MmS 1205	SWy-1	3.14	0.50	150	480	5.00	4.75		48 gel	26	40 gel
MmS 1301	WyNa/Ca	3.14	1.00	150	480	0.00	0.06	30	grad	30	30+grad
MmS 1302	WyNa/Ca	3.14	1.00	150	480	0.50	0.43		grad	31	grad
MmS 1303	WyNa/Ca	3.14	1.00	150	480	0.50	0.46		grad	30	grad
MmS 1304	WyNa/Ca	3.14	1.00	150	480	4.00	4.51		grad	29	grad
MmS 1305	WyNa/Ca	3.14	1.00	150	480	4.00	3.66		grad	29	grad

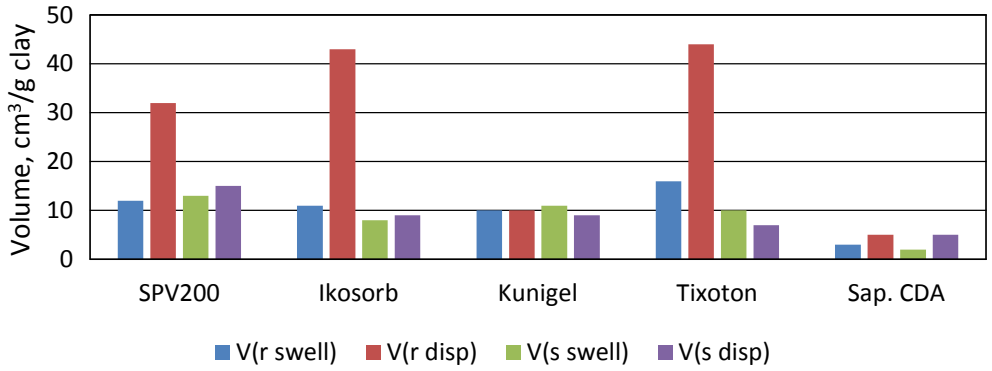

Fig. 5-2: Clay/water volumes for five materials in Series MmS-1000.

V(r swell) represents the volume of passive water uptake in reference materials, V(r disp) represents the volume of material (actively dispersed) after settlement, and V(s swell) and V(s disp) represents the corresponding volumes for materials exposed to steam.

The laser beams in Fig. 5-3 expose that there was no colloidal particles in the supernatant in the reference sample of Ikosorb (left photo), but there was a significant amount of colloidal particles in the upper part of the test tube in the steam exposed material (right photo). This illustrates the ability to form stable gels in some of the reference materials, such as SPV 200, Ikosorb and Tixoton, and that this ability seems to be strongly reduced by the steam treatment in these samples.

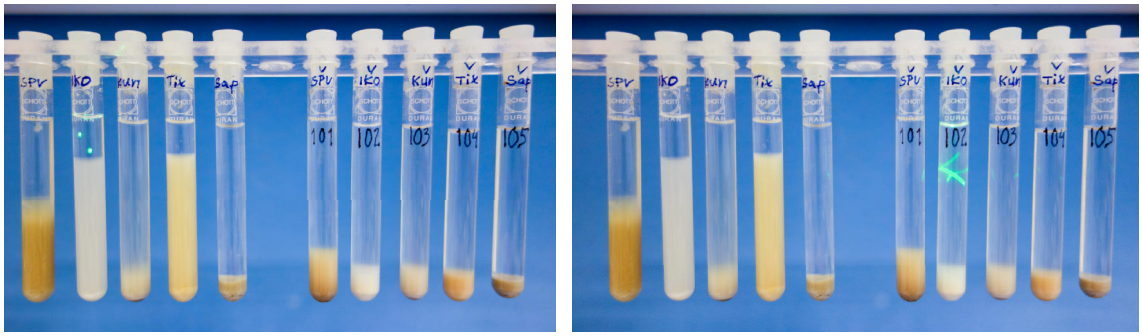

Fig. 5-3: Illustration of the clay/water volume after active dispersion and settlement for five materials in Series MmS-1000.

Both photos show the volumes of reference material (left) and after steam exposure (right). Note the laser beam in both photos. In the reference sample of Ikosorb (left photo) the lack of Tyndall effect shows that no colloidal particles are present in the supernatant. In contrast, there was a significant amount of colloidal particles in the upper part of the test tube in the corresponding steam exposed material (right photo).

The pure monovalent montmorillonites in Series MmS-800 formed sols in pure water, and there was no significant effect of the exposure to steam (Fig. 5-4, left photo). Also at 200 °C, the two sodium montmorillonite samples were not significantly affected by the exposure to steam (Fig. 5-4, right photo). The pure calcium montmorillonite samples were slightly discolored but there was no significant difference in clay/water volume compared to the reference sample.

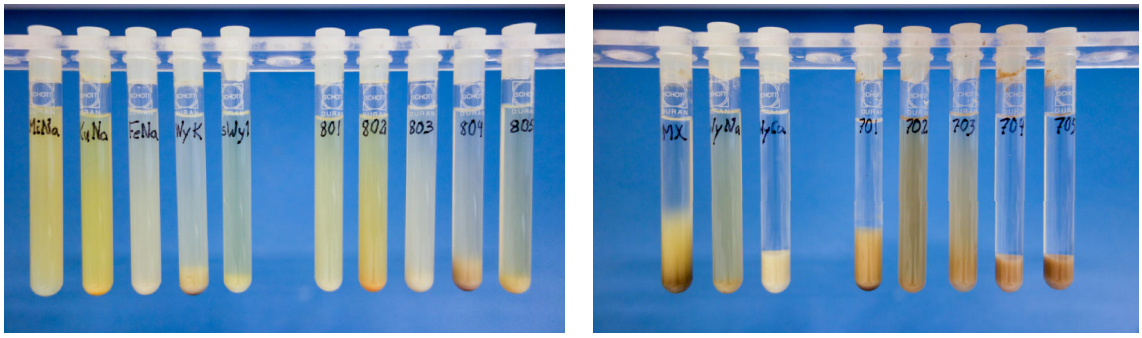

Fig. 5-4: Left photo: reference (left) and steam (150 °C) exposed (right) montmorillonites from Series MmS-800, right photo: reference (left) and steam (200 °C) exposed (right) materials from the Series MmS-700.

The results by Couture (1985) show dramatic effects of steam for most conditions, especially at relatively low water-to-solid ratios during the exposure for steam (Fig. 5-5).

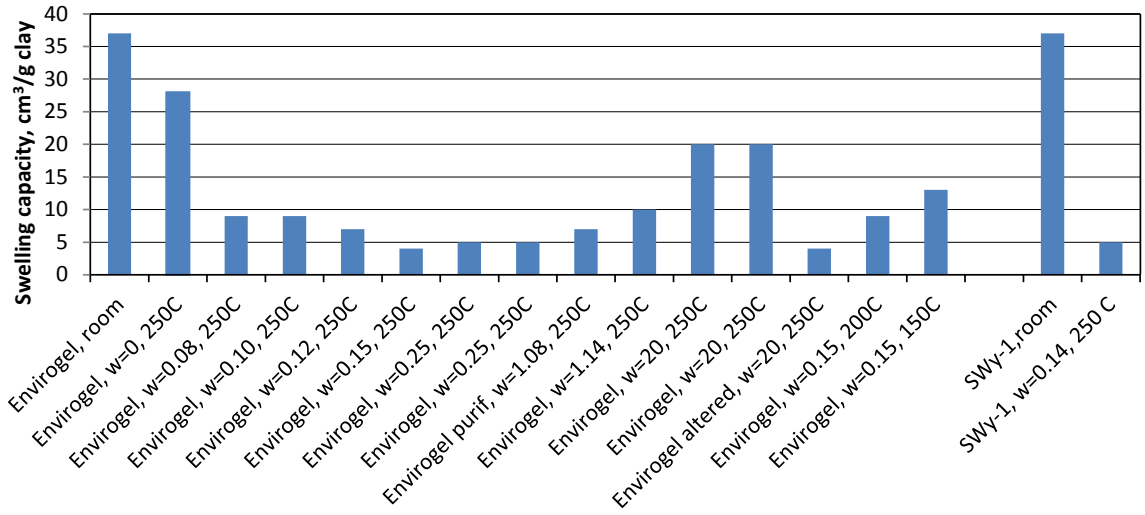

Fig. 5-5: "Swelling capacity" of different materials according to the publication by Couture (1985).

Labels denote type of clay, water-to-solid ratio and temperature during the steam exposure.

Haas et al. (1999) exposed the commercial bentonites Montigel and MX-80 for water steam and analysed them afterwards with respect to both geotechnical and mineralogical changes. Cyclic steam treatment of the Montigel material resulted in a reduction of the swelling pressure by up to 50 %. The pressure was however restored after ultrasonic treatment, drying and milling, and in some cases, higher swelling pressures were measured compared to the reference material. Standard tests concerning shrinking, liquid limit, sedimentation and water adsorption showed no, or insignificant, changes compared to reference material. The mineralogical analyses concerned cation exchange capacity, basal spacing (XRD) and BET-area. All analyses showed insignificant differences in comparison to the reference material independent of temperature and exposure time.

Oscarson & Dixon (1990) exposed bentonite with various degree of water saturation (0, 50, 85 and 100 %) for temperatures up to 150 °C. The exposed materials were thereafter water saturated and swelling pressure and hydraulic conductivity were determined both at elevated and room temperatures. No significant changes in these properties were found compared to reference material. Morphological and mineralogical analyses by use of scanning electron microscopy and X-ray diffraction did not show any changes compared to the reference material.

The present study measured differences, between reference and steam exposed material, of the same magnitude as those identified by Couture in some of the materials, but only after active dispersion and sedimentation. The dispersion of the reference material resulted in formation of voluminous sols and gels with much larger volume than what was formed after passive swelling in pure water in these materials. Obviously, the ability to form such voluminous structures by dispersion and subsequent sedimentation was reduced by exposure to steam in these materials, but not the ability to swell. In general, sedimentation and sol/gel formations are a delicate processes, which are sensitive to small changes in ionic strength, pH etc. (Birgersson et al. 2009).

There are consequently no significant results showing negative effects of steam on the passive uptake of water in bentonite, usually termed swelling capacity, and there are no indications that steam should change the physical properties of a bentonite buffer in a long-term perspective except for the statements presented by Couture. Couture defined the swelling capacity of a clay as the maximum specific volume in water, and according to the tests procedure given by Couture (1985), all samples were actively dispersed ultrasonically and then allowed to settle. We therefore find it plausible that the conclusions in that study were related to the formation of voluminous sols/gels in the reference materials.

The statement by Couture (1985) that "the reduced swelling capacity corresponds to reduced uptake of water by hydrated layers of the montmorillonite" is consequently questioned, not only based on the above discussion, but also on the statement that "montmorillonite altered by water vapour at 250 °C expands only to a maximum basal spacing of 19 Å, which corresponds to three water layers per 10 Å silicate layers in the structure". No reference or experimental results which supported the statement were provided. On the contrary, the lowest reported clay volume was 4 cm^3/g clay, which corresponds to a mean interlayer distance of approximately ten times the stated distance of 9 Å.

5.5 Conclusions

In the present study, large differences in final volume after active dispersion were found between reference and steam exposed material in some of the examined bentonites. These results were qualitatively similar to those found in (Couture 1985), who used the term "swelling capacity", although the results clearly relates to sedimentation properties rather than to swelling properties.

The term "swelling capacity" is thus normally used to describe the maximum volume after passive water uptake (free swelling or unconfined swelling). No such tests were performed in the study by Couture, but results from the present study show no significant effect of steam at the examined temperatures (up to 200 °C). There are consequently no experimental indications in the two studies that short term exposure to steam impairs the swelling properties of bentonite.

6 Summary and conclusions

Bentonite and bentonite/sand mixtures are used as buffers, seals, or backfills in almost every program for radioactive-waste disposal worldwide. The development of the concepts started in the late 1970s and extensive research and technology development has been going on since then. The key features of bentonite in this application are its low hydraulic permeability, self-sealing ability due to the swelling pressure, and long-term mineralogical stability. The functionality of bentonite has been demonstrated in a large spectrum of laboratory and in situ experiments. In a crystalline, fractured host rock below the groundwater table, practically no alternatives to a bentonite buffer are possible for a repository for spent fuel or high level waste. In a clay host rock, the geological medium itself acts as a self-sealing hydraulic barrier and other options may be possible (e.g. backfilling with host rock or using a concrete barrier), but a bentonite clay buffer has clear advantages (e.g. high sorption capacity, inherently low hydraulic conductivity). Bentonite is still the main option for seals in shafts and galleries, both in crystalline and clay host rocks.

The present report offers a broad overview of the current understanding of the thermal stability of montmorillonite. The first part of this report is dedicated to a literature review focusing on the transformation of montmorillonite to a non-swelling clay mineral illite. The additional studies presented here examined potential changes to the safety-relevant properties of bentonite during the high temperature period of a repository. This report should provide improved insights regarding safety-relevant properties of montmorillonite under prevailing repository conditions.

- The literature review revealed that the transformation of smectite-to-illite is induced by increasing temperature and potassium activity. The conversion process is complex and still not completely understood. Nonetheless, it displays very slow kinetics over a wide range of environmental conditions for the temperatures of interest here.
- The various models for illitisation of smectites suggest negligible transformation in a repository because of the relatively short period of elevated temperatures. Because of uncertainties and a number of conservatisms in the application of such models (for example K^+ supply is assumed to be instantaneous and bentonite barriers are partially saturated for some period), the results of such calculations should be considered as bounding and indicative and not as quantitative predictions.
- The hydrothermal "illitisation" experiments described in this report at temperatures of around 270 °C with Wyoming bentonite explored unrealistic "high-K" conditions in the presence of 0.1 M KCl solution, "realistic" conditions with raw Wyoming bentonite and conditions with Na-exchanged and purified Wyoming bentonite with added powdered K-feldspar. There was no evidence of illitisation in reacted samples from raw bentonite or Na-exchanged bentonite reacted in "granite-type" solution regardless of the presence of added K-feldspar or the more abundant accessory mineral content in the raw bentonite. The only distinct increase in illite content occurred in the samples based on K-bentonite reacted in a 0.1 M KCl solution. It appears that the much higher potassium activity in these samples promoted illitisation. The smectite-to-illite conversion appears to have been faster in the beginning and decreased afterwards.

- The batch tests run at temperatures between 20 °C and 150 °C showed that montmorillonite dissolved and released silica and resulted in a layer charge increase located in the tetrahedral sheets. The montmorillonite was consequently altered in the direction towards beidellite. Dissolution of the raw bentonite was comparable to the corresponding purified montmorillonite, showing that the presence of accessory minerals in the bentonite does not significantly influence the process. No fixation of potassium was observed in samples ion-exchanged to basically pure K^+-montmorillonite. Actually, no fixation of potassium was observed in any test, although explicit potassium exchange was performed post-heating in all test materials.
- The last part of the report focused on the relatively long period in the repository evolution (potentially decades to hundreds of years) during which the near-field is only partially saturated and the bentonite is expected to be exposed to steam. Couture (1985) reported that the swelling capacity of bentonite might be significantly reduced if exposed to steam. Couture used the term "swelling capacity" to describe the volume of a bentonite which was actively dispersed and allowed to settle. This volume has no relevance to swelling, but more to gel formation from a solution. Oscarson & Dixon (1990) instead used the term "maximum volume". Based on the experimental findings presented in this report it can be concluded that:
  - The results reported by Couture (1985) could principally be reproduced if the steam-treated bentonite was subsequently actively dispersed and allowed to settle. However, at temperatures of 150 °C and 200 °C the maximum passive uptake of water, usually termed swelling capacity, did not change significantly. The Couture effect relates the effect of steam to a reduction in maximum specific volume rather than to swelling capacity. The findings suggest that the relatively short term high temperature period (> 100 °C) and the period during which the partial saturation in a repository causes a high water vapour pressure do not cause any significant reduction of the water uptake capacity of montmorillonite. It can be further concluded that safety function indicators such as the swelling pressure or the hydraulic conductivity which are directly related to the water uptake are not expected to be reduced.

Impact of the thermal transient for the repository safety

The spectrum of experimental conditions explored (Sections 3 – 5) encompasses the range in thermo-hydro-chemical conditions in a HLW repository and in fact goes beyond it.

The overall experimental findings confirm that the montmorillonite mineral is sufficiently stable over the transient thermal period to fulfil the safety requirements of the bentonite buffer. The observed tendency of mineral alteration in the bentonite from montmorillonite towards beidellite does not impede any safety function criteria to be fulfilled.

The repository near-field is expected to have a low water-to-solid ratio (smectite). Thus, the effects observed in the high water-to-solid ratio experiments will be greater than those under expected repository conditions and the stability of the smectite clay barrier will be greater than that of the clays in the experiment.

Scientific appraisal and impact on the understanding of montmorillonite to illite transformation processes

The changes in mineral composition of the smectites shown in some of the 90 and 150 °C experiments suggest a shift of the mineral composition towards a beidellite composition and an increase in overall layer charge. The difference in mineral composition between the low temperature experiments and those which are more closely allied to diagenetic (burial) conditions is worth pointing out in the project:

- The smectite to illite transformation is a selective chemical change and results in an inter-layered mineral (illite and smectite) as seen in the K-bentonite experiments at 270 °C. This produces a growing number of non-smectite layers in the overall mineral structure which changes the physical and chemical properties of the smectite material.
- In the experiments performed on smectite at lower temperatures a gradual increase in layer charge in all layers or randomly in the structure is observed. This does not lead to a significant change in mineral behaviour as far as swelling or cation absorption is concerned. This process will preserve the overall fundamental physical and chemical behaviour of the smectite for a longer time than that of the classical smectite to illite via mixed layered mineral process. This is a fundamentally new observation.

It should be stressed that the experiments have been carried out under conditions of chemical under-saturation with respect to the chemical components of the smectites through the use of a high water to solid ratio. This is probably the reason why there is a loss of silica but why other elements remain within the minerals is not yet understood. One would expect the integral dissolution of the minerals instead of the obvious elemental diffusion within the structure which compensates the lost silica with aluminium ions. The partial loss of silica (the fundamental element in clays) shows the effects of dissolution under conditions of strong under-saturation but the re-arrangement by internal diffusion of the remaining elements, notably aluminium, has not been foreseen.

Acknowledgements

The authors would like to thank Dr. Bruce Velde and Lawrence Johnson for their critical review, helpful and interesting discussions and useful comments.

7 References

Aagard, P. & Helgeson, H.C. (1983): Activity/composition relations among silicates and aqueous solutions: II. Chemical and thermodynamic consequences of ideal mixing of atoms on homological sites in montmorillonites, illite and mixed-layer clays. Clays and Clay Minerals 31, 207-217.

Abercrombie, H.J., Hutcheon, I.E., Bloch, J.D. & De Caritat, P. (1994): Silica activity and the smectite-illite reaction. Geology 22, 539-542.

Ahn, J.H. & Peacor, D.R. (1986): Transmission and analytical electron microscopy of the smectite-to-illite conversion. Clays and Clay Minerals 34, 165-179.

Aja, S.U. & Rosenberg, P.E. (1996): The thermodynamic status of compositionally-complex clay minerals; discussion of Clay mineral thermometry; a critical perspective. Clays and Clay Miner. 44, 560-568.

Alexander, W.R., Milodowski, A.E., Pitty, A.F., Hardie, S.M.L., Kemp, S.J., Rushton, J.C., Siathas, A., Siathas, A., Mackenzie, A.B., Korkeakoski, P., Norris, S., Sellin, P. & Rigas, M. (2013): Bentonite reactivity in alkaline solutions: interim results of the Cyprus Natural Analogue Project (CNAP). Clay Miner. 48, 235-249.

Altaner, S.P. (1989): Calculation of K diffusional rates in bentonite beds. Geochim. Cosmochim. Acta 53, 923-931.

Altaner, S.P., Hower, J., Whitney, G. & Aronson, J.L. (1984): Model for K-bentonite formation: Evidence from zoned K-bentonites in the disturbed belt, Montana. Geology 12, 412-415.

Amram, K. & Ganor, J. (2005): The combined effect of pH and temperature on smectite dissolution rate under acidic conditions. Geochim. Cosmochim. Acta 69, 2535-2546.

Andra (2005): Dossier 2005: Référentiel des matériaux d'un stockage de déchets à haute activité et à vie longue. Tome 1: Matériaux à base d'argiles gonflantes. Andra report C.RP. ASCM.04.0015.A, Châtenay-Malabry, France.

Arcos, D., Grandia, F. & Domènech, C. (2006): Geochemical evolution of the near field of a KBS-3 repository. SKB Tech. Rep. TR-06-16. SKB Svensk Kärnbränslehantering AB, Stockholm, Sweden.

Bauer, A. & Berger, G. (1998): Kaolinite and smectite dissolution rate in high molar KOH solutions at 35° and 80 °C. Appl. Geochem. 13, 905-916.

Bauer, A. & Velde, B. (1999): Smectite transformation in high molar KOH solutions. Clays Minerals 34, 259-273.

Beaufort, D., Berger, G., Lacharpagne, J.C. & Meunier, A. (2001): An experimental alteration of montmorillonite to a di + trioctahedral smectite assemblage at 100 and 200 °C. Clays and Clay Minerals 36, 211-225.

Bell, T.E. (1986): Microstructure in mixed-layer illite/smectite and its relationship to the reaction of smectite to illite. Clays and Clay Minerals 34, 146-154.

Bethke, C.M. & Altaner, S.P. (1986): Layer-by-layer mechanism of smectite illitization and application to a new rate law. Clays and Clay Minerals 34, 136-145.

Birgersson, M. (*in prep.*): Computational assessment of transport of dissolved silica from a KBS-3 deposition hole. Posiva Report (draft). Posiva Oy, Finland.

Birgersson, M. & Wersin, P. (2014): KBS-3H reactive transport modelling of iron-bentonite interactions, an update for the Olkiluoto case. Posiva Working Report No. 2013-02. Posiva Oy, Finland.

Birgersson, M., Börgesson, L., Hedström, M., Karnland, O. & Nilsson, U. (2009): Bentonite erosion – Final report. SKB Tech. Rep. TR-09-34. SKB Svensk Kärnbränslehantering AB, Stockholm, Sweden.

Blanc, P., Bieber, A., Fritz, B. & Duplay, J. (1997): A short range interaction model applied to illite-smectite mixed-layer minerals. Physics and Chemistry of Minerals 24, 574-581.

Blanc, P., Vieillard, P., Gailhanou, H. & Gaboreau, S. (2013): Thermodynamics of clay minerals. *In:* F. Bergaya & G. Lagaly (eds.): Handbook of Clay Science, Chapter 6, 173-210.

Bouchet, A., Cassagnabère, A. & Parneix, J.C. (2004): Batch experiments: results on MX80. *In:* Ecoclay II: Effect of cement on clay barrier performance phase II. Final report. European contract FIKW-CT-2000-28.

Bradbury, M.H., Berner, U., Curti, E., Hummel, W., Kosakowski, G. & Thoenen, T. (2014): The long term geochemical evolution of the nearfield of the HLW repository. Nagra Tech. Rep. NTB 12-01. Nagra, Wettingen.

Cama, J., Ganor, J., Ayora, C. & Lasaga, C.A. (2000): Smectite dissolution kinetics at 80 °C and pH 8.8. Geochim. Cosmochim. Acta 64, 2701-2717.

Carstea, D.D., Harward, M.E. & Knox, E.G. (1970): Comparison of iron and aluminum hydroxy interlayers in montmorillonite and vermiculite: I. formation. Soil Sci. Soc. Amer. Proc. 34, 517-521.

Chang, H.K., Mackenzie, F.T. & Schoonmaker, J. (1986): Comparisons between the diagenesis of dioctahedral and trioctahedral smectite, Brazilian offshore basins. Clays and Clay Minerals 34, 407-423.

Colten, V.A. (1986): Hydration states of smectite in NaCl brines at elevated pressure and temperature. Clays and Clay Minerals 34, 179-193.

Couture, R.A. (1985): Steam rapidly reduces the swelling capacity of bentonite. Nature 318, 50-52.

Cuadros, J. & Linares, J. (1996): Experimental kinetic study of the smectite-to-illite transformation. Geochim. Cosmochim. Acta, 60, 439-453.

Dubacq, B., Vidal, O. & De Andrade, V. (2010): Dehydration of dioctahedral aluminous phyllosilicates: thermodynamic modelling and implications for thermobarometric estimates. Contrib. Mineral. Petrol. 159, 159-174.

Dueck, A. (2004): Hydro-mechanical properties of a water unsaturated sodium bentonite. Laboratory study and theoretical interpretation. Ph. D. Thesis, Lund University, Sweden.

Dueck, A. (2010): Thermo-mechanical cementation effects in bentonite investigated by unconfined compression tests. SKB Tech. Rep. TR-10-41. SKB Svensk Kärnbränslehantering AB, Stockholm, Sweden.

Eberl, D. (1978): The reaction of montmorillonite to mixed-layer clay: the effect of interlayer alkali and alkaline earth cations. Geochim. Cosmochim. Acta 42, 1-7.

Eberl, D.D. (1980): Alkali cation selectivity and fixation by clay minerals. Clays and Clay Minerals 28, 161-172.

Eberl, D.D. (1993): Three zones for illite formation during burial diagenesis and metamorphism. Clays Clay Minerals 41, 26-37.

Eberl, D.D. & Hower, J. (1976): Kinetics of illite formation. Bull. Geol. Soc. Am. 87, 1326-1330.

Eberl, D.D. & Hower, J. (1977): The hydrothermal transformation of sodium and potassium smectite into mixed-layer clay. Clays and Clay Minerals 25, 215-227.

Eberl, D.D., Whitney, G. & Khoury, H. (1978): Hydrothermal reactivity of smectite. American Mineralogist 63, 401-409.

Eberl, D.D., Środoń, J. & Northrop, H.R. (1987): Potassium Fixation in Smectite by Wetting and Drying. *In:* Geochemical Processes at Mineral Surfaces, ACS Symposium Series. American Chemical Society, 296-326.

Eberl, D.D., Velde, B. & Mccormick, T.D. (1993): Synthesis of illite-smectite from smectite at earth surface temperatures and high pH. Clays and Clay Minerals 28, 49-60.

Elliott, W.C. & Matisoff, G. (1996): Evaluation of kinetic models for the smectite to illite transformation. Clays and Clay Minerals 44, 77-87.

Elliott, W.C., Aronson, J.L., Matisoff, G. & Gautier, D.L. (1991): Kinetics of the smectite to illite transformation in the Denver basin: clay mineralogy, K-Ar data and mathematical modelling. Bull. Amer. Assoc. Petrol. Geol. 75, 436-462.

Esposito, K.J. & Whitney, G. (1995): Thermal effects of thin igneous intrusions on diagenetic reactions in a Tertiary basin of southwestern Washington. US Geol. Surv. Bull 2085-C, 40 p.

Essene, E.J. & Peacor, D.R. (1997): Illite and smectite; metastable, stable or unstable? Further discussion and a correction; reply. Clays and Clay Minerals 45, 116-122.

Fernandez, R., Cuevas, J., Sanchez, L., Vigil De La Villa, R. & Leguey, S. (2006): Reactivity of the cement – bentonite interface with alkaline solutions using transport cells. Applied Geochemistry 21, 977-992.

Ferrage, E., Vidal, O., Mosser-Ruck, R., Cathelineau, M. & Cuadros, J. (2011): A reinvestigation of smectite illitisation in experimental hydrothermal conditions: Results from X-ray diffraction and transmission electron microscopy. American Mineralogist 96, 207-223.

Garrels, R.M. (1984): Montmorillonite/illite stability diagrams. Clays and Clay Minerals 32, 161-166.

Gaucher, E. (1998): Interaction eaux-argiles. Etude experimentale. PhD thesis, University of Paris VII, 265 p.

Giggenbach, W. (1981): Geothermal mineral equilibria. Geochim. Cosmochim. Acta 45, 393-410.

Greene-Kelly, R. (1953): Irreversible Dehydration in Montmorillonte. Clay Miner. Bull 2, 52-56.

Haas, R., Teysseire, Ph. & Bucher, F. (1999): Einfluss von Wasserdampf auf Quellpotential von Bentonit. Unpubl. Nagra Internal Rep. Nagra, Wettingen.

Hillier, S. (1993): Origin, diagenesis, and mineralogy of chlorite minerals in Devonian lacustrine mudrocks, Orcadian basin, Scotland. Clays and Clay Minerals 41, 240-259.

Hoffman, J. & Hower, J. (1979): Clay mineral assemblages as low grade metamorphic geothermometer – Application to the thrust-faulted disturbed belt of Montana. *In:* P.A. Scholle & P.R. Schluger (eds.): Aspects of Diagenesis. SEPM Special Publication 26, 55-79.

Hoffmann, U. & Klemen, R. (1950): Verlust der Austauschfähigkeit von Lithiumionen an Bentonit durch Erhitzung. Z. Anorg. Allg. Chemie 262, 95-99.

Howard, J.J. & Roy, D.M. (1985): Development of layer charge and kinetics of experimental smectite alteration. Clays and Clay Minerals 33, 81-88.

Hower, J.J., Eslinger, E.V., Hower, M.E. & Perry, E.A. (1976): Mechanism of burial metamorphism of argillaceous sediment. 1. Mineralogical and chemical evidence. Geol. Soc. Am. Bull. 87, 725-737.

Huang. W.-L., Longo, J.M. & Pevear, D.R. (1993): An experimentally derived kinetic model for smectite-to-illite conversion and its use as a geothermometer. Clays and Clay Minerals 41, 162-177.

Huertas, F.J., Caballero, E., Jiménez de Cisneros, C., Huertas, F. & Linares, J. (2001): Kinetics of montmorillonite dissolution in granitic solutions. Appl. Geochem. 16, 397-407.

Idiart, A., Maia, F. & Arcos, D. (2013): Geochemical evaluation of the near-field for future HLW repository at Olkiluoto. Posiva 2013-05. Posiva Oy, Eurajoki, Finland.

Inoue, A. (1983): Potassium fixation by clay minerals durig hydrothermal treatment. Clays and Clay Minerals 31, 81-91.

Inoue, A. (1995): Formation of clay minerals in hydrothermal environments. *In:* B. Velde (ed.): Origin and Mineralogy of Clays. Springer, 268-329.

Inoue, A., Velde, B., Meunier, A. & Touchard, G. (1988): Mechanism of illite formation during smecite to illite conversion in a hydrothermal system. Am. Miner. 73, 1325-1334.

Johnston, R.M. & Miller, H.G. (1985): Hydrothermal stability of bentonite-based buffer materials. AECL report AECL-8376. AECL, Pinawa, Manitoba, Canada.

Kamei, G., Mitsui, M.S., Futakuchi, K., Hashimoto, S. & Sakuramoto, Y. (2005): Kinetics of long-term illitization of montmorillonite – a natural analogue of thermal alteration of bentonite in the radioactive waste disposal system. J. Phys. Chem. Solids 66, 612-614.

Karnland, O. & Birgersson, M. (2006): Montmorillonite stability with special respect to KBS-3 conditions. SKB Tech. Rep. TR-06-11. SKB Svensk Kärnbränslehantering AB, Stockholm, Sweden.

Karnland, O., Olsson, S. & Nilssson, U. (2006): Mineralogy and sealing properties of various bentonites and smectite-rich clay materials. SKB Tech. Rep. TR-06-30. SKB Svensk Kärnbränslehantering AB, Stockholm, Sweden.

Karnland, O., Olsson, S., Nilsson, U. & Sellin, P. (2007): Experimentally determined swelling pressures and geochemical interactions of compacted Wyoming bentonite with highly alkaline solutions. Physics and Chemistry of the Earth, Parts A/B/C 32, 275-286.

Karnland, O., Olsson, S., Dueck, A., Birgersson, M., Nilsson, U. & Hernan-Hakansson, T. (2009): Long term test of buffer material at the Äspö Hard Rock Laboratory, LOT project. Final report on the A2 test parcel. SKB Tech. Rep. TR-09-29. SKB Svensk Kärnbränslehantering AB, Stockholm, Sweden.

Kaufhold, S. & Dohrmann, R. (2009): Stability of bentonites in salt solutions I. sodium chloride. Applied Clay Science 45, 171-177.

Kaufhold, S. & Dohrmann, R. (2010): Stability of bentonites in salt solutions: II. Potassium chloride solution – Initial step of illitization? Appl. Clay Sci. 49, 98-107.

Kaufhold, S. & Dohrmann, R. (2011). Stability of bentonites in salt solutions III – Calcium hydroxide. Applied Clay Science 51, 300-307.

Kim, J., Dong, H., Seabaugh, J., Newell, S.W. & Eberl, D.D. (2004): Role of microbes in the smectite-to-illite reaction. Science 303, 830-832.

Köhler, S.J., Dufaud, F. & Oelkers, E.H. (2003): An experimental study of illite dissolution kinetics as a function of ph from 1.4 to 12.4 and temperature from 5 to 50 °C. Geochim. Cosmochim. Acta 67, 3583-3594.

Lahann, R.W. & Roberson, H.E. (1980): Dissolution of silica from montmorillionite: effect of solution chemistry. Geochim. Cosmoschim. Acta 44, 1937-1943.

Lanson, B. & Velde, B. (1992): Decomposition of X-ray-diffraction patterns – A convenient way to describe complex I/S diagenetic evolution. Clay Clay Miner. 40, 629-643.

Lee, J.O., Kang, I.M. & Cho, W.J. (2010): Smectite alteration and its influence on the barrier properties of smectite clay for a repository. Appl. Clay Sci. 47, 99-104.

Leupin, O. & Lawrence, J. (2014): Requirements for buffer for a repository for SF/HLW in Opalinus Clay. Nagra Working Report NAB 13-46. Nagra, Wettingen.

Lippmann, F. (1977): The solubility products of complex minerals, mixed crystals, and three-layer clay minerals. N. Jb. Abh. 130, 243-263.

Lippmann, F. (1980): Phase diagrams depicting aqueous solubility of binary mineral system. Neues Jb. Mineral. Abh. 139, 1-25.

Lippmann, F. (1982): The thermodynamic status of clay minerals. Proc. 7th Int. Clay Conf., 475-485.

Mäder, U.K. (2009): Reference pore waters for the Opalinus Clay and 'Brown Dogger' for the provisional safety-analysis in the framework of sectoral plan – interim results (SGT-ZE). Nagra Working Report NAB 09-14. Nagra, Wettingen.

Marty, N.C.M., Cama, J., Sato, T., Chino, D., Villiéras, F., Razafitianamaharavo, A., Brendlé, J., Giffaut, E., Soler, J.M., Gaucher, E.C. & Tournassat, C. (2011): Dissolution kinetics of synthetic Na-smectite. An integrated experimental approach. Geochim. Cosmochim. Acta 75, 5849-5864.

May, H.M., Kinniburgh, D.G., Helmke, P.A. & Jackson, M.L. (1986): Aqueous dissolution, solubilities, and thermodynamic stabilities of common aluminosilicate clay minerals: Kaolinite and smectites. Geochim. Cosmochim. Acta 50, 1667-1677.

Meier, L.P. & Kahr, G. (1999): Determination of the cation exchange capacity (CEC) of clay minerals using the complexes of copper (II) ion with triethylenetetramine and tetraethylenepentamine. Clays Clay Min. 47, 386-388.

Metz, V., Amram, K. & Ganor, J. (2005): Stoichiometry of smectite dissolution reaction. Geochim. Cosmochim. Acta 69, 1755-1772.

Meunier, A. (2005): Clays. Springer, 472 p.

Meunier, A. & Velde, B. (2004): Illite. Springer, 286 p.

Meunier, A., Velde, B. & Griffault, L. (1998): The reactivity of bentonites: a review. An application to clay barrier stability for nuclear waste storage. Clay Minerals 33, 187-196.

Mosser-Ruck, R. & Cathelineau, M. (2004): Experimental transformation of Na,Ca-smectite under basic conditions at 150 C. Applied Clay Science 26, 259-273.

Mosser-Ruck, R., Cathelineau, M., Baronnet, A. & Trouiller, A. (1999): Hydrothermal reactivity of K-smectite at 300 °C and 100 bar: dissolution-crystallization processes and non-expandable dehydrated smectite formation. Clays and Clay Minerals 34, 275-290.

Myllykylä, E., Tanhua-Tyrkkö, M., Bouchet, A. & Tiljander, M. (2013): Dissolution experiments of Na- and Ca-montmorillonite in groundwater simulants under anaerobic conditions. Clay Miner. 48, 295-308.

Nadeau, P.H., Wilson, M.J., McHardy, W.J. & Tait, J.M. (1985): The conversion of smectite to illite during diagenesis: Evidence from some illitic clays from bentonites and sandstones. Mineral. Mag. 49, 393-400.

Nagra (2002): Project Opalinus Clay: Safety report: Demonstration of disposal feasibility for spent fuel, vitrified high-level waste and long-lived intermediate-level waste (Entsorgungsnachweis). Nagra Tech. Rep. NTB 02-05. Nagra, Wettingen.

Nagra (2010): Beurteilung der geologischen Unterlagen für die provisorischen Sicherheitsanalysen in SGT Etappe 2 – Klärung der Notwendigkeit ergänzender geologischer Untersuchungen. Nagra Tech. Rep. NTB 10-01. Nagra, Wettingen.

Nagra (2014): SGT Etappe 2: Vorschlag weiter zu untersuchender geologischer Standortgebiete mit zugehörigen Standortarealen für die Oberflächenanlage – Charakteristische Dosisintervalle und Unterlagen zur Bewertung der Barrierensysteme. Nagra Tech. Rep. 14-03. Nagra, Wettingen.

Newman, A.C.D. & Brown, G. (1987): The chemical constitution of clays. Mineralogical Society Monograph 6.

Niu, B., Yoshimura, T. & Hirai, A. (2000): Smectite diagenesis in Neogene marine sandstone and mudstone of the Niigata basin, Japan. Clays and Clay Minerals 48, 26-42.

Oscarson, D.W. & Dixon, D.A. (1989): The effect of steam on montmorillonite. Applied Clay Science 4, 279-292.

Oscarson, D.W. & Dixon, D.A. (1990): Effect of heating unsaturated bentonite on the swelling and hydraulic properties of subsequently saturated clay. *In:* Proc. of the Annual Conf. and 1st Bienial Environmental Speciality Conf. of the Canadian Soc. of Civil Engineering II-1, 312-223. Hamilton, Ontario.

Patrier, O.,Papapanagiotou, P., Beaufort, D.,Traineau, H., Bril, H. & Rojas, J. (1996): Role of permeability versus temperature in the distribution of the fine (< 0.2 μm) clay fraction in the Chipilapa geothermal system (El Salvador, Central America). J. Volcanology and Geothermal Research 72, 101-120.

Pellegrini, R., Horseman, S., Kemp, S., Rochelle, C., Boisson, J.-Y., Lombardi, S., Bouchet, A. & Parneix, J.-C. (1999): Natural analogues of the thermo-hydro-chemical and thermo-hydro-mechanical response. EC Nuclear Science and Technology Report, EUR 19114. EC, Luxembourg.

Pusch, R. (2000): On the effect of hot water vapor on MX-80 clay. SKB Tech. Rep. TR-00-16. SKB Svensk Kärnbränslehantering AB, Stockholm, Sweden.

Pusch, R., Bluemling, P. & Johnson, L. (2003): Performance of strongly compressed MX-80 pellets under repository-like conditions. Applied Clay Science 23, 239-244.

Pusch, R. & Madsen, F.T. (1995): Aspects of the illitization of the Kinnekule bentonites. Clays and Clay Minerals 43, 261-270.

Pytte, A. (1982): The kinetics of the smectite to illite reaction in contact metamorphic shales. M.A. Thesis, Dartmouth College.

Pytte, A.M. & Reynolds, R.C. (1989): The thermal transformation of smectite to illite. *In:* Naeser, N.D. & McCulloh, T.H.: Thermal history of Sedimentary Basins. Springer-Verlag New York, 133-140.

Rai, D. & Kittrick, J.A. (1989): Mineral equilbria and the soil system. *In:* J.B. Dixon & S.B. Weed (eds.): Minerals in Soil Environments. Soil Science Society of America Book Series, Madison, Wisconsin, USA, 161-198.

Reynolds, C.R. & Moore, D.M. (1989): X-Ray diffraction and the identification and analysis of clay minerals – Chapter 8: Quantitative Analysis. Oxford University Press.

Reynolds, Jr. R.C. & Reynolds, III R.C. (1995): NEWMOD 2.1 for Windows.

Ribeiro, F.R., Fabris, J.D., Kostka, J. E., Komadel, P. & Stucki, J.W. (2009): Comparisons of structural iron reduction in smectites by bacteria and dithionite: II. A variable-temperature Mössbauer spectroscopic study of Garfield nontronite. Pure and Applied Chemistry 81, 1499-1509.

Roaldset, E., He Wei & Grimstad, S. (1998): Smectite to illite conversion by hydrous pyrolysis. Clays and Clay Minerals 33, 147-158.

Roberson, H.E. & Lahann, R.W. (1981): Smectite to illite conversion rates: effects of solution chemistry. Clays and Clay Minerals 29, 129-135.

Rozalén, M., Huertas, F.J. & Brady, P.V. (2009): Experimental study of the effect of pH and temperature on the kinetics of montmorillonite dissolution. Geochim. Cosmochim. Acta 73, 3752-3766.

Rozalén, M.L., Huertas, F.J., Brady, P.V., Cama, J., García-Palma, S. & Linares, J. (2008): Experimental study of the effect of pH on the kinetics of montmorillonite dissolution at 25 °C. Geochim. Cosmochim. Acta 72, 4224-4253.

Sass, B.M., Rosenberg, P.E. & Kittrick, J.A. (1987): The stability of illite/smectite during diagenesis: An experimental study. Geochim. Cosmochim. Acta 51, 2103-2115.

Sato, T., Murakami, I. & Watanabe, T. (1996): Change in layer charge of smectites and smectite layers in illite/smectite during diagenetic alteration. Clays and Clay Minerals 44, 460-469.

Savage, D. (2014): An assessment of the impact of the long term evolution of engineered structures on the safety-relevant functions of the bentonite buffer in a HLW repository. Nagra Tech. Rep. NTB 13-02. Nagra, Wettingen.

Senger, R.K. & Ewing, J. (2008): Evolution of temperature and water content in the bentonite buffer: Detailed modelling of two-phase flow processes associated with the early closure period – Complementary simulations. Nagra Working Report NAB 08-53. Nagra, Wettingen.

Senger, R., Papafotiou, A. & Marschall, P. (2014): Thermo-hydraulic simulations of the near-field of a SF/HLW repository during early- and late-time post-closure period. Nagra Working Report NAB 14-11. Nagra, Wettingen.

Sena, C., Salas, J. & Arcos, D. (2010): Aspects of geochemical evolution of the SKB near field in the frame of SR-Site. SKB Tech. Rep. TR-10-59. SKB Svensk Kärnbränslehantering AB, Stockholm, Sweden.

SKB (2010): Buffer, backfill and closure process report for the safety assessment SR-Site. SKB Tech. Rep. TR-10-47. SKB Svensk Kärnbränslehantering AB, Stockholm, Sweden.

SKB (2011): Long-term safety for the final repository for spent nuclear fuel at Forsmark. SKB Tech. Rep. TR-11-01. SKB Svensk Kärnbränslehantering AB, Stockholm, Sweden.

Son, B-K., Yoshimura, T. & Fukasawa, H. (2001): Diagenesis of dioctahedral and trioctahedral smectites from altering beds in miocene to pleistocene rocks of the Niigata basin, Japan. Clays and Clay Minerals 49, 333 – 346.

Stroes-Gascoyne, S. (2011): Microbiological characteristics of compacted bentonite fo a dry density of 1'450 kg/m^3: A literature review. Nagra Working Report NAB 11-05. Nagra, Wettingen.

Stucki, J.W., Golden, D.C. & Roth, C.B. (1984): Effects of reduction and reoxidation of structural iron on the surface charge and dissolution of dioctahedral smectites. Clays and Clay Minerals 32, 350-356.

Sucha, V., Kraus, I., Gerthofferova, H., Petes, J. & Serekova, M. (1993): Smectite to illite conversion in bentonites and shales of the east Slovak basin. Clays and Clay Minerals 28, 243-253.

Svensson, D., Dueck, A., Nilsson, U., Olsson, S., Sandén, T., Lydmark, S., Jägerwall, S., Pedersen, K. & Hansen, S. (2011): Alternative buffer material. Status of the ongoing laboratory investigation of reference materials and test package 1. SKB Tech. Rep. TR-11-06. SKB Svensk Kärnbränslehantering AB, Stockholm, Sweden.

Tardy, Y., Duplay, J. & Fritz, B. (1987): Stability fields of smectites and illites as a function of temperature and chemical composition. SKB Tech. Rep. 87-20. SKB Svensk Kärnbränslehantering AB, Stockholm, Sweden.

Van Groos, A.F.K. & Guggenheim, S. (1984): The effect of pressure on the dehydration reaction of interlayer water in Na-montmorillonite (Swy-1). American Mineralogist 69, 872-879.

Velde, B. (1995a): Composition and mineralogy of clay minerals. *In:* B. Velde (ed.): Origin and Mineralogy of Clays: Clay and the Environment. Springer, New York Chapter 2, 8-41.

Velde, B. (1995b): Compaction and diagenesis. *In:* B. Velde (ed.): Origin and Mineralogy of Clays: Clay and the Environment. Springer, New York, Chapter 5, 220-245.

Velde, B. & Lanson, B. (1993): Comparison of I/S transformation and maturity of organic matter at elevated temperatures. Clays and Clay Minerals 41, 178-183.

Velde, B. & Vasseur, G. (1992): Estimation of the diagenetic smectite to illite transformation in time-temperature space. American Mineralogist 77, 967-976.

Vidal, O. & Dubacq, B. (2009): Thermodynamic modelling of clay dehydration, stability and compositional evolution with temperature, pressure and water activity. Geochim. Cosmochim. Acta 73, 6544-6564.

Vieillard, P. (2000): A new method for the prediction of Gibbs free energies of formation of hydrated clay minerals based on the electronegativity scale. Geochim. Cosmochim. Acta 48, 459-473.

Wersin, P., Johnson, L.H. & McKinley, I.G. (2007): Performance of the bentonite barrier beyond 100°C: a critical review. Physics and Chemistry of the Earth 32, 780-788.

Whitney, G. (1990): Role of water in the smectite-to-illite reaction. Clays and Clay Minerals 38, 343-350.

Whitney, G. & Northrop, H.R (1988): Experimental investigation of the smectite to illite reaction: Dual reaction mechanisms and oxygen-isotope systematics. Amer. Mineral. 73, 77-90.

Yamada, H. & Nakazawa, H. (1993): Isothermal treatments of regularly interstratified montmorillonite-beidellite at hydrothermal conditions. Clays and Clay Minerals 41, 726-730.

Yau, Y.-C., Peacor, D.R., Essene, E.J., Lee, J.-H., Kuo, L.C. & Cosca, M.A. (1987): Hydrothermal treatment of smectite, illite, and basalt to 460 Degrees Celsius: Comparison with hydrothermally formed clay minerals. Clays and Clay Minerals 35, 241-250.

Ylagan, R., Altaner, S.P. & Pozzuoli, A. (2000): Reaction mechanisms of smectite illitization associated with hydrothermal alteration from Ponza Island, Italy. Clays and Clay Minerals 48, 610-631.

Zysset, M. & Schindler, P.W. (1996): The proton promoted dissolution kinetics of K-montmorillonite. Geochim. Cosmochim. Acta 60, 921-931.

Zhang, G.X., Dong, H., Kim, J. & Eberl, D.D. (2007): Microbial Reduction of Structural Fe^{3+} in Nontronite by a Thermophilic Bacterium and its Roles in Promoting the Smectite to Illite Reaction. American Mineralogist 92, 1411-1419.